Award Number: W81XWH-11-1-0557

TITLE: Social Behavior in Medulloblastoma: Functional Analysis of Tumor-Supporting Glial Cells

PRINCIPAL INVESTIGATOR: Hui Zong

CONTRACTING ORGANIZATION: University of Virginia
Charlottesville, VA 22908

REPORT DATE: October 2015

TYPE OF REPORT: Final

PREPARED FOR: U.S. Army Medical Research and Materiel Command
Fort Detrick, Maryland 21702-5012

REPORT DOCUMENTATION PAGE

Form Approved
OMB No. 0704-0188

1. REPORT DATE	2. REPORT TYPE	3. DATES COVERED
October 2015	Final	1Jul2011 - 31Jul2015

4. TITLE AND SUBTITLE
Social Behavior in Medulloblastoma: Functional Analysis of Tumor-Supporting Glial Cells

5a. CONTRACT NUMBER
W81XWH-11-1-0557

5b. GRANT NUMBER

5c. PROGRAM ELEMENT NUMBER

6. AUTHOR(S)
Hui Zong

E-Mail: hz9s@virginia.edu

5d. PROJECT NUMBER

5e. TASK NUMBER

5f. WORK UNIT NUMBER

7. PERFORMING ORGANIZATION NAME(S) AND ADDRESS(ES)
University of Virginia
Charlottesville, VA 22908

8. PERFORMING ORGANIZATION REPORT NUMBER

9. SPONSORING / MONITORING AGENCY NAME(S) AND ADDRESS(ES)
U.S. Army Medical Research and Materiel Command
Fort Detrick, Maryland 21702-5012

10. SPONSOR/MONITOR'S ACRONYM(S)

11. SPONSOR/MONITOR'S REPORT NUMBER(S)

12. DISTRIBUTION / AVAILABILITY STATEMENT
Approved for Public Release; Distribution Unlimited

13. SUPPLEMENTARY NOTES

14. ABSTRACT

Medulloblastoma is the most common malignant pediatric brain tumor. Granule neuron precursors (GNPs) in developing cerebellum proliferate exponentially, and the misregulation of which has been linked to medulloblastoma formation. GNPs are unipotent and only give rise to granule neurons. However, using MADM, a mouse genetic mosaic model, we found that medulloblastoma contain glial cells that are trans-differentiated from transformed GNPs. Our preliminary data showed that specific ablation of tumor glia without harming tumor GNPs led to complete tumor remission, suggesting a tumor-supporting role for these trans-differentiated glia. Here we propose to analyze the tumor "social behavior" with two specific aims. First, we will investigate the tumor regressing process at the cellular level *in vivo*, and determine therapeutic parameters of glial ablation for medulloblastoma treatment. Second, we will investigate the molecular basis for glia-tumor crosstalk that sustains the tumor growth. In the past year, we have completed most of the work proposed in aim 1. Our data showed that the glial-ablation treatment not only results in complete remission free of relapses, but also remains quite effective for mice with late-stage tumors. These findings are particularly encouraging since they point to great potentials in targeting glial cells for treating medulloblastoma in human

15. SUBJECT TERMS
Medulloblastoma, granule neuron precursors (GNPs), tumor-derived glial cells, niche support, genetic ablation

16. SECURITY CLASSIFICATION OF:			17. LIMITATION OF ABSTRACT	18. NUMBER OF PAGES	19a. NAME OF RESPONSIBLE PERSON
a. REPORT	b. ABSTRACT	c. THIS PAGE			USAMRMC
U	U	U	UU	101	19b. TELEPHONE NUMBER *(include area code)*

Table of Contents

Introduction

Medulloblastoma is the most common malignant pediatric brain tumor, resulting from the deviation from normal process of cerebellar development. Immediately after birth, granule neuron precursors (GNPs) on the surface of developing cerebellum proliferate exponentially. The misregulation of GNP proliferation has been linked to medulloblastoma formation. Fate mapping experiments demonstrated that GNPs are unipotent and only give rise to granule neurons. However, using MADM, a mouse genetic mosaic model with lineage tracing capability, we found that medulloblastoma contain glial cells that trans-differentiate from malignantly transformed GNPs. Our preliminary data showed that specific ablation of tumor glia with a genetic tool (GFAP-TK) without harming tumor GNPs led to complete tumor remission, suggesting a critical role for these trans-differentiated glia in supporting the growth of tumor GNPs. Here we propose to establish a co-culture system to investigate the molecular basis for glia-tumor crosstalk that sustains the tumor growth.

Key words

Medulloblastoma, spontaneous reprogramming, tumor microenvironment, tumor-derived astrocytes

Overall project summary

This project started in 2011 at University of Oregon, based on the original Statement of Work (SOW). In the beginning of 2013, our lab moved to University of Virginia. We resumed our work after the approval of the revised SOW. In this final report, the outcomes in all years are reported in a chronological order, with the reference to tasks in the corresponding SOW (original or revised).

For **original task 1**, we worked closely with the IACUC committee at University of Oregon and ACURO, and successfully went through the regulatory review processes for animal studies to get the approval in the beginning of the funding period prior to starting our animal work.

For **original task2**, we set up a well-organized mouse colony to generate MADM-based medulloblastoma model with GFAP-TK (referred to as medullo-TK mice hereafter). We optimized the mouse stocks and established the breeding routines that consistently generate a steady supply of medullo-TK mice for treatment schemes proposed in this grant.

For **original task 3**, we performed histological analysis of cellular events during glial ablation-induced tumor regression. After injecting GCV in medullo-TK mice at P35, we first analyzed tumor brains 6-hour post treatment. For five individual brains that we examined, GFP+ tumor cells were still visible in all of them (Figure 1A shows a representative image). When we stained for Ki67, almost all of these cells are still proliferating, evidenced by the positive staining of Ki67 (Figure 1B & C). Therefore, at this early stage, tumor cells have not started reacting to the consequences of glial ablation.

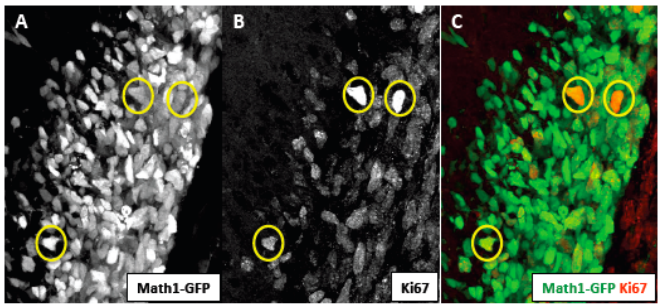

Figure 1. Histological analysis of tumors in medullo-TK mice 6-hour post GCV-injection showed no signs of regression medulloblastoma.

Based on this finding, next we decided to examine a set of brains at 1-day post treatment. Interestingly, at this time point we often observe the progressive death of tumor cells. In one representative brain, there was a massive loss of Math1+ GNPs in the region outlined by the red margin (Figure 2A). However, in other regions there were still significant amount of GFP+ tumor GNPs (Figure 2A). To investigate whether these tumor cells are still proliferative or going through apoptosis, we stained the tissue slice with Ki67 and TUNEL, respectively. While these cells were Ki67 negative indicating the cease of proliferation (data not shown), most tumor GNPs stained positive for TUNEL (Figure 2B). Interestingly, while many cells undergoing apoptosis were green, some of them were neither glial cells (TK negative) nor tumor GNPs (GFP negative) (Figure 2C). The identify of these cells were serendipitously revealed while we co-stained Annexin V (another apoptotic marker) with a GFAP antibody raised in the mouse, which can cross-reacting with mouse vasculature during secondary antibody detection (Figure 2D). Further co-staining of CD34 (endothelial cell marker) and Annexin V confirmed the death of vasculature in glia-ablated tumor mass (Figure 2E). Data from this series of experiments showed that while tumor cells still proliferate 6-hour post GCV treatment, by 1-day post treatment, massive cell death has begun. It is interesting that some tumor regions seem to be more susceptible than other areas, and that the death of tumor cells even led to apoptosis of vasculatures within the tumor mass, an effect could be exploited for medulloblastoma therapy if more data support this finding.

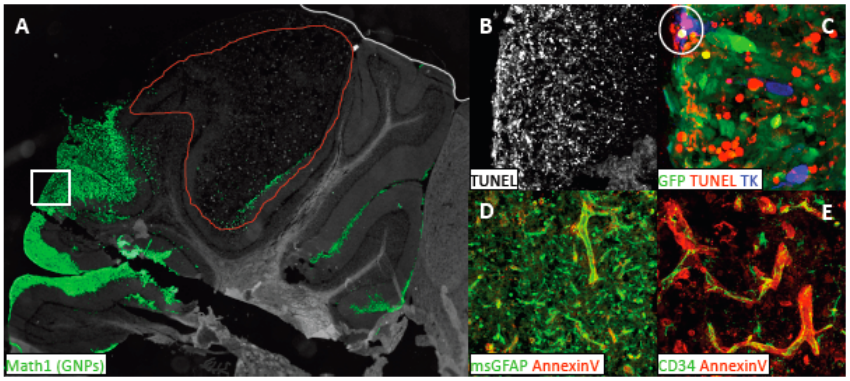

Figure 2. Histological analysis of tumors in medullo-TK mice 1-day post GCV-injection. A) Low magnification image shows that part of the tumor mass regressed while some GFP+ tumor cells persisted in other regions. B) TUNEL staining revealed massive cell death in remaining GFP+ tumor cells. C) Both GFP+ tumor cells and GFP- by-standing cells went through apoptosis. D-E) Endothelial cells in the tumor mass went through apoptosis after glial ablation.

Original task 4 and task 5 is to assess the possibility of relapses of glia-ablated tumors after the initial regression observed in the preliminary data of our proposal and in Figure 2 of this report. Specifically, in **original task 4**, we stained remnant tumor GNPs with Ki67 and NeuN at 7-day post treatment to see whether they remain proliferative or have fully differentiated (Figure 3). To make sure that the cells that we examined were dividing tumor cells prior to the GCV treatment, we co-injected BrdU with GCV. While we did observe some BrdU positive tumor cells at 7-day post treatment, almost all of them are Ki67 negative, suggesting that they are no longer proliferative (Figure 3, A-C). When we co-stained these cells with NeuN, a mature neuron

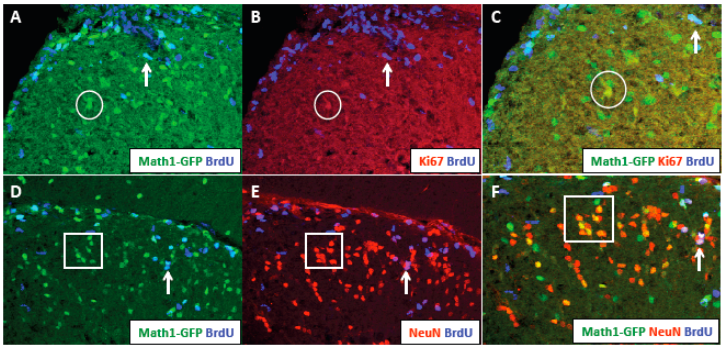

Figure 3. Tumor cells at 7-day post treatment undergo massive neuronal differentiation with few dividing mutant GNPs remaining. (A-C) Few remaining tumor cells are Ki67+ although many of them were dividing at the time of treatment and stained positive for BrdU. (D-F) Many remaining tumor cells are NeuN+, indicating that they are fully differentiated into neuronal fate.

marker, we found many tumor GNPs have fully differentiated into neurons, further supporting the notion that they lost the relapsing capability (Figure 3, D-F). For **original task 5**, we investigated whether GCV-treated, regressed tumors could still relapse by waiting an extended period prior to dissection. In this experiment, we treated medullo-TK mice with GCV at P35, then waited three to four months, at least twice the lifespan of untreated control mice, to monitor the relapse potentials in these mice. We found that there were no tumors in any mice in the experimental group, suggesting that the treatment leads to complete remission free of any relapses. When we sectioned these brains, we often found cluster of green cells under the meninges, which are most likely remnant cells at original tumor locations (Figure 4A). When we co-stained these cells with NeuN, we found that many of these cells are fully differentiated neurons (Figure 4B). Some of them still retained BrdU that was co-injected during the GCV treatment months ago, suggesting that these cells withdrew from cell cycle completely after the glial ablation (Figure 4B). We also found some remnant tumor cell-derived GFP+ glial cells that evaded the ablation (Figure 4C-D). However, they appear to be harmless since they are neither proliferating nor supporting tumor growth at this time. Overall, the results from these two tasks are very encouraging, suggesting that the treatment paradigm could be highly effective for human patients if it advances into clinics.

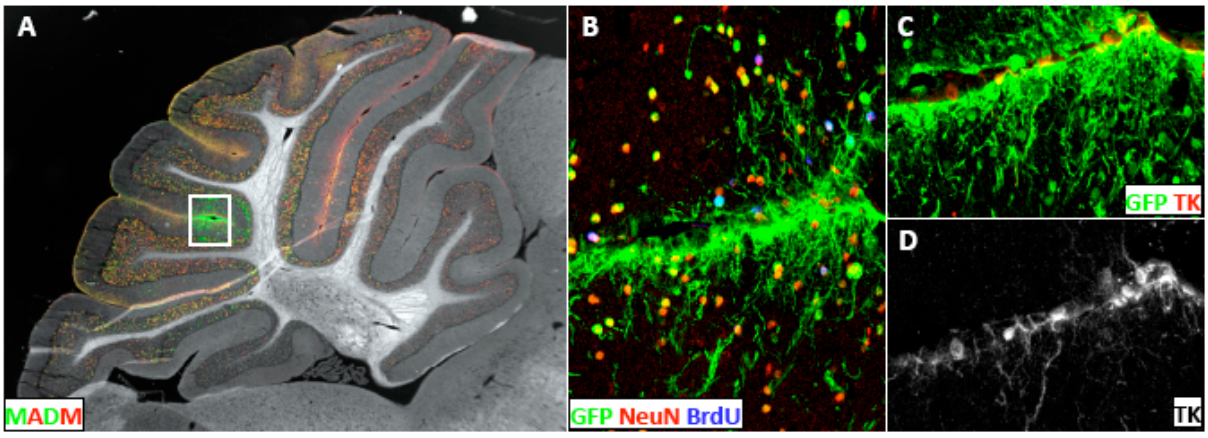

Figure 4. Glia ablation via GCV treatment leads to complete remission of tumors. A) Treated medullo-TK cerebellum showed relatively "normal" tissue organization 3-month following treatment. B) Higher magnification of boxed region A, showing remnant mutant GFP+ cells. Most mutant cells have differentiated into NeuN+ neurons (yellow), some are traced from the treatment period with BrdU (purple) demonstrating that differentiation can occur very early after treatment. C) Remnant tumor glial cells appear not to contribute to further malignancy. D) Nuclei of GFAP-TK+ tumor glia, from panel C, remain at remission stages.

The findings from the above two tasks made **original task 6** particularly important. Since most of the time human patients come to the clinics when neurological symptoms start to appear, at which time tumor sizes tend to be quite large. In this task, we Injected GCV in medullo-TK mice at different time points to determine the treatment

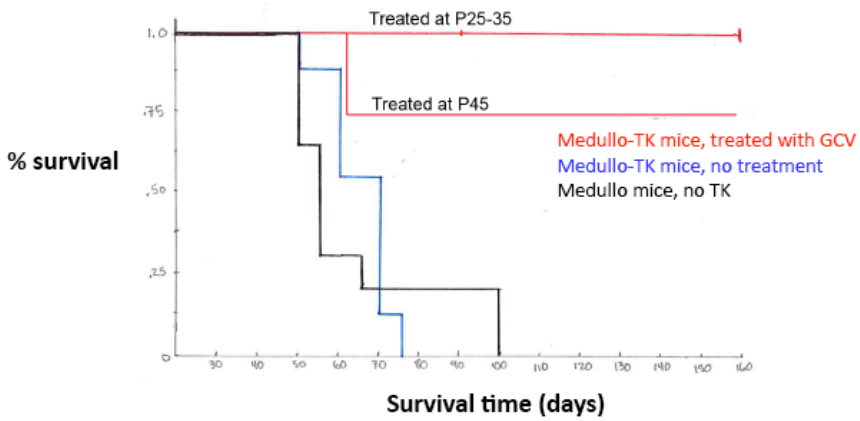

Figure 5. Glial ablation treatment at different tumor progression stages appears to be very effective.

efficacy of glial ablation during different tumor progression stages. In total we examined four experimental groups with at least five mice per group: 1) P25-35 injection of GCV into Medullo-TK mice, when tumors are generally small to medium in size; 2) P45 injection of GCV into Medullo-TK mice, when tumors are generally very large that often cause mouse death in 1-2 weeks; 3) Medullo-TK mice without any GCV injections; 4) Medullo mice without TK and injected with GCV to control for unlikely tumor-shrinking activity of GCV on its own. We found that while mice from two control groups died at around 2-month of age, GCV-treated mice lived for five months or longer (Figure 5). While all Medullo-TK treated at P25 to P35 lived symptom-free to more than five-month of age, two out of eight Medullo-TK mice treated at P45 died around 2-month of age but the remained six mice lived symptom-free for many months (Figure 5). We postulate that the death of two mice with late treatment could be caused by irreversible neurological damages caused by tumors prior to the treatment, and that large tumors could be treated as long as the brain damage is not permanent. This piece of encouraging data suggest that even large tumors could be treated quite effectively.

After we successfully completed **original tasks 1-6**, our lab moved from University of Oregon to University of Virginia in early 2013. As required by the terms and conditions of the funding, we revised the Statement of Work to adjust the timeline of some tasks to compensate for the loss of time during the move.

For **revised task 0**, we successfully moved relevant lab personnel, equipment, and reagents to University of Virginia (UVa).

For **revised task 1**, we submitted our animal protocol to UVa Animal Care and Use Committee, and got the approval. We then submitted ACURO documents and IACUC approval by UVa to USAMRMC Office of Research Protections (ORP), and got the approval.

For **revised task 2**, upon the approval by IACUC and ACURO, we set up a well-organized mouse colony to generate a steady supply of medulloblastoma-bearing mice for experiments proposed in this grant.

For **revised task 7**, we successfully purified tumor GNPs from the tumor mass with a Purcoll-gradient based centrifugation method. Isolated tumor-GNPs have high purity, free of glial cell contamination (Figure 6A,B). However, purification of adequate amount of tumor-derived astrocytes has been extremely difficult due to the destruction of this rare cell population during the tumor dissociation procedure. As an alternative, we successfully purified and cultured normal astrocytes (Figure 6C), and optimized the culture conditions that can accommodate both GNPs and astroctyes, a prerequisite for co-culture experiment. When we cultured tumor GNPs either alone or with normal astrocytes, we found that tumor GNPs co-cultured with normal astrocytes had a 2-fold increase in their proliferative rate (attached manuscript, Supplemental Figure 7A, B). We also observed that tumor GNPs spread out and intimately associated with astrocytes in the co-culture, in stark contrast to self-aggregation when they are

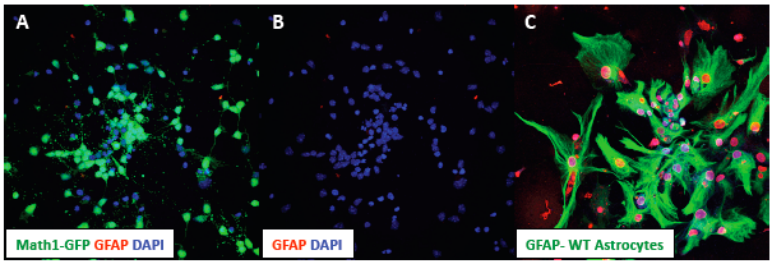

Figure 6. Sub-fractionate glial cells and GNPs from mixed tumor mass. (A-B) Tumor GNPs can be sub-fractionated to high purity, free to GFAP+ astrocyte contamination. (C) Successful culturing of WT astrocytes.

cultured alone (attached manuscript, Supplemental Figure 7C). To investigate the long-term effect of astrocytes on tumor GNPs, we performed a time course experiment, and found that proliferation of tumor GNPs is enhanced while cell death and differentiation are suppressed in comparison to those cultured alone (attached manuscript, Supplemental Figure 7D-F). It should be noted that astrocytic support is specific, since NIH3T3 cells showed no sign of support to tumor cells in a co-cultured assay although tumor cells form close contact with them (data not shown). Overall, these data indicate that normal astrocytes can support tumor GNPs.

To investigate the tumor-supporting roles of tumor-derived astrocytes, we made additional attempts, including immuno-affinity purification and FACS, but were not successful due to cell death caused by procedure. As the next best option, we dissociated medulloblastoma and cultured all cells in a medium containing heparin binding epidermal growth factor (HB-EGF) that is critical for astrocyte survival (Foo et al., 2011), in hope that some tumor GNPs will reprogram into astrocytes in this condition. After 3 days *in vitro* (DIV), only a small percentage of cells survived (0.8-1.4% of initial seeded cells) since this medium is not tailored for tumor GNP growth (attached manuscript, Figure 7A top). We were excited to find that most of cells display the characteristic astrocytic morphology and are GFAP-positive (attached manuscript, Figure 7B). Therefore, we used these cells as tumor-derived astrocytes in subsequent co-culture assays. For visual clarity, we seeded *Math1-GFP*-positive tumor GNPs onto red tumor-derived astrocytes (attached manuscript, Figure 7A, middle). Initially green tumor GNPs were evenly distributed (attached manuscript, Figure 7C). After a longer incubation period (3 DIV), we expect two possible outcomes. If tumor-derived astrocytes do not provide support for tumor GNPs, then tumor GNPs would proliferate irrespective of their distance from tumor-derived astrocytes. On the other hand, if tumor-derived astrocytes provide support to tumor GNPs, then tumor GNPs in proximity to tumor-derived astrocytes would proliferate at a much higher rate than those far from tumor-derived astrocytes (attached manuscript, Figure 7A, bottom). When we quantified the total number of surviving tumor GNPs in relation to their distance to tumor-derived astrocytes (within or beyond 30mm, which is the approximate radial length of tumor-derived astrocytes processes), we found that ~80% of surviving tumor GNPs resides within 30mm of tumor-derived astrocytes (attached manuscript, Figure 7E, left graph). Next we quantified the proliferative rate of all surviving tumor GNPs, and found that more than half of tumor GNPs within 30mm of tumor-derived astrocytes were proliferating, while those beyond 30mm from tumor-derived astrocytes had a significantly reduced proliferative rate (~25% EdU-positive) (attached manuscript, Figure 7D, and E right graph). In conclusion, these data suggest that tumor-derived astrocytes support tumor GNP survival and proliferation.

In **revised task 8** we proposed to use *in situ* analysis of candidate trophic factors in tumor glial cells. Using Angiopoietin 1 (Ang-1) as a candidate probe, we found that, in normal cerebellum, Ang-1 is highly expressed in Purkinje neurons and Bergmann glial cells based on their cell body location and possibly protoplasmic astrocytes in the inner granule layer (Figure 7, top panels). We also found high-level of Ang-1 expression in tumors (Figure 7, bottom panels).

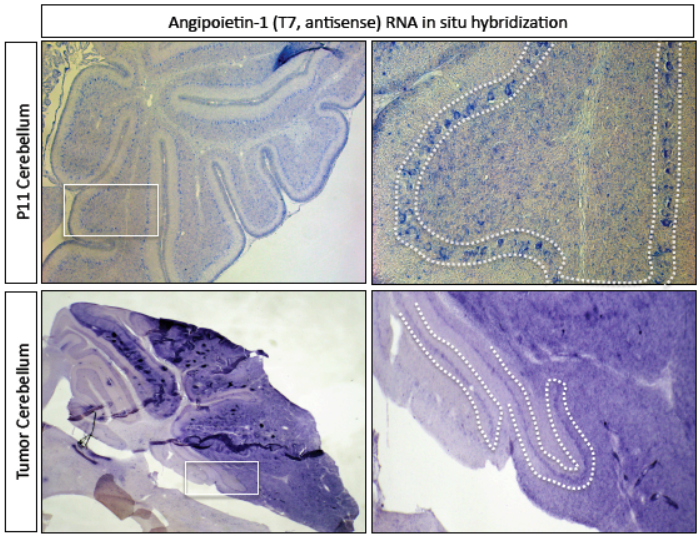

Figure 7. In situ hybridization of Ang-1 in normal developing cerebellum (top panels) and medulloblastoma (bottom panels).

The understanding of molecular mechanisms also requires us to identify candidate genes. For **revised task 9**, our original plan was to purify both tumor-derived astrocytes and tumor GNPs for RNAseq analysis, then look for candidate ligand-receptor pairs in each of the cell type. While we performed RNAseq analysis of tumor GNPs, we were not able to obtain sufficient number of tumor-derived astrocytes due to reasons mentioned above. To get around this problem, we examined the level of a panel of candidate growth factors with realtime PCR in tumor mass vs. purified tumor GNPs vs. normal cerebellum, following the notion that microenvironmental factors would express at a high level in the tumor mass but be absent from tumor GNPs. For each tumor that we analyzed, we first took a piece of tumor mass then used percoll gradient centrifugation to purify tumor GNPs from the remaining tumor tissue. When we compared the expression level of candidate growth factors in paired tumor mass-tumor GNP samples in comparison to the normal brain, we found that, while only IGF1, HGF, and PDGF-AA are consistently up-regulated in multiple tumor samples [Figure 8A], only IGF1 and HGF are made by microenvironmental cells whereas PDGF-AA is produced by tumor GNPs [Figure 8B]. In culture, IGF1 promoted the proliferation of tumor GNPs to a much higher level than HGF did [Figure 8C]. Finally, we found that IGF1 mRNA levels in a set of human medulloblastoma samples are significantly higher than that in normal cerebellum [Figure 8D].

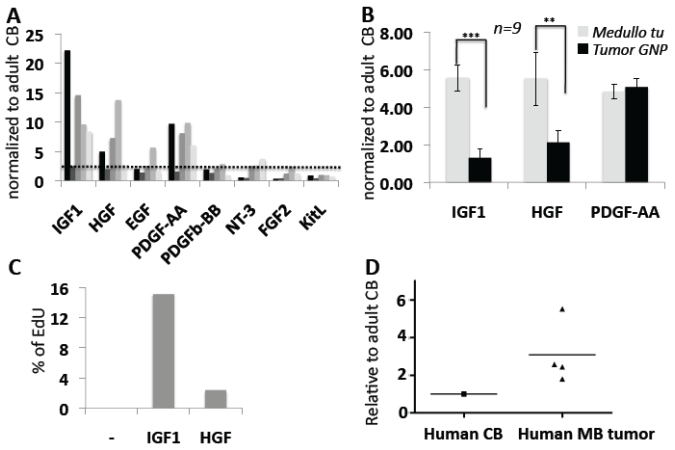

Figure 8. IGF1 is identified as a TME factor from the screening of a panel of growth factors. **A**. IGF1, HGF, PDGF-AA are consistently up-regulated in medulloblastoma. **B**. IGF1 and HGF are TME factors; while PDGF-AA is made by tumor GNPs. **C**. IGF1 greatly promote tumor cell proliferation in vitro. **D**. IGF1 level is elevated in human medulloblastoma in comparison to normal cerebellum.

While identifying gene expression changes is an important first step to understand molecular events in the tumor development, it is as important to master techniques for molecular perturbation so we could investigate cause-and-consequence problems. With that in mind, we advanced our work along the line of **revised task 10**. We have successfully constructed lentiviral vectors and optimized viral production and infection procedures. After the successful purification of tumor GNPs, we tested the infection on them and got a ~40% of efficiency (Figure 9). To investigate the role of IGF1 signaling in medulloblastoma, we have constructed a few lentiviral vectors that contain shRNA against different regions of IGF1R (Figure 10). To avoid the off-target effect, we designed multiple shRNA probes targeting different regions spanning the coding sequence (Figure 10A). We designed an RNAi reporter system similar to that described by Fellmann et al. (2) to quickly evaluate the efficacy of shRNAs to any target of interest. In this reporter system a 50bp-DNA fragment from the target gene (shRNA recognition site) was fused at the 3' end of a cDNA encoding the red fluorescent protein mCherry (Figure

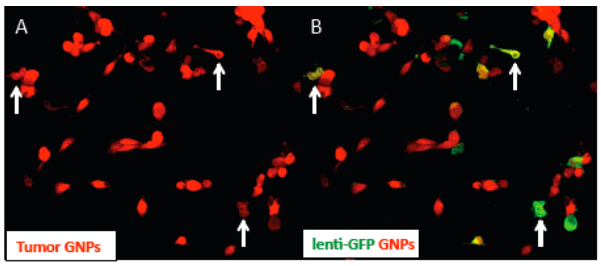

Figure 9. Infection of tumor cells with GFP-expressing lentiviral vector. A) Purified tumor GNPs from red MADM tumor. B) Expression of GFP in infected tumor GNPs.

10B). A shRNA that effectively target that fragment will suppress the expression of mCherry, which serves as a surrogate marker to indicate the potency of the shRNA. Using this system, we found that shRNA-3329 is moderately effective while shRNA-3437 is fully effective in suppressing their targets based on the reduction of mCherry expression (Figure 10C, top and middle panels, respectively). To further validate the potency of these shRNA in knocking down the endogenous IGF1R, we transiently transfected these shRNA-encoding vectors into tumor cells and performed the Western blot experiments. Concordant with the results by using the surrogate reporter system, data in Figure 10D clearly demonstrate the endogenous IGF1R were significantly knocked down by both shRNAs.

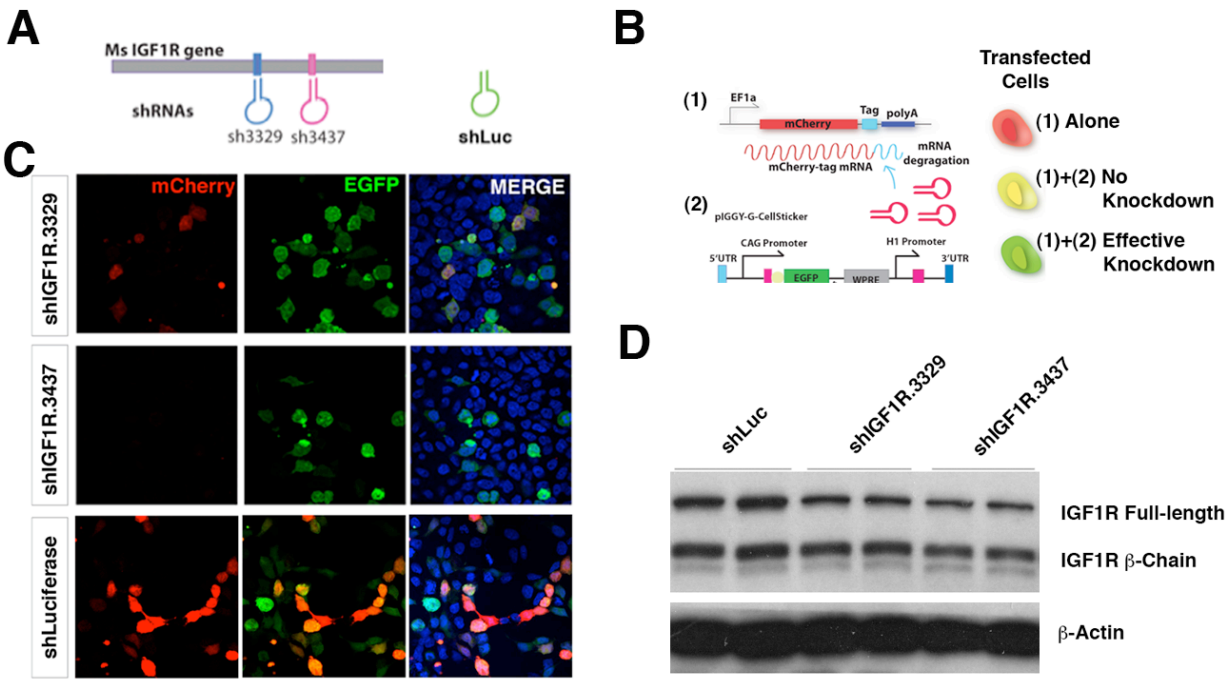

Figure 6. Construction of lentiviral vectors to knockdown IGF1R. **A.** Diagram to show the two shRNAs against different regions in the mouse IGF1R coding sequence. An shRNA against luciferase was used as a non-specific control. **B.** Diagram to show the working mechanism of the surrogate reporter system to evaluate the potency of the shRNAs. **C.** Efficacy of the two shRNAs specific to mouse IGF1R gene to knockdown the cognate targets in HEK293T cells by using the reporter system. **D.** Same set of shRNA effectively knockdown the endogenous IGF1R protein in tumor cells, shown in western blots.

For **revised task 11 and 12**, we followed up the IGF1 finding, and showed that the addition of IGF1 promoted tumor cell proliferation while the inhibition of IGF1R did the opposite. However, while we are confident that IGF1 is an important microenvironmental factor for medulloblastoma, our in situ analysis later showed that it is secreted by tumor-associated microglia rather than tumor-derived astrocytes (data not shown). Therefore, this project has reached a new beginning since the relationships among tumor and microenvironmental cells turned out to be more complex than our original hypothesis: there are at least two type of microenvironmental cells (tumor-derived astrocytes and tumor-associated microglia), which likely work in concert to support tumor progression. To identify factors from tumor-derived astrocytes, we will use laser-guided microdissection method to isolate these cells and perform RNAseq analysis after the funding period of this grant, with lab's startup funding from UVa.

For **revised task 13**, we have completed all data analysis and written the report to CDMRP. We have also submitted the manuscript describing our findings about tumor-derived astrocytes to Cancer Cell, which is currently under "pending revision" (see the manuscript in Appendices). We also submitted a NIH R01 on the role of IGF1 and tumor-associated microglia in medulloblastoma, which will be reviewed in February 2016.

Key Research Accomplishments

- We demonstrated the critical role of tumor-derived astrocytes for medulloblastoma progression, making them a novel target for this type of cancer.
- We established a lentiviral system that can be used for investigating molecular mechanisms of the support from tumor-derived astrocytes toward tumor GNPs.
- We established a co-culture system and a mouse model for medulloblastoma that is amenable for drug testing to disrupt the support from tumor-derived astrocytes and to halt tumor progression.
- Serendipitously, we identified IGF1 as a microenvironmental factor from tumor-associated microglia (TAM), and are in a good position to further investigate molecular mechanisms and therapeutic potentials based on this finding.

Conclusion

Understanding the interaction between tumor and microenvironmental cells not only is of great interest for basic biology, but also carries great potential in developing novel and effective therapeutic strategies. Upon the completion of proposed studies in this grant, we have now firmly established the critical role of tumor-derived astrocytes in the progression of medulloblastoma. This finding opens up an entirely novel area of research, which could lead to paradigm-shift treatment strategies against medulloblastoma. Rather than using drugs or radiation that kill brain cells indiscriminately, interventions that specifically disrupt the crosstalk between tumor-derived astrocytes and tumor GNPs should be not only highly effective but also minimally toxic to other cells in the developing brain of young patients. Our serendipitous finding of IGF1 from tumor-associated microglia as a critical tumor-supporting factor opens up a new direction for further investigation. It is highly promising since IGF1R inhibitor has been used in clinical trials for other cancer types. Follow-up studies along this direction could provide rationales for drug repurposing, which could push this finding to the bedside at a rather fast pace. Curing brain tumors without causing life-long devastating disabilities in children should have a great impact for patients and their families. We are grateful for the financial support by the DoD grant that made our studies possible.

Publications, Abstracts, and Presentations

- **Selected Speaker** at Models and Mechanisms of Cancer, Salk Institute – August 2011. Title: "Mosaic Analysis with Double Markers (MADM) in Mice Reveals Community Building Behaviors in Medulloblastoma."
- **Selected Speaker** at Glia in Health and Disease, Cold Spring Harbor Laboratories – July 2012. Title: "Medulloblastoma Builds Its Own Glial Niche."
- **Selected Speaker** for *Neuro tumor club dinner meeting, Society of Neuro-oncology,* Washington DC, April 8, 2013
- **Invited Speaker** for *AACR Annual Meeting*, Washington DC, April 6-10, 2013
- **Invited Speaker** for Brain Tumor Meeting in Berlin, Germany

- **Invited speaker**. In vivo analysis of genetic contribution to glial development and functions at cellular resolution using MADM mouse model. XI European Meeting on Glial Cells in Health and Disease, Berlin, Germany, July 3-6, 2013
- **Invited speaker.** Use MADM, a mouse genetic mosaic model, to study how tumor cells attack. Mini-symposium on Cancer Biology, University of Chile, Santiago, Chile, January 10, 2014
- **Invited speaker.** UC Santa Cruz, Department of Molecular, Cell, and Developmental Biology, Santa Cruz, CA, April 14, 2014
- **Manuscript** under revision in Cancer Cell (attached as appendices).

Other Achievements

The following researchers were involved in studies proposed in this grant, and got valuable training along the process.

Name	P. Brit Ventura
Project role	Graduate Student
Contribution to project	Performed glia ablation experiments and co-culture experiments.

Name	Kate Karfilis
Project role	Graduate Student
Contribution to project	Performed in situ analysis of potential factors in the tumor mass.

Name	Maojin Yao
Project role	Postdoc
Contribution to project	Characterization of the tumor-derived astrocytes in the genetic model. In situ analysis of candidate factors in the tumor mass.

Name	Ying Jiang
Project role	Research Scientist
Contribution to project	Identification of IGF1 as a microenvironmental factor, and functional validation.

References:

1. Foo LC*, et al.* (2011) Development of a method for the purification and culture of rodent astrocytes. *Neuron* 71(5):799-811.
2. Fellmann C*, et al.* (2011) Functional identification of optimized RNAi triggers using a massively parallel sensor assay. *Molecular cell* 41(6):733-746.

Appendices

1. Meeting abstracts
2. Manuscript under revision in Cancer Cell

Microglial voltage-gated proton channel, Hv1, contributes to brain damage in ischemic stroke
Long-Jun Wu, Gongxiong Wu, Edward P. Feener, David E. Clapham.
Presenter affiliation: Harvard Medical School, Boston, Massachusetts. 131

TGF-β signaling regulates complement C1q expression and developmental synaptic refinement
Allison M. Rosen, Arnaud Frouin, Alexander Stephan, Ben A. Barres, Beth Stevens.
Presenter affiliation: Children's Hospital Boston, Boston, Massachusetts; Harvard Medical School, Boston, Massachusetts. 132

Bone marrow transplant arrests disease in an Mecp2-null mouse model of Rett syndrome—Microglia as potential key players in Rett
NC Derecki, JC Cronk, J Kipnis.
Presenter affiliation: University of Virginia, Charlottesville, Virginia. 133

SUNDAY, July 22

BANQUET

Cocktails 6:00 PM Dinner 6:45 PM

MONDAY, July 23—9:00 AM

SESSION 10 ROLE OF GLIA IN CNS INJURY AND DISEASE

Chairperson: **R. Armstrong,** Uniformed Services University of the Health Sciences, Bethesda, Maryland

Phenotypic conversions of "protoplasmic" to "reactive" astrocytes in Alexander disease
Alexander Sosunov, Eileen Guilfoyle, Xiaoping Wu, Guy McKhann, James E. Goldman.
Presenter affiliation: Columbia University, New York, New York. 134

MEDULLOBLASTOMA BUILDS ITS OWN GLIAL NICHE

Brit Ventura, Kate Karfilis, Kelsey Wahl, Hui Zong

University of Oregon, Institute of Molecular Biology, Eugene, OR, 97403

Understanding the interactions between tumor cells and their microenvironment are paramount for the design of novel treatments. However, conventional research methods, including mouse cancer models, lack the in vivo single-cell resolution to tease apart tumor versus niche cell types for mechanistic insights. To circumvent this problem, our lab makes use of a novel mouse genetic system termed MADM (Mosaic Analysis with Double Markers) to model cancers. Starting with a mouse heterozygous for a tumor suppressor gene (TSG), MADM can generate sporadic mutant cells that are null for candidate TSG(s) with unequivocal GFP labeling, enabling us to trace the lineage of mutant cells and distinguish them from other niche cells.

In this study, we used MADM to model medulloblastoma, the most prevalent type of pediatric brain tumors. It is known that such tumors, especially the desmoplastic subtype relying on Shh pathway hyperactivation, originate from granule neuron precursors (GNPs). It is puzzling that although GNPs are unipotent toward the granule neuron lineage, the tumor mass contains many glia. Moreover, medulloblastomas are often highly vascularized even though GNPs are known not to produce angiogenic factors. Using GNP-specific Math1-Cre, the MADM model generated GFP+ p53-null GNPs in a heterozygous patched mutation background, resulting in fully penetrant cerebellar tumors. Although the majority of GFP+ cells in the tumor mass resemble GNPs, a closer look revealed green cells with large cell bodies, reminiscent of astroglial morphologies. We further confirmed their glial identity by staining with multiple astrocyte markers. Importantly, these cells are GFP+ suggesting that they are derived from mutant GNPs. It's surprising since normal GNPs are known not to give rise to any glial cells. To investigate the molecular mechanisms that enable mutant GNPs to generate glia within the tumor, we performed transcriptome analysis of tumor GNPs in comparison to wildtype GNPs. This revealed increased expression of transcription factors that are normally restricted to a small time window during embryonic GNP lineage development. It suggests that tumorigenic transformation may lead to a reversion of the fate of some tumor GNPs to an earlier developmental stage with broader potentials. In addition to investigating the mechanisms of trans-differentiation, we are also analyzing the functional roles of tumor glia, in particular their roles in inducing angiogenesis to support tumor GNPs.

In summary, our MADM-based medulloblastoma model seems to have revealed a community building behavior of tumor cells, through which some of them convert their fate to non-proliferative glial cells, which in turn provide cues for the establishment and maintenance of the tumor microenvironment.

Saturday, August 13 - 9:00 am

SESSION VI: TUMOR MICROENVIRONMENT
Chair: MARTINE ROUSSEL

46 Martine Roussel
St. Jude Children's Research Hospital
Role of Myc Genes in Pediatric Medulloblastoma

47 P. Britten Ventura, Kate Karfilis, Peter Kim, Kelsey Wahl, and Hui Zong
University of Oregon
Mosaic Analysis with Double Markers (MADM) in Mice Reveals Community Building Behaviors in Medulloblastoma

48 Sourav Ghosh, Yael Kusne, Anthony S. Perry, Maurice Jabbour, Edward Mandell, Michael E. Berens, Joseph C. Loftus, and Elisabeth J. Rushing
The University of Arizona, Tucson
aPKC-dependent EGFR and NF-kappaB Signaling Cooperate to Promote Glioblastoma Invasion

49 Vicki A. Sciorra, Michael A. Sanchez, Emily Ho, and Andrew E. Wurmser
University of California, Berkeley
Glioma Cells Participate in the Formation Tumor Capillaries by Competitively Inducing Endothelial Cell Death

Mosaic Analysis with Double Markers (MADM) in Mice Reveals Community Building Behaviors in Medulloblastoma

P. Britten Ventura, Kate Karfilis, Peter Kim, Kelsey Wahl, and Hui Zong
Institute of Molecular Biology, University of Oregon, Eugene, OR 97403

Medulloblastoma is the most common pediatric brain cancer manifesting in the developing cerebellum. The etiology of desmoplastic medulloblastoma implicates that perturbation in the Sonic Hedgehog signaling pathway can lead unipotent granule neuron precursors (GNPs) to overproliferate and tumor formation. To investigate the course of tumorigenesis originating in GNPs, we have employed a mouse genetic mosaic model termed Mosaic Analysis using Double Markers (MADM). MADM-induced loss of heterozygosity of the tumor suppressor, *p53*, mediated by the GNP-specific *Math1*-Cre, in a *Ptc+/-* background leads to consistent and fully penetrant medulloblastoma formation. The permanent labeling of both mutant (GFP+) and wildtype (RFP+) GNPs allows us to visualize the behaviors of mutant GNPs compared to wildtype GNPs originating from the same cell. To our surprise, when we looked at the cellular level in GFP+ tumors, we noticed that although the majority of the tumor mass is made up of dividing mutant GNPs, there was also a significant population of larger GFP+ cells with glial morphology. Marker staining for glial antigens confirmed that these large cells are indeed glial cells. This observation suggests that transformed unipotent GNPs can switch fates in the tumor to produce glia in addition to GNPs. Given this interesting fate switching phenomenon we sought to determine if these glia were important for tumor progression with a genetic ablation experiment to selectively kill the tumor glia using a *Gfap* promoter driven thymidine kinase (TK) transgene. Conversion of the substrate ganciclovir (GCV) into cytotoxic agents by TK in both early and late stage tumors resulted in complete tumor remission, demonstrating the essential role of these glial cells for tumor maintenance. Preliminary results indicate that using this method of ablation, we can cause not only tumor regression but complete tumor remission. This evidence suggests that these fate-switched glia play an important role in the tumor community and its successful growth and maintenance. Currently we are focusing on determining the molecular mechanisms by which tumor glia are generated via a fate-switch process, and by which they facilitate and sustain tumor growth. Dissecting the mode of support and tumor regression afforded by tumor-generated glia should provide targets for more specific therapeutic strategies, circumventing the devastating side effects of current surgical, radio- and chemotherapies.

18th Annual Neuro-Tumor Club Dinner Meeting at AACR

Time: Monday April 8, 2013; 6:30–10:00pm

Location: Washington Plaza Hotel, 10 Thomas Circle, NW, Washington, DC 20005

✷ ***Yes, I would like to present at the Neuro-Tumor Club Dinner Meeting!***
(Abstract deadline Friday, March 8, 2013)

☐ ***Yes, I plan to attend the Neuro-Tumor Club Dinner Meeting!***
(RSVP required even if you are not presenting)

Name: _____Hui Zong_____

Institution: ___University of Virginia, Dept of Microbiology, Immunology, and Cancer Biology_____

Title (student / postdoc / professor, etc): _____Associate Professor_____

Phone: __434-982-1956_____Email: _____hz9s@virginia.edu_____

Presentation Title: ___Genetic mosaic mouse models for brain tumors: basic research and pre-clinical applications__

I would like to present* in one the following areas:

☐ Geno/Phenotyping and Personalized/Combinatorial Therapy
☐ Angiogenesis and Tumor Microenvironment
☐ New Gene and Immunotherapy
☐ New Tools and Translational Approaches
☐ CNS Metastases
☐ Biomarkers in Gliomas?
☐ Stem Cells
✷ Animal Models
☐ Other category? _____

* Presentation is **5-minutes**, no more than 5 slides (without animation), PowerPoint file to be e-mailed to SNO by Monday, April 1.

Key Message of Presentation (< or = 3 sentences): (instead of formal abstract)

We developed a genetic mosaic model called MADM that can generate sparse, GFP-labeled mutant cells in the mouse brain, mimicking the clonal origin of human tumor physiology [Zong 2005 Cell, Muzumdar 2007 PNAS].

Single-cell resolution provided by the model allows one to study brain tumor at pre-transforming stages for cell of origin issues [Liu et al 2011 Cell], and to study tumor-niche interactions without ambiguity.

As a pre-clinical model, MADM allows one to 1) quantify drug efficacy by cell number rather than tumor size; 2) analyze drug effects on mutant/tumor cells outside of tumor mass; 3) monitor tumor cell migration; 4) assess tumor-prevention effects of a given drug on pre-transforming cells.

I would be interested to deliver a 3-minute INTRODUCTION on the following theme:

☐ Geno/Phenotyping and Personalized/Combinatorial Therapy
☐ Angiogenesis and Tumor Microenvironment
☐ New Gene and Immunotherapy
☐ New Tools and Translational Approaches
☐ CNS Metastases
☐ Biomarkers in Gliomas?
☐ Stem Cells
☐ Animal Models
☐ Other category? _____

Presenter Application Form Due: Friday, March 8, 2013

*Please **email** this form to Linda Greer: linda@soc-neuro-onc.org or **FAX** to: **713-583-1345***

Human cancers frequently arise from the loss of both copies of a tumor suppressor gene (TSG) in sporadic cells. We have established a mouse genetic system termed MADM (Mosaic Analysis with Double Markers) that limits TSG inactivation in very few cells for physiologically relevant cancer modeling. MADM unequivocally labels sporadic mutant and wildtype sibling cells with GFP and RFP respectively, to confer the *in vivo* single cell resolution and lineage tracing capability. The research theme of our lab is focused on brain tumor modeling with two questions that are particularly interesting to us: 1) What is the developmental origin of brain tumors? 2) How do tumor cells evolve along their lineage potentials during malignant transformation?

The cell-of-origin for glioma has long been thought to be neural stem cells (NSCs) based on two observations. First, purified tumor cells manifest stem cell features. Second, the introduction of p53 and NF1 mutations into NSCs in mouse models led to glioma formation. However, endpoint features may not reliably reflect the nature of tumor initiating cells, thus the analysis should focus on early, pre-transforming stages. Furthermore, conceptually there is a critical difference between cell-of-origin and cell-of-mutation. The former is the cell type that transforms into malignancy, while the latter is the one in which initial mutations occur but may not directly transform. We used MADM to probe into early phases of gliomagenesis, and surprisingly found the lack of overpopulation of mutant NSCs. Among NSC-derived cell types, we only detected dramatic over-expansion of mutant oligodendrocyte precursor cells (OPCs) at pre-transforming stages. Consistently, terminal-stage tumor cells displayed salient OPC features by both histological criteria and transcriptome profiling. Most importantly, introducing the same mutations directly into OPCs was sufficient for malignant transformation. Our findings strongly implicate OPC as a cell-of-origin for glioma, and highlight the importance of analyzing early phases of tumorigenesis to pinpoint its origin.

Our lab also generated a medulloblastoma model by introducing TSG mutations into uni-potent granule neuron precursors (GNPs). Preliminary findings indicated that tumor GNPs divert from their uni-potency to give rise to glial cells. We are currently investigating two critical questions on these tumor-derived glial cells: 1) how do uni-potent GNPs reprogram themselves during malignant transformation to generate cell types beyond the original lineage potential? 2) how do glial cells contribute to the progression of medulloblastoma?

In summary, our work has started unraveling the importance of lineage potentials during the tumorigenic process. While the same mutations could occur in many cell types, often times only one cell lineage would be able to transform into malignancy. Teasing apart the differences in signaling context between transforming and non-responsive cell types could provide critical insights for devising highly effective treatment strategies. It's also important to note that tumor cells have the capacity to deviate from normal developmental program and alter their original lineage potentials. The mechanisms and significance of "tumor-reprogramming" still await further investigations.

ZELLULÄRE NEURO-
WISSENSCHAFTEN
FG Prof. Dr. Helmut Kettenmann

MDC
MAX-DELBRÜCK-CENTRUM
FÜR MOLEKULARE MEDIZIN
BERLIN-BUCH

MDC ♆ Zelluläre Neurowissenschaften ♆ Robert-Rössle-Str. 10 ♆ 13092 Berlin-Buch

Robert-Rössle-Str. 10
13092 Berlin

Tel. (030) 9406 3133
Fax: (030) 9406 3819
E-Mail: gibson@mdc-berlin.de

Hui Zong
Assistant Professor of Biology
Institute of Molecular Biology
University of Oregon
215 Streisinger Hall
Eugene, OR 97403-1229
USA

Berlin, 21.08.12

Brain Tumor Meeting 2013, Berlin

Dear Dr. Zong:

Berlin has a very large neuroscience community, and one major focus is on brain tumors. Several Berlin-based research groups have specialized on investigating the impact of parenchymal interactions of brain tumor cells. A focus is given on the interaction of brain tumor cells with immune cells (microglia) and neural stem- and precursor-cells.

For the Departments of Neurosurgery at the Charité and the Clinics in Berlin-Buch the properties and the treatment of brain tumors are a major topic. There are close and stimulating collaborations between several groups doing basic research and the clinics. This led to the idea to organize a small conference on brain tumors and to complement the local expertise with external experts. We started the first meeting in 2000 and will have the sixth meeting of this series in 2013. Last time over 170 participants attended the meeting. The meeting will take place at the Max Delbrück Center for Molecular Medicine (MDC) in Berlin-Buch. It will start on Thursday, May 23, 2013, after lunch and will end in the afternoon of the next day on Friday, May 24, 2013.

We would like to invite you to join this meeting and to give a lecture on the role of tumor stroma interactions in cancer. We feel that it would be very stimulating for brain tumor-researchers to get an overview on the many important pathological roles that have been uncovered for tumor-parenchyma interactions in peripheral tumors.

We can cover your travel costs (economy flight) and accommodation. We are convinced that this will be an exciting meeting and we would be very happy if you could accept our invitation.

Looking forward to hearing from you,

Sincerely,

Helmut Kettenmann

Contact

Meino Alexandra Gibson
Max Delbrück Center for Molecular Medicine
Robert-Rössle-Straße 10, D-13125 Berlin
gibson@mdc-berlin.de
Telefon: +49 30 94 06-33 36
Telefax: +49 30 94 06-28 13

Registration fee

Participants (early)	Euro 30,--
Students (early)	Euro 10,--
Participants (late)	Euro 50,--
Students (late)	Euro 30,--

Registration

Important Deadlines

March 1, 2013:	Abstract submission
March 1, 2013:	Early registration
Until April 15, 2013:	Late registration

For registratiaon and abstract submission please visit:
http://www.braintumor-berlin.de
Onsite registration will be available.

Public transportation

S-Bahnhof Berlin-Buch (S2)
Bus 158

Final program available April 2013.

Anfahrt

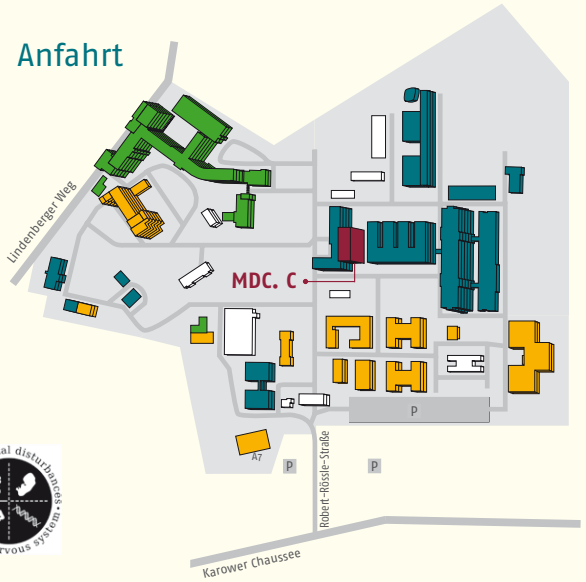

SFB 665 developmental disturbances in the nervous system

NeuroCure Cluster of Excellence

SFB TRR 43 The Brain as a Target of Inflammatory Processes

Organized by

Max Delbrück Center for Molecular Medicine (MDC)
Cellular Neuroscience
Robert-Rössle-Str. 10 • D-13125 Berlin
http://www.mdc-berlin.de

Department of Neurosurgery
Charité-Universitätsmedizin Berlin
Augustenburger Platz 1 • D-13353 Berlin
http://neurochirurgie.charite.de

Department of Neurosurgery
HELIOS Klinikum Berlin-Buch
Schwanebecker Chaussee 50 • D-13125 Berlin
http://www.helios-kliniken.de/berlin

Impressum:
Verleger: HELIOS Klinikum Berlin-Buch · Schwanebecker Chaussee 50 · 13125 Berlin
Druckerei: Schmohl & Partner · Gustav-Adolf-Straße 150 · 13086 Berlin

Bln. / 11.2012

HELIOS Kliniken
Jeder Moment ist Medizin

CHARITÉ

MDC MAX-DELBRÜCK-CENTRUM FÜR MOLEKULARE MEDIZIN BERLIN-BUCH IN DER HELMHOLTZ-GEMEINSCHAFT e.V.

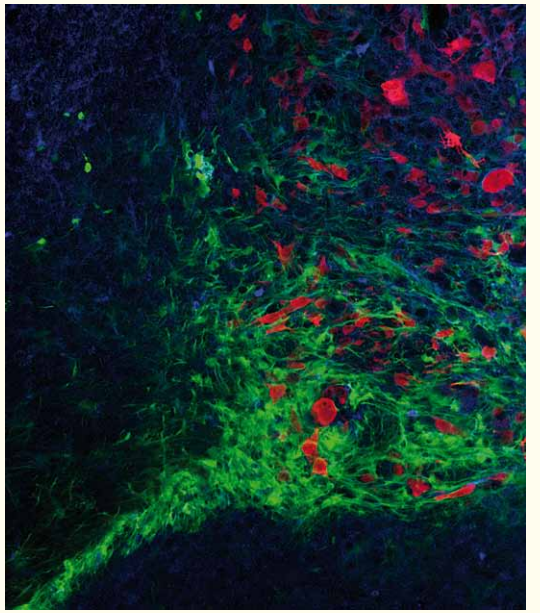

Max Delbrück Center for Molecular Medicine (MDC)
Charité-Universitätsmedizin Berlin
HELIOS Klinikum Berlin-Buch

Brain Tumor 2013

Announcement

May 23-24, 2013
Campus Berlin-Buch
Max Delbrück Communications Center (MDC.C)
Robert-Rössle-Str. 10 • D-13125 Berlin

Dear Colleagues,

We are pleased to announce that the Brain Tumor Meeting 2013 will take place at the Max Delbrück Center für Molecular Medicine (MDC) in Berlin (Germany) on May 23-24, 2013.

In summer 2000, Berlin neuroscientists, neuro-surgeons and neurologists focusing on brain tumors initiated this scientific conference. It was repeated in 2001, 2004, 2006, 2008 and 2011 - throughout this time the Brain Tumor Meeting gained national and international attention and attracted many leading scientist working on gliomas and other brain tumors.

The main focus of the meeting is to provide a platform for an interdisciplinary scientific exchange especially between scientists and clinicians. Recent discoveries on the role of glioma stem cells, on the interaction of gliomas with their microenvironment and on glioma cell death pathways have altered our understanding of glioma biology.

Internationally and nationally renowned speakers were invited to present their newest data on these topics. Furthermore, abstracts for oral- and poster-presentations are invited and the best resentations will be awarded prizes.

We expect exciting scientific exchange and invite you to join this meeting.

Scientific Program Committee

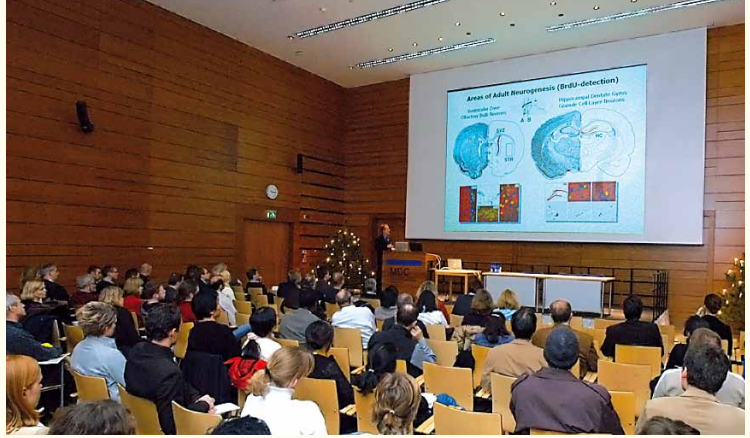

Invited Speaker

Gabriele Bergers (San Francisco, USA)

Ruggero De Maria (Rome, Italy)

Bozena Kaminska (Warsaw, Poland)

Michael Platten (Heidelberg, Germany)

Jeremy N. Rich (Cleveland, USA)

Peter Vajkoczy (Berlin, Germany)

Michael Weller (Zurich, Switzerland)

Hui Zong (Oregon, USA)

Scientific Program Committee

Rainer Glass, Frank Heppner, Helmut Kettenmann, Jürgen Kiwit, Michael Synowitz

Abstracts

Abstract submissions for oral or poster presentation are welcome.

Deadline for abstract submission is March 1, 2013.

Duration of oral presentation:

talk:	15 min
discussion:	5 min

The official meeting language is English.

Best Abstract Prize Competition

Prizes are awarded for the best five abstracts presented at the Brain Tumor 2013 meeting.

1. prize	IPad
2. prize	IPad mini
3. prize	Ipod touch 64G
4. prize	Ipod touch 32G
5. prize	Ipod nano

A two-tier assessment will be used to determine Best Abstracts Prize: First by the members of the program committee and second by a voting system of the meeting participants.

Tumor-derived glial cells comprise a niche for medulloblastoma progression

P Britten Ventura[1], Maojin Yao[1], Fausto J Rodriguez[4], Kelsey Wahl[3], Ying Jiang[1], Lin Qi[5], Jennifer M Munson[2], Charles G Eberhart[4], Xiao-Nan Li[5], Hui Zong[1*]

[1]Department of Microbiology, Immunology, and Cancer Biology

[2]Department of Biomedical Engineering, University of Virginia; Charlottesville, VA, 22908; USA.

[3]Department of Biology, University of Oregon; Eugene, OR, 97403; USA

[4]Department of Pathology, Division of Neuropathology, Johns Hopkins University School of Medicine; Baltimore, MD, 21231; USA

[5]Brain Tumor Program, Texas Children's Cancer Center, Department of Pediatrics, Baylor College of Medicine; Houston, TX, 77030; USA

* Correspondence author: Hui Zong, hz9s@virginia.edu

Running title: tumor cells build their own niche

Summary

Niche cells play critical roles in tumor initiation, progression, and metastasis. However, our understanding of niche function has been hampered by the complex cell composition in the tumor mass. Although the cerebellar tumor, desmoplastic medulloblastoma, comprises glial elements, their origins and functions are unclear. Here we used a mouse genetic system called Mosaic Analysis with Double Markers (MADM) to analyze the tumor niche in medulloblastoma, taking advantage of the unambiguous GFP-labeling of tumor cells by the system. While tumor-infiltrating blood vessels and immune cells are GFP-negative, surprisingly, all astrocytes within tumors are GFP-positive, suggesting that they are derived from tumor cells. Karyotype comparisons in human medulloblastoma confirmed the lineage relationship between tumor cells and niche astrocytes. Finally, tumor-derived astrocytes enable tumor cell survival and proliferation *in vitro* and strictly correlate with tumor progression *in vivo*. In summary, our findings revealed a tumor-derived glial niche in medulloblastoma that support tumor progression.

Highlights

- MADM allows analyses of tumor-niche interactions at single cell resolution
- Niche astrocytes in medulloblastoma are transdifferentiated from tumor cells
- The presence of niche astrocytes strongly correlate with tumor progression
- Tumor-derived astrocytes provide support to tumor cells

eTOC

Tumor cells rely on niche support to survive and thrive. Taking advantage of the unequivocal GFP-labeling of mutant cells in a mouse model, we investigated tumor-niche interactions in medulloblastoma, a type of malignant pediatric brain tumor. Surprisingly, we found that one type of niche cell is derived from tumor cells rather than being recruited from normal tissue, and provides critical support for tumor progression. Strategies to block the transdifferentiation process or the tumor-supporting niche signals could provide highly effective treatment for medulloblastoma.

Introduction

Interactions between distinct cell types ensure normal embryonic development and adult tissue homeostasis. Such interactions are also important in human diseases, particularly tumor-niche interactions in cancer. Rather than simply over-proliferating on their own, tumor cells often coerce surrounding cells to form a supportive niche (Hanahan and Weinberg, 2011). For example, in a hypoxic environment, tumor cells secrete vascular endothelial growth factor (VEGF) to promote stroma-derived angiogenesis to provide nutrients and oxygen to sustain tumor growth (Plate et al., 1992; Pugh and Ratcliffe, 2003; Shweiki et al., 1992). Therapeutic targeting of niche factors, such as anti-VEGF drug (bevacizumab), has been used in clinics to curb tumor progression (Bergers and Hanahan, 2008).

While our knowledge of tumor-niche interactions is largely derived from studies of the tumor microenvironment in carcinomas, the understanding of the niche in brain cancers is still evolving. For example, trans-differentiation of tumor-derived vasculature has been observed in glioma (Carmeliet and Jain, 2011), suggesting that tumors themselves can contribute to niche biology that enhances progression.
Medulloblastoma is the most common malignant pediatric brain tumor arising in the cerebellum (Gilbertson and Ellison, 2008). Many medulloblastoma are thought to originate from granule neuron progenitors (GNPs), and the SHH molecular subtype are all believed to arise from this superficial layer of precursors (Gibson et al., 2010; Goodrich et al., 1997; Pietsch et al., 1997; Schüller et al., 2008; Yang et al., 2008). In mice, from embryonic day 11.5 (E11.5), GNPs are generated from a small group of neural stem cells (NSCs) that migrate from the ventricular zone (VZ) through the

rhombic lip (RL) and finally settle on the surface of cerebellar primordium, forming the external granule layer (EGL) (Figure 1A) (Roussel and Hatten, 2011). GNPs are specified through the expression of transcription factor *Math1*, and are fate-restricted to only give rise to granule neurons, while NSCs generate all other neurons and astrocytes in the cerebellum (Figure 1B) (Ben-Arie et al., 1997; Lumpkin et al., 2003; Machold and Fishell, 2005; Wang et al., 2005). During postnatal day 0-21 (P0-P21) in mice, GNPs proliferate in the EGL in response to Sonic hedgehog (SHH) secreted from underlying Purkinje neurons (Wallace, 1999; Wechsler-Reya and Scott, 1999), then exit the cell cycle and migrate inward along the processes of specialized astrocytes, Bergmann glia. Upon reaching the inner granule layer (IGL), they completely differentiate and mature into granule neurons (Figure 1C) (Rakic, 1971). Dysregulation of the SHH pathway, such as mutations in the negative regulator *Patched* (*Ptch*) (Cowan et al., 1997; Goodrich et al., 1997; Raffel et al., 1997), leads to hyperproliferation of GNPs and eventual malignant transformation into medulloblastoma.

Pathological analyses over the past 100 years have revealed multiple niche cell types within human medulloblastoma (Bailey and Cushing, 1925; Burger et al., 1987; Delpech et al., 1977; Gilhuis et al., 2006; Mannoji et al., 1981; Roggendorf et al., 1996; Salsman et al., 2011; Wright, 1910). When we examined a set of SHH subgroup of medulloblastoma samples, we found that most tumors contained blood vessels, microglia/macrophages, and astrocytes (Figure S1A-B). Interestingly, while tumor GNPs proliferate at a high rate *in vivo*, culturing them *in vitro* has been almost impossible, prompting considerable efforts to maintain human medulloblastoma cells through serial transplantation in the brain of immune-compromised NOD/SCID mice (Shu et al., 2008).

Taken together, these observations suggest that tumor GNPs may rely on support from niche cells, mirroring the reliance of normal GNPs on SHH secreted from Purkinje neurons and the scaffolding of Bergmann glia for proper development.

To study tumor-niche interactions, an ideal model should mimic the clonal origin of human tumors and allow one to distinguish tumor from niche cells at single cell resolution. Here we used a mouse genetic system termed Mosaic Analysis with Double Markers (MADM) that generates sparse mutant cells unequivocally labeled with fluorescent proteins (Zong et al., 2005) to generate a medulloblastoma model by specifically introducing oncogenic mutations relevant to human patients into GNPs (Henner et al., 2013). Since this model generated tumors with high penetrance and consistent latency, we analyzed the niche establishment in great detail throughout tumor progression. Whereas most niche cells were GFP-negative, we were surprised to find that cells bearing astrocytic markers and morphologies were GFP-positive and thus tumor-derived. Furthermore, we found that, in human desmoplastic/nodular medulloblastoma of the SHH subtype, tumor cells and niche astrocytes share the same chromosomal aberrations, suggesting that such a lineage relationship exists in human tumors as well. Finally, our data demonstrate that the presence of astrocytes strongly correlates with tumor progression *in vivo*, and that astrocytes provide support to tumor GNPs *in vitro* to sustain proliferation and inhibit differentiation and apoptosis. In summary, we have identified a niche-building behavior in medulloblastoma that appears to be critical for tumor progression. Future determination of the molecular mechanisms of transdifferentiation and tumor-niche communications should provide critical insights for the development of highly effective therapeutic strategies.

Results

The establishment of MADM model for medulloblastoma to study tumor niche

To study tumor-niche interactions in medulloblastoma, we established a mouse genetic model with mutations commonly found in human medulloblastoma patients, specifically *PTCH and TP53* (Goodrich et al., 1997; Pietsch et al., 1997; Zhukova et al., 2013). Heterozygous loss of *Ptch* sensitize mice toward medulloblastoma formation, while the loss of *p53* increases the penetrance and decreases the latency of tumor formation (Goodrich et al., 1997; Wetmore et al., 2001), coinciding with a dismal prognosis of human medulloblastoma patients carrying *TP53* mutation (Zhukova et al., 2013). To mimic the clonal origin of human cancer, we used *Math1-Cre* transgene (Matei et al., 2005) with MADM to target *p53* mutation to a small number of GNPs, the cell of origin for SHH subtype medulloblastoma (Schüller et al., 2008; Uziel et al., 2005; Yang et al., 2008). The resulting mice have GNPs with three different genotypes labeled by distinct colors: red GNPs are $p53^{+/+}$; $Ptch^{+/-}$, green GNPs are $p53^{-/-}$; $Ptch^{+/-}$ (Figure 1D), while colorless and yellow GNPs are $p53^{+/-}$; $Ptch^{+/-}$ (not shown). Whereas red, yellow, or colorless GNPs differentiate into neurons and rarely transform, some green $p53^{-/-}$; $Ptch^{+/-}$ GNPs further transform to become tumorigenic, albeit the vast majority of them differentiate into neurons (Figure 1D). Taking advantage of specific GFP-labeling of tumor GNPs, we set out to study intricate interactions between colorless niche cells and green tumor cells throughout tumor progression (see schematic illustration in Figure 1E).

Considering the labeling of any cells other than GNPs by *Math1-Cre* could fundamentally compromise our data interpretation, we verified the faithfulness of *Math1-*

Cre-mediated recombination and found that 100% of labeled cells in the adult cerebellum are granule neurons in the IGL (Figure 1F,G), and that no potential niche cell types are labeled, including blood vessels, microglia, and astrocytes (Figure S1C-E). Next, we characterized the progress of tumor development in MADM medulloblastoma (MADM-MB) mice, and found that tumors originated focally from green mutant GNPs and progressed along a relatively consistent time course (Figure 1H). Around 60-day of age, tumors are small and focal (Figure H left panel and Figure I), despite of the great number of GFP-labeled cells (granule neurons) in the rest of the cerebellum, suggesting the clonal origin of tumors in this model. Medium-sized lesions form around P75, with tumor cells infiltrating into normal tissues (Figure 1H, middle panel). Finally, late-stage malignant tumors that distort normal cerebellar structure are mostly found in mice older than 90-days of age (Figure 1H, right panel). In summary, we have successfully established a MADM-based medulloblastoma model that allows further analyses of niche establishment during tumor progression.

Analyses of tumor niche with the MADM model during all stages of tumor progression and the discovery of a transdifferentiation phenomenon

Using a panel of markers for blood vessels, microglia/macrophages, and glial cells, we investigated whether niche cell types commonly found in human tumors (Figure S1A-B) exist in the MADM-based medulloblastoma model, timing of appearance, and their prevalence in the tumor mass. Blood vessels (CD34+) are prominent in all tumor sizes, with enlarged lumen size in comparison to adjacent normal tissue (Figure 2A). The coverage of vessels throughout tumor area steadily increases as tumors

progress from small to large sizes (Figure S2A), suggesting an augmentation of angiogenic signals during tumor progression. Similarly, IBA-1-positive microglia/macrophages are enriched in tumors with 4~5-fold increase in density compared to normal brain regions (Figure 2B, S2B) even in small tumors. While microglia in adjacent normal brain regions maintain highly branched morphology indicative of resting state, tumor-associated microglia/macrophages (TAMs) manifest the amoeba-like morphology and often contain GFP+ cellular fragments within their cell bodies, suggesting that they are in an activated state to engulf tumor cells (Figure 2B, circled). It should be noted that the prevalence and activated state of TAMs are evident at early stages of tumor progression, implicating their potential roles for tumor initiation. The fact that there are no microglia in EGL where tumors initiate suggests that TAMs are either recruited microglia from normal cerebellar tissue or infiltrated macrophages from blood vessels.

Next, we assessed the presence of glial cells in the tumor niche, including oligodendrocyte progenitor cells (OPCs), a dynamic cell population in the adult brain that can give rise to myelinating oligodendrocytes (Crawford et al., 2014; Hughes et al., 2013) and astrocytes, a cell type that is known to become “reactive” to provide protection during the injury state (Sofroniew, 2009; Sofroniew and Vinters, 2010). While PDGFRα-positive OPCs are not abundant in normal cerebellum, they were highly enriched in tumor regions from early to late stage tumors (Figure 2C, S2B). GFAP-positive astrocytes are prominently present in all-sizes of tumors and cover a large portion of the tumor mass with their extended processes (Figure 2D, S2D). Surprisingly, while vessels, immune cells, and OPCs are GFP-negative, all astrocytes in the tumor

mass are GFP-positive (Figure 2A-C vs. D). Since we verified that only GNPs are initially labeled in this model, the fact that GFAP-positive cells are green suggests that some tumor GNPs deviated from their unipotent fate and transdifferentiated into tumor "astrocyte-like" cells (herein referred to as, TuAstros). Transdifferentiation is tumor-specific since all astrocytes outside of the tumor region are GFP-negative (Figure 2E-F), and happens early during tumor initiation since TuAstros in very small lesions already have the same color labeling as tumor cells (Figure 2G). To investigate whether or not the transdifferentiation is caused by p53 loss, we examined spontaneous tumors in a few mice with the *Ptch+/-; WT-MADM; Math1-Cre* genotype, in which all tumor GNPs do not carry *p53* mutations. The fact that astrocytes in these tumors are also labeled by MADM (data not shown) suggests that transdifferentiation is not dependent on p53 mutations.

In addition to comparing the prevalence of niche cell types in tumor versus normal brain regions (Figure S2A, B), we also assessed the composition of niche cells by calculating the percentage of each cell type in the tumor mass. We found that TAMs make up ~5% and OPCs make up 5~10% of all DAPI+ cells in the tumor, while TuAstros are only ~1% of total tumor cells and remain steady throughout all tumor stages (Figure S2C), suggesting a possible mechanism to maintain the stoichiometry of TuAstros for tumor progression (see discussion). While TuAstros could provide niche support, we wondered how such a small number of TuAstros could function as a supportive niche. Therefore we used an Aldh1L1-GFP transgene to reveal all of the major astrocytic processes in order to assess the extent of coverage of TuAstros throughout the tumor area (Figure S2D, E). We observed that TuAstros processes

infiltrate into the entirety of the tumor area and maintain close contact with many tumor GNPs (Figure S2D, E).

In summary, our findings revealed that niche cells start appearing in the tumor even at early tumor initiation stages, implicating a heavy reliance of tumor GNPs on the microenvironment throughout the transformation process. We also serendipitously uncovered that astrocytes in the tumor mass are derived from tumor GNPs rather than entrapped from surrounding normal tissues.

Detailed characterization of TuAstros

First, we assessed whether TuAstros behave similarly to normal astrocytes. In normal cerebellum, Bergmann glia form distinctive radial fibers that project through the ML toward the surface of folia (Figure 3A). When we examined TuAstros in medulloblastoma, similar structures are also evident especially at the edge of small- to mid-sized tumors (Figure 3B, outlined), where TuAstros have radially organized process with endfeet touching the pia surface (Figure 3C-D versus A). Additionally, one of the important functions of astrocytes is the wrapping of blood vessels for blood-brain barrier maintenance and blood flow regulation (Foo et al., 2011; Iadecola and Nedergaard, 2007; Sofroniew and Vinters, 2010; Takano et al., 2005). We found close contact between TuAstros and blood vessels throughout tumor regions (Figure 3E), reminiscent of supportive functions of normal astrocytes to blood vessels. In summary, TuAstros display morphological resemblance to normal astrocytes in addition to their expression of multiple astrocyte-specific markers GFAP, BLBP, and Aldh1L1, suggesting a complete fate change of these cells from GNPs.

While our data demonstrate the transdifferentiation of TuAstros from Math1+ tumor cells, it is possible that they could be derived from rhombic lip progenitors that express *Math1* but have not fully committed to GNP fate (Machold and Fishell, 2005; Schüller et al., 2008; Wang et al., 2005). To determine whether or not fate-restricted, unipotent GNPs could transdifferentiate when transformed, we established a different medulloblastoma model in which *p53* mutation is induced specifically in postnatal GNPs by *Math1-CreER* (Figure 3F). Cre activity was induced by Tamoxifen injection starting at P7, and mice were analyzed for tumor formation and possible transdifferentiation at postnatal day 90 (see experimental scheme in Figure 3F). We found that, while vehicle injected mice rarely form tumors by 3-month of age, 7 out of 10 Tamoxifen-injected mice formed tumors. The fact that all these tumors had RFP-positive and BLBP-positive TuAstros (Figure 3G) suggests that transdifferentiation can occur in tumors originated from postnatal unipotent GNPs and thus does not depend on developmental plasticity of embryonic Math1+ progenitor cells.

Finally, we used a grafting assay to investigate whether transdifferentiation is an intrinsic program within tumor GNPs (Figure S3). After Percoll gradient centrifugation to remove all other cell types (Hatten, 1985), we cultured purified tumor GNPs briefly *in vitro* under conditions that do not support astrocyte survival. After confirming the lack of astrocyte contamination based on qRT-PCR of astrocytic genes, tumor cells were injected into brains of NOD/SCID mice to assess their transdifferentiation ability (Figure S3B,C). While no TuAstros can be found in grafted brains 10-day post injection (10dpi), further confirming the purity of injected tumor GNPs, at 30dpi transdifferentiation was evident since GFAP- and BLBP- positive TuAstros were abundant in secondary tumors

(Figure S3D,E). Therefore, the ability of tumor GNPs to transdifferentiate into TuAstros appears to be driven by intrinsic mechanisms.

In human medulloblastoma, tumor astrocytes are lineage-related to tumor cells

While we revealed the transdifferentiation phenomenon in the mouse medulloblastoma model, we wondered whether this finding has any human relevance since this has not been reported from pathological analyses of patient samples. Therefore, we sought to determine whether or not astrocytes in human SHH subtype medulloblastoma were derived from tumor cells. While genetic lineage tracing in human samples is impossible, we investigated the lineage relationship between astrocytes (GFAP+) and tumor cells based on cytogenetic aberrations unique to tumor cells using fluorescent *in situ* hybridization (FISH) in combination with immunofluorescent staining for GFAP. If astrocytes and tumor cells are not lineage-related, we expect to see distinct FISH patterns in tumor cells and astrocytes (Figure 4A, left). However, if astrocytes and tumor cells share lineage, they would bear the same cytogenetic aberrations (Figure 4A, right). Using *PTCH1* (9q22.33) and a Chromosome 9 control (*9q21.33*) loci (Ellison et al., 2006) as the FISH marker, we examined 21 human SHH subtype medulloblastoma samples, 6 (29%) of which demonstrated 9q loss and were studied further with double FISH and GFAP immunofluorescence. CD34-positive endothelial cells in these tumors have two FISH signals (retained 9q), serving as an internal control and demonstrating that no germline alteration was present in these patients (Figure 4B). When we compared tumor cells and GFAP+ cells in these tumors, we found that both cell types exhibited the loss of heterozygosity at the *9q21.33* and *PTCH1* loci representing 9q arm

loss (Figure 4C, and quantified in Table 1), suggesting that astrocytes in human medulloblastoma are likely derived from tumor GNPs.

Next, we assessed the distribution of astrocytes in human medulloblastoma. We found GFAP-positive cells with astrocytic morphologies often organize into nodule-like structures throughout tumor samples and form varied levels of contact with tumor cells (Figure S4A) (Barnard and Pambakian, 1980; Deck et al., 1978; Delpech et al., 1977; Mannoji et al., 1981; Rubinstein et al., 1974; Velasco et al., 1980). As observed in the mouse samples (Figure 3E), GFAP-positive astrocytes in human medulloblastoma form close contact with blood vessels (Figure S4B). Therefore, it appears that astrocytes could be a critical niche component in human medulloblastoma as well.

Finally, we assessed whether human medulloblastoma cells could transdifferentiate into astrocytes with a xenograft assay. To avoid culture-induced artifacts, we use a primary human SHH-subgroup medulloblastoma line that has been propagated through serial xenografting into the brains of NOD-SCID mice and verified for its authentic gene expression profiles (Shu et al., 2008; Zhao et al., 2012). First we needed to establish a method to detect this transdifferentiation since tumor cells are not labeled for lineage tracing. Fortunately we found an antibody that is specific for human GFAP since it differs significantly from mouse GFAP (Figure S4C). While many astrocytes in xenografted tumors are murine in origin (Figure S4C), we could easily find cells positive for human GFAP with typical astrocytic morphology (Figure 4D). It is unlikely that these are residual human astrocytes from patients since normal cells would unlikely survive extensive grafting for more than 12 generations. Therefore, it appears that human medulloblastoma cells can give rise to astrocytes.

Tumor astrocytes do not function as cancer stem cells to generate tumor GNPs

It is well known that neural stem cells express many astrocytic markers including GFAP (Alvarez-Buylla et al., 2001; Sofroniew and Vinters, 2010). One potential function of TuAstros could be to serve as cancer stem cells in the tumor. To address this possibility we performed a lineage tracing experiment of TuAstros to assess whether they could give rise to tumor GNPs. *Glast-CreER* and *ROSA26-LSL-tdT* transgenes were used to permanently label TuAstros in spontaneously formed tumors in *Ptch+/-* mice (Figure 5A). First, we confirmed specific labeling of TuAstros by examining tumor brains two days after Tamoxifen administration and found that only TuAstros are tdT-positive but tumor GNPs are not labeled (Figure S5). Next, we analyzed tumors with labeled TuAstros at much later time points. If TuAstros were cancer stem cells, we would expect to see tdT-positive tumor GNPs. On the other hand, if TuAstros were not cancer stem cells, labeling would be restricted to TuAstros (illustrated in Figure 5A). When we examined two tumors 2-weeks after Tamoxifen administration, we confirmed that all tdT-positive cells in tumors are GFAP-positive and display the characteristic TuAstro morphology (Figure 5B), whereas tumor cells (DAPI-positive cells surrounding TuAstros) are never labeled. To test whether TuAstros could give rise to tumor GNPs, the waiting period was extended 1-2 months following initial Tamoxifen administration. Since waiting for 1-2 months in *Ptch+/-* primary tumors was not feasible due to animal morbidity, we performed such experiment in secondary tumors generated by cells from primary *Glast-CreER; ROSA26-LSL-tdT; Ptch+/-* tumors that did not receive tamoxifen. TuAstros were labeled by tamoxifen administration at 14 and 21 dpi, and tumors were

analyzed 2 months later. All tdT-positive cells in tumors are GFAP-positive, whereas surrounding tumor cells remain unlabeled (n=2) (Figure 5C). Together, these experiments strongly suggest that TuAstros do not serve as cancer stem cells in medulloblastoma.

Strong correlation between the presence of TuAstros and mutant GNP proliferation in pre-neoplastic lesions

Since TuAstros appear not to act as cancer stem cells, next we assessed potential supportive roles of TuAstros in medulloblastoma. Previously it was reported that while all normal GNPs migrate inward and differentiate into granule neurons at the end of cerebellar development, *Ptch*+/- GNPs tend to form distinct focal accumulations on the surface of the cerebellum (Oliver et al., 2005). These GNP clusters are termed pre-neoplastic lesions (PNLs), since some of them can further progress toward full malignancy while others eventually exit the cell cycle (Figure 6A). While there could be many possible explanations for the different fates of PNLs, we wondered if it could be determined by the presence or absence of TuAstros.

To investigate this possibility, we analyzed more than 30 PNLs in pre-malignant brains, which were located by visualizing DAPI-positive clusters on the surface of cerebellum. To determine whether there was any correlation between the presence of TuAstros and malignant progression, we co-stained sections of PNLs with GFAP and Ki67. In 14 cases, the presence of TuAstros correlates with the proliferation of mutant GNPs; in 16 cases, the absence of TuAstros correlates with the lack of proliferation of mutant GNPs (Figure 6B-D). Therefore, among 33 PNLs that we examined, 30 of them

showed strong correlation between the presence of TuAstros and tumor progression. There were instances where multiple proliferating PNLs could be identified in the same cerebellum (Figure S6A-C), which invariantly stained strongly for GFAP. Among proliferating PNLs, the degree of astrocyte presence varies, which correlates well (Figure S6D-E) with the abundance and spatial distribution of dividing mutant GNPs most of the time. In summary, these data suggest a strong correlation between the presence of TuAstro and the progression of PNLs.

TuAstros support tumor GNP survival and proliferation.

While the presence of TuAstros correlate with PNL progression, it would be important to directly investigate whether TuAstros support tumor GNPs with a co-culture assay. Due to the scarceness of TuAstros in the tumor mass (~1% of total cells, Figure S2) and cell death due to sheer stress, our attempt to purify them with FACS was not successful. As the next best option, we dissociated RFP-labeled medulloblastoma and cultured all cells in a medium containing heparin binding epidermal growth factor (HB-EGF) that is critical for astrocyte survival (Foo et al., 2011). After 3 days *in vitro* (DIV), only a small percentage of cells survived (0.8-1.4% of initial seeded cells) since this medium is not tailored for tumor GNP growth (Figure 7A top). Since most of cells display the characteristic astrocytic morphology and are GFAP-positive (Figure 7B), we used these cells as TuAstros in subsequent co-culture assays.

For visual clarity, we seeded *Math1-GFP*-positive tumor GNPs onto RFP-positive TuAstros (Figure 7A, middle). Initially green tumor GNPs were evenly distributed and divided regardless of their proximity to red TuAstros (Figure 7C). After a longer

incubation period (3 DIV), we expect two possible outcomes. If TuAstros do not provide local support for tumor GNPs, then tumor GNPs would proliferate irrespective of their distance from TuAstros. On the other hand, if TuAstros provide support to tumor GNPs, then tumor GNPs in proximity to TuAstros would proliferate at a much higher rate than those far from TuAstros (Figure 7A, bottom). When we quantified the total number of surviving tumor GNPs in relation to their distance to TuAstros (within or beyond 30μm, which is the approximate radial length of TuAstros processes), we found that ~80% of surviving tumor GNPs resides within 30μm of TuAstros (Figure 7E, left graph). Next we quantified the proliferative rate of all surviving tumor GNPs, and found that more than half of tumor GNPs within 30μm of TuAstros were proliferating, while those beyond 30μm from TuAstros had a significantly reduced proliferative rate (~25% EdU-positive) (Figure 7D, and E right graph). In conclusion, these data suggest that TuAstros support tumor GNP survival and proliferation.

In addition to endpoint measurements, we also used live imaging to visualize the dynamics of tumor GNPs co-cultured with TuAstros to examine the mode of support. With the same experimental setup described above (Figure 7A), we began live imaging upon the seeding of GFP-positive tumor GNPs onto RFP-positive TuAstros at 2hr intervals over the course of 48hr (Figure 7F-I). Initially, tumor GNPs were evenly distributed, settling at varied distances from TuAstros (Figure 7F). We made several important observations after careful analysis of the time-lapse videos: 1) GNPs that initially landed on TuAstros tend to survive and proliferate; 2) GNPs residing within 30 μm from TuAstros tend to migrate toward TuAstros (Figure 7H); 3) Of tumor GNPs that were farther than 30 μm from a TuAstro, even though some underwent cell division

initially, most eventually died (Figure 7G). To quantify our observation that tumor GNPs residing within 30 μm survive better and divide more (Figure 7J), we calculated the fold-change of tumor GNP numbers for those either within or beyond 30 μm of a TuAstro, and found that the number of GNPs within 30 μm of TuAstros almost doubled while the number of GNPs beyond 30 μm reduced by half over 48 hours (Figure 7K). These real time imaging data suggest that TuAstros support the growth of tumor GNPs by means of direct contact or short-range signals.

Finally, we wondered whether the support of TuAstros to tumor GNPs is a cancer-specific phenomenon or simply a recapitulation of the supportive roles of normal astrocytes during cerebellar development. First, we investigated whether normal astrocytes purified from neonatal brains could support wildtype GNPs in a co-culture assay. Compared to those cultured alone, GNPs co-cultured with normal astrocytes had a 2-fold increase in their proliferative rate (Figure S7A, B), suggesting that the tumor-supporting function of TuAstros could be a recapitulation of normal developmental process. To further probe the nature of astrocytic support to tumor GNPs, we performed additional co-culture experiments using wild-type astrocytes that are much more abundant than TuAstros. We observed that tumor GNPs spread out and intimately associated with astrocytes in the co-culture, in stark contrast to self-aggregation when they are cultured alone (Figure S7C), implicating physical support of astrocytes to tumor GNPs. When we examined the activities of tumor GNPs co-cultured with normal astrocytes, we found that proliferation is enhanced while cell death and differentiation are suppressed in comparison to those cultured alone (Figure S7D-G). It should be noted that mere cell contact is not enough for such a support, since NIH3T3 cells

showed no sign of support to tumor cells in a co-cultured assay although tumor cells form close contact with them (data not shown). Overall, these data indicate that normal astrocytes can support tumor GNPs, suggesting that the supportive functions of TuAstros may be an intrinsic activity of astrocytes.

Discussion

Solid tumors are often composed of many niche cell types that intimately interact with tumor cells and contribute to tumor progression. In this study, we investigated the diverse cellular niche for medulloblastoma that includes blood vessels, immune cells, and glial cells. Surprisingly, we found that niche astrocytes are derived from tumor GNPs, even though normal GNPs are known to be unipotent and never give rise to astrocytes. Further we confirmed that such a lineage relationship also exists in human desmoplastic/nodular SHH subtype medulloblastoma based on common cytogenetic aberrations shared between tumor cells and astrocytes. Finally, we showed that TuAstros do not behave like cancer stem cells, but rather directly promote the survival and proliferation of tumor GNPs. These findings highlight a self-building supportive network within medulloblastoma. Our finding resonates with recent reports in other types of cancers. For example, endothelial differentiation of cancer stem-like cells (CSCs) has been reported in leukemia, myeloma, neuroblastoma, and glioblastoma, as well as renal, ovarian, and breast cancers (Alvero et al., 2009; Bonfanti et al., 2011; Bussolati et al., 2008; Gunsilius et al., 2000; Ricci-Vitiani et al., 2010; Rigolin, 2006; Shen et al., 2008; Soda et al., 2011; Wang et al., 2006). Particularly in human glioma, it appears that CSC-to-endothelial transdifferentiation may contribute to neovascularization and possibly chemoresistance (Ricci-Vitiani et al., 2010; Soda et al., 2011; Wang et al., 2010). Therefore, the aberrant lineage plasticity of tumor cells could serve as a common mechanism for promoting robust tumor progression.

MADM is a powerful tool to study tumor-niche interactions

While the importance of niche cells in tumor progression have been well established (Egeblad et al., 2010; Quail and Joyce, 2013), many aspects remain unclear indicating the need for further studies in model organisms. First of all, niche establishment during tumor initiation is greatly understudied – when do each niche cell type appear during tumor progression and how do they interact with each other and with tumor cells? Second, what is the composition of each niche cell type and how are they distributed in the tumor mass? Last but not least, what is the lineage relationship between tumor and niche cells? Studying tumor niche with refined temporal and spatial resolution should greatly deepen our understanding of cancer biology that may lead to paradigm-shifting therapeutic strategies.

To study the tumor niche in detail, one prerequisite is the availability of genetic tools with high resolution for *in vivo* phenotypic analysis. As a genetic mosaic system, MADM generates rare mutant cells that closely mimics human physiology of tumor development, and unequivocally labels them with fluorescent proteins that enables detailed analysis of tumor niche throughout all stages of tumor progression, even at pre-malignant stages (Liu et al., 2011; Muzumdar et al., 2007). Using MADM, our data showed that, while blood vessels gradually increase their coverage as tumors progress, microglia/macrophages are significantly enriched from early stages and maintain the composition throughout tumor development (Figure 2, S2). As importantly, findings of transdifferentiation from conventional conditional knockout (CKO) models could have alternative explanations since one could argue that aberrant Cre expression could be induced by the tumor microenvironment to drive the expression of reporter gene in niche cells. In the case of the MADM model, the double color scheme enables easy

distinction between these two possibilities, because promiscuous Cre activity in astrocytes would lead to yellow (if they don't divide) or green plus red astrocytes (if they divide) while truly transdifferentiated cells would only share the same color as tumor cells (Zong et al., 2005). Since all TuAstros are GFP-positive in the MADM model, we are confident that they are derived from green tumor GNPs. Therefore, MADM is a powerful tool not only for its resolution to facilitate the analysis of tumor-niche interactions, but also for its lineage tracing capacity to reveal unsuspected lineage relationships in the tumor mass.

The discovery of tumor GNP-to-TuAstros transdifferentiation, potential mechanisms and remaining questions

While a prominent astrocytic presence in human desmoplastic medulloblastoma has been reported before (Bailey and Cushing, 1925; Deck et al., 1978; Delpech et al., 1977; Eng and Rubinstein, 1978; Mannoji et al., 1981; Palmer et al., 1981; Velasco et al., 1980), the origin of these astrocytes has been unclear. Using the MADM model, we provide definitive evidence that TuAstros are transdifferentiated from tumor GNPs, a process that starts from early stages of tumorigenesis and persists throughout tumor progression to maintain a consistent composition within the tumor mass. Further examination of human medulloblastoma samples showed that tumor cells and astrocytes share the same chromosomal aberrations, suggesting that they are lineage related as well.

For unipotent GNPs to give rise to astrocytes, it could go through direct transdifferentiation or alternatively through a de-differentiation then re-differentiation

process. If tumor GNPs do de-differentiate to acquire stem cell properties then re-differentiate, we would expect GFP-labeling of multiple cell types other than astrocytes, such as neurons, OPCs, and oligodendrocytes. Since we have never observed that, TuAstros are likely directly transdifferentiated from tumor GNPs. It should be noted that, during cerebellar development, a small fraction of GNPs displays transient *Gfap* promoter activity, suggesting that some GNPs could have plasticity although it doesn't manifest in normal development (Silbereis et al., 2010). Interestingly, GNP-to-astrocyte transdifferentiation was also seen in cell culture either after SV40 T antigen-mediated immortalization or the treatment of high level of BMP and SHH (Okano-Uchida et al., 2004; Gao and Hatten, 1994), suggesting certain stimuli could unleash the hidden developmental potential from GNPs. A previous report showing that rare olig2-expressing cells in human medulloblastoma share the same myc amplification as other tumor cells (Schüller et al., 2008). Since olig2 is a transcription factor critical for gliogenesis, its over-expression could mediate transdifferentiation of tumor cells into astrocytes, although further evidence would still be needed to support this hypothesis.

One puzzling question is how TuAstros maintain a relatively consistent composition in the tumor mass since they don't appear to divide. Is there a specific sub-population of GNPs that transdifferentiate at a steady rate to keep up with tumor growth? Or, do all tumor GNPs possess the plasticity but transdifferentiate in a stochastic fashion? Probing into tumor GNP heterogeneity with stochastic profiling methods (Janes et al., 2010) and clonal level analysis in an *in vivo* setting should help tease apart these two possibilities.

TuAstros promote the growth and survival of tumor GNPs

While the transdifferentiation is an interesting observation, an important question is whether TuAstros functionally contribute to tumorigenesis. Astrocytic support for the self-renewal and survival of neural progenitors has been previously reported (Lim and Alvarez-Buylla, 1999; Song et al., 2002). During normal cerebellar development, astrocytes are essential for ensuring survival and inward migration of GNPs (Delaney et al., 1996; Roussel and Hatten, 2011). Furthermore, we found that cultured normal astrocytes promote the proliferation of wildtype GNPs (Figure S7). These findings suggest an innate supportive role of astrocytes to GNPs. Using a co-culture assay, we demonstrated that the proliferation and survival of tumor GNPs are greatly enhanced in the presence of both TuAstros and wildtype astrocytes. Further studies are warranted to identify candidate factors from TuAstros that sustain tumor GNP growth.

It should be noted that TuAstros only cover 20% of tumor areas, even when most processes are revealed by the Aldh1L1-GFP reporter gene. How can such a limited coverage support the entire tumor mass? First of all, it is possible that TuAstros have fine processes beyond detection that contact most/all tumor cells. Second, TuAstros could secret soluble supporting factors that diffuse toward tumor cells that they are not in direct contact with. Finally, the support of 20% of tumor GNPs may be enough to tip the balance between proliferation and differentiation/apoptosis in enough tumor cells to maintain the tumor mass.

Since wildtype astrocytes can support tumor GNPs in culture, why do medulloblastoma cells generate TuAstros rather than simply rely on existing astrocytes in the brain for the support? There are at least two probable explanations: physical

distance and age-dependent functional changes of astrocytes. First, PNLs, the precursor to medulloblastoma, initiate at the surface of cerebellum, where they can only access the end feet tips of Bergmann glia (Figure S2F) (Oliver et al., 2005). Such limited contact may not be enough to support tumor progression. Second, the functions of astrocytes may change along the developmental process. While newly born astrocytes provide mitogenic support, older ones likely specialize into neural supportive functions (Barres, 2008). Therefore, tumor-derived astrocytes form a niche that can co-evolve with the expanding tumor mass and provide optimal support for the intrinsic robustness of medulloblastoma.

Concluding remarks and perspectives: a self-building tumor niche reveals increased complexity in tumor development

While our current studies established the importance of TuAstros for medulloblastoma, it is important to further investigate the molecular mechanisms that would allow us to block the transdifferentiation process and to remove tumor-supporting factors from TuAstros as highly effective treatment strategies. Additionally, targeting the close interaction between TuAstros and tumor vasculature could also become a unique opportunity for therapy development. In summary, our work revealed previously under-appreciated complexity of niche components in medulloblastoma, and calls for careful examination of tumor niches in all types of tumors both to enhance our understanding of cancer biology and to promote the development of paradigm-shifting therapeutic strategies.

Experimental Procedures

Mouse Lines and Genotyping Methods

All animal procedures were based on animal care guidelines approved by the Institutional Animal Care and Use Committee. Mouse lines used in this study can be found in the Supplemental Experimental Procedures.

Tissue Preparation and Histology

Following anesthesia, mice were perfused with 4% cold paraformaldehyde (PFA) following standard procedures. Brains were isolated, postfixed (overnight at 4^{o}C), cryoprotected in 30% sucrose (overnight at 4^{o}C), and embedded into optimal cutting temperature (O.C.T.) prior to cryosectioning on a cryostat.

Imaging

All confocal images were collected on a Zeiss LSM710 upright laser confocal microscope and analyzed with ImageJ software. Adobe Photoshop CS4 was used for image processing. Live imaging was performed on an EVOS FL Auto Cell Imaging System (Life Technologies) and time series were analyzed with ImageJ.

Immunohistochemistry

Immunohistochemistry was performed using standard methodology. Details regarding antibodies and procedures are described in the Supplemental Experimental Procedures and Table S1.

Quantification

All quantification was performed based on systematic sampling described in Supplemental

Experimental Procedures. Statistical analysis was performed in Excel and Graph Pad Prism.

Purification of Tumor Cells and Astrocytes

Tumor GNPs and wildtype astrocytes were purified as previously described (Foo et al., 2011, Hatten., 1985) with minor modifications. Detailed procedures regarding *in vitro* culture conditions are described in Supplemental Experimental Procedures.

Tumor Cell Grafting

Tumor cells were suspended into Neurobasal medium with a density of 5,000 viable cells /μl. Tumor cell suspension (2 μl) was injected into right striata of NOD-SCID mice (JAX laboratory) as described in Supplemental Experimental Procedures.

Author Contributions

P.B.V., M.Y., K.W., Y.J. performed all experiments with mouse tissues and cell culture. F.J.R. and C.E. provided all IHC and FISH/IF images of human medulloblastoma samples and inputs for relevant writing. J.M.M. analyzed *in vitro* live imaging data and assembled respective figure panels. L.Q. and X.L. provided human medulloblastoma cells for the grafting experiment. P.B.V and H.Z. conceived and direct projected, designed experiments, and wrote the manuscript with inputs from all authors. All authors reviewed the manuscript.

Acknowledgements

We thank Chris Doe, David Rowitch, and Praveen Raju for critical discussions and insightful feedback for our manuscript. This project is partially supported by grants to H.Z. (DoD W81XWH-11-1-0557) and C.G.E. (R01NS055089). P.B.V. is supported by NIH/NINDS pre-doctoral fellowship (F31-NS076313). H.Z. is a Pew Scholar in Biomedical Sciences, supported by the Pew Charitable Trusts.

References

Alvarez-Buylla, A., García-Verdugo, J.M., and Tramontin, A.D. (2001). A unified hypothesis on the lineage of neural stem cells. Nat Rev Neurosci *2*, 287–293.

Alvero, A.B., Fu, H.-H., Holmberg, J., Visintin, I., Mor, L., Marquina, C.C., Oidtman, J., Silasi, D.-A., and Mor, G. (2009). Stem-Like Ovarian Cancer Cells Can Serve as Tumor Vascular Progenitors. Stem Cells *27*, 2405–2413.

Bailey, P., and Cushing, H. (1925). Medulloblastoma cerebelli: a common type of midcerebellar glioma of childhood. Arch NeurPsych *14*, 192.

Barnard, R.O.R., and Pambakian, H.H. (1980). Astrocytic differentiation in medulloblastoma. J Neurol Neurosurg Psychiatry *43*, 1041–1044.

Barres, B.A. (2008). The magic and mystery of glia: A perspective on their roles in health and disease. Neuron *60*, 430–440.

Ben-Arie, N., Bellen, H.J., Armstrong, D.L., McCall, A.E., Gordadze, P.R., Guo, Q., Matzuk, M.M., and Zoghbi, H.Y. (1997). Math1 is essential for genesis of cerebellar granule neurons. Nature *390*, 169–172.

Bonfanti, P., Claudinot, S., Amici, A.W., Farley, A., Blackburn, C.C., and Barrandon, Y. (2011). Microenvironmental reprogramming of thymic epithelial cells to skin multipotent stem cells. Nature *466*, 978–982.

Burger, P.C., Grahmann, F.C., Bliestle, A., and Kleihues, P. (1987). Differentiation in the medulloblastoma. Acta Neuropathol *73*, 115–123.

Bussolati, B., Bruno, S., Grange, C., Ferrando, U., and Camussi, G. (2008). Identification of a tumor-initiating stem cell population in human renal carcinomas. The FASEB Journal *22*, 3696–3705.

Carmeliet, P., and Jain, R.K. (2011). Molecular mechanisms and clinical applications of angiogenesis. Nature *473*, 298–307.

Cowan, R.R., Hoban, P.P., Kelsey, A.A., Birch, J.M.J., Gattamaneni, R.R., and Evans, D.G.D. (1997). The gene for the naevoid basal cell carcinoma syndrome acts as a tumour-suppressor gene in medulloblastoma. Br J Cancer *76*, 141–145.

Crawford, A.H., Stockley, J.H., Tripathi, R.B., Richardson, W.D., and Franklin, R.J.M. (2014). Oligodendrocyte progenitors: adult stem cells of the central nervous system? Exp Neurol *260*, 50–55.

Deck, J., Eng, L.F., Bigbee, J., and Woodcock, S.M. (1978). The role of glial fibrillary acidic protein in the diagnosis of central nervous system tumors. Acta Neuropathol *42*, 183–190.

Delaney, C.L., Brenner, M., and Messing, A. (1996). Conditional ablation of cerebellar astrocytes in postnatal transgenic mice. J Neurosci *16*, 6908–6918.

Delpech, B., Delpech, A., Vidard, M.N., Girard, N., Tayot, J., Clement, J.C., and Creissard, P. (1977). Glial fibrillary acidic protein in tumours of the nervous system. Br J Cancer *37*, 33–40.

Egeblad, M., Nakasone, E.S., and Werb, Z. (2010). Tumors as Organs: Complex Tissues that Interface with the Entire Organism. Developmental Cell *18*, 884–901.

Ellison, D.W., Clifford, S.C., and Giangaspero, F. (2006). Medulloblastoma. In Russell & Rubinstein's Pathology of Tumors of the Nervous System, R.E. McLendon, M.K. Rosenblum, and D.D. Bigner, eds. (New York: Oxford University Press, Inc.), pp. 247–264.

Eng, L.F., and Rubinstein, L.J. (1978). Contribution of immunohistochemistry to diagnostic problems of human cerebral tumors. Journal of Histochemistry & Cytochemistry *26*, 513–522.

Foo, L.C., Allen, N.J., Bushong, E.A., Ventura, P.B., Chung, W.-S., Zhou, L., Cahoy, J.D., Daneman, R., Zong, H., Ellisman, M.H., et al. (2011). Development of a Method for the Purification and Culture of Rodent Astrocytes. Neuron *71*, 799–811.

Gao, W.Q., and Hatten, M.E. (1994). Immortalizing oncogenes subvert the establishment of granule cell identity in developing cerebellum. Development *120*, 1059–1070.

Gibson, P., Tong, Y., Robinson, G., Thompson, M.C., Currle, D.S., Eden, C., Kranenburg, T.A., Hogg, T., Poppleton, H., Martin, J., et al. (2010). Subtypes of medulloblastoma have distinct developmental origins. Nature *468*, 1095–1099.

Gilbertson, R.J., and Ellison, D.W. (2008) The Origins of Medulloblastoma Subtypes. Annu. Rev. Pathol. Mech. Dis. *3*, 341–65.

Gilhuis, H.J., Laak, J.A.W.M., Pomp, J., Kappelle, A.C., Gijtenbeek, J.M.M., and Wesseling, P. (2006). Three-dimensional (3D) reconstruction and quantitative analysis of the microvasculature in medulloblastoma and ependymoma subtypes. Angiogenesis *9*, 201–208.

Goodrich, L.V., Milenković, L., Higgins, K.M., and Scott, M.P. (1997). Altered Neural Cell Fates and Medulloblastoma in Mouse patched Mutants. Science *277*, 1109–1113.

Gunsilius, E., Duba, H.-C., Petzer, A.L., Kahler, C.M., Grunewald, K., Stockhammer, G., Gabl, C., Dirnhofer, S., Clausen, J., and Gastl, G. (2000). Evidence from a leukaemia model for maintenance of vascular endothelium by bone-marrow-derived endothelial cells. Lancet *355*, 1688–1691.

Hanahan, D., and Weinberg, R.A. (2011). Hallmarks of Cancer: The Next Generation.

Cell *144*, 646–674.

Hatten, M.E. (1985). Neuronal regulation of astroglial morphology and proliferation in vitro. J Cell Biol *100*, 384–396.

Henner, A., Ventura, P.B., Jiang, Y., and Zong, H. (2013). MADM-ML, a Mouse Genetic Mosaic System with Increased Clonal Efficiency. PLoS ONE *8*.

Hughes, E.G., Kang, S.H., Fukaya, M., and Bergles, D.E. (2013). Oligodendrocyte progenitors balance growth with self-repulsion to achieve homeostasis in the adult brain. Nature Publishing Group *16*, 668–676.

Iadecola, C., and Nedergaard, M. (2007). Glial regulation of the cerebral microvasculature. Nat Neurosci *10*, 1369–1376.

Janes, K.A., Wang, C.-C., Holmberg, K.J., Cabral, K., and Brugge, J.S. (2010). identifying single-cell molecular programs by stochastic profiling. Nat Meth *7*, 311–317.

Jones, D.T.W., Jäger, N., Kool, M., Zichner, T., Hutter, B., Sultan, M., Cho, Y.-J., Pugh, T.J., Hovestadt, V., Stütz, A.M., et al. (2012). Dissecting the genomic complexity underlying medulloblastoma. Nature *488*, 100–105.

Lim, D.A., and Alvarez-Buylla, A. (1999). Interaction between astrocytes and adult subventricular zone precursors stimulates neurogenesis. Proc Natl Acad Sci USA *96*, 7526–7531.

Liu, C., Sage, J.C., Miller, M.R., Verhaak, R.G.W., Hippenmeyer, S., Vogel, H., Foreman, O., Bronson, R.T., Nishiyama, A., Luo, L., et al. (2011). Mosaic Analysis with Double Markers Reveals Tumor Cell of Origin in Glioma. Cell *146*, 209–221.

Lumpkin, E.A., Collisson, T., Parab, P., Omer-Abdalla, A., Haeberle, H., Chen, P., Doetzlhofer, A., White, P., Groves, A., Segil, N., et al. (2003). Math1-driven GFP expression in the developing nervous system of transgenic mice. Gene Expression Patterns *3*, 389–395.

Machold, R., and Fishell, G. (2005). Math1 is expressed in temporally discrete pools of cerebellar rhombic-lip neural progenitors. Neuron *48*, 17–24.

Mannoji, H.H., Takeshita, I.I., Fukui, M.M., Ohta, M.M., and Kitamura, K.K. (1981). Glial fibrillary acidic protein in medulloblastoma. Acta Neuropathol *55*, 63–69.

Matei, V., Pauley, S., Kaing, S., Rowitch, D., Beisel, K.W., Morris, K., Feng, F., Jones, K., Lee, J., and Fritzsch, B. (2005). Smaller inner ear sensory epithelia in Neurog1 null mice are related to earlier hair cell cycle exit. Dev. Dyn. *234*, 633–650.

Muzumdar, M.D., Luo, L., and Zong, H. (2007). Modeling sporadic loss of heterozygosity in mice by using mosaic analysis with double markers (MADM). Proc Natl Acad Sci USA *104*, 4495–4500.

Okano-Uchida, T., Himi, T., Komiya, Y., and Ishizaki, Y. (2004). Cerebellar granule cell precursors can differentiate into astroglial cells. Proc Natl Acad Sci USA *101*, 1211–1216.

Oliver, T.G., Read, T.A., Kessler, J.D., Mehmeti, A., Wells, J.F., Huynh, T.T.T., Lin, S.M., and Wechsler-Reya, R.J. (2005). Loss of patched and disruption of granule cell development in a pre-neoplastic stage of medulloblastoma. Development *132*, 2425–2439.

Palmer, J.O., Kasselberg, A.G., and Netsky, M.G. (1981). Differentiation of Medulloblastoma. Studies including immunohistochemical localization of glial fibrillary acidic protein. J Neurosurg *55*, 161–169.

Pietsch, T., Waha, A., Koch, A., Kraus, J., Albrecht, S., Tonn, J., Sörensen, N., Berthold, F., Henk, B., Schmandt, N., et al. (1997). Medulloblastomas of the desmoplastic variant carry mutations of the human homologue of Drosophila patched. Cancer Research *57*, 2085–2088.

Plate, K.H., Breier, G., Weich, H.A., and Risau, W. (1992). Vascular endothelial growth factor is a potential tumour angiogenesis factor in human gliomas in vivo. Nature *359*, 845–848.

Pugh, C.W., and Ratcliffe, P.J. (2003). Regulation of angiogenesis by hypoxia: role of the HIF system. Nature Medicine *9*, 677–684.

Pugh, T.J., Weeraratne, S.D., Archer, T.C., Krummel, D.A.P., Auclair, D., Bochicchio, J., Carneiro, M.O., Carter, S.L., Cibulskis, K., Erlich, R.L., et al. (2012). Medulloblastoma exome sequencing uncovers subtype-specific somatic mutations. Nature *488*, 106–110.

Quail, D.F., and Joyce, J.A. (2013). Microenvironmental regulation of tumor progression and metastasis. Nature Medicine *19*, 1423–1437.

Raffel, C., Jenkins, R.B., Frederick, L., Hebrink, D., Alderete, B., Fults, D.W., and James, C.D. (1997). Sporadic medulloblastomas contain PTCH mutations. Cancer Research *57*, 842–845.

Rakic, P. (1971). Neuron-glia relationship during granule cell migration in developing cerebellar cortex. A Golgi and electronmicroscopic study in Macacus Rhesus. J Comp Neurol *141*, 283–312.

Ricci-Vitiani, L., Pallini, R., Biffoni, M., Todaro, M., Invernici, G., Cenci, T., Maira, G., Parati, E.A., Stassi, G., Larocca, L.M., et al. (2010). Tumour vascularization via endothelial differentiation of glioblastoma stem-like cells. Nature *468*, 824–828.

Rigolin, G.M. (2006). Neoplastic circulating endothelial cells in multiple myeloma with 13q14 deletion. Blood *107*, 2531–2535.

Roggendorf, W., Strupp, S., and Paulus, W. (1996). Distribution and characterization of

microglia/macrophages in human brain tumors. Acta Neuropathol *92*, 288–293.

Roussel, M.F., and Hatten, M.E. (2011). Cerebellum development and medulloblastoma. Curr. Top. Dev. Biol. *94*, 235–282.

Rubinstein, L.J.L., Herman, M.M.M., and Hanbery, J.W.J. (1974). The relationship between differentiating medulloblastoma and dedifferentiating diffuse cerebellar astrocytoma. Light, electron microscopic, tissue, and organ culture observations. Cancer *33*, 675–690.

Salsman, V.S., Chow, K.K.H., Shaffer, D.R., Kadikoy, H., Li, X.-N., Gerken, C., Perlaky, L., Metelitsa, L.S., Gao, X., Bhattacharjee, M., et al. (2011). Crosstalk between Medulloblastoma Cells and Endothelium Triggers a Strong Chemotactic Signal Recruiting T Lymphocytes to the Tumor Microenvironment. PLoS ONE *6*, e20267.

Schüller, U., Heine, V.M., Mao, J., Kho, A.T., Dillon, A.K., Han, Y.-G., Huillard, E., Sun, T., Ligon, A.H., Qian, Y., et al. (2008). Acquisition of granule neuron precursor identity is a critical determinant of progenitor cell competence to form Shh-induced medulloblastoma. Cancer Cell *14*, 123–134.

Shen, R., Ye, Y., Chen, L., Yan, Q., Barsky, S.H., and Gao, J.-X. (2008). Precancerous Stem Cells Can Serve As Tumor Vasculogenic Progenitors. PLoS ONE *3*, e1652.

Shu, Q., Wong, K.K., Su, J.M., Adesina, A.M., Yu, L.T., Tsang, Y.T.M., Antalffy, B.C., Baxter, P., Perlaky, L., Yang, J., et al. (2008). Direct Orthotopic Transplantation of Fresh Surgical Specimen Preserves CD133 +Tumor Cells in Clinically Relevant Mouse Models of Medulloblastoma and Glioma. Stem Cells *26*, 1414–1424.

Shweiki, D., Itin, A., Soffer, D., and Keshet, E. (1992). Vascular endothelial growth factor induced by hypoxia may mediate hypoxia-initiated angiogenesis. Nature *359*, 843–845.

Silbereis, J.J., Heintz, T.T., Taylor, M.M.M., Ganat, Y.Y., Ment, L.R.L., Bordey, A.A., and Vaccarino, F.F. (2010). Astroglial cells in the external granular layer are precursors of cerebellar granule neurons in neonates. Molecular and Cellular Neuroscience *44*, 12–12.

Soda, Y., Marumoto, T., Friedmann-Morvinski, D., Soda, M., Liu, F., Michiue, H., Pastorino, S., Yang, M., Hoffman, R.M., and Kesari, S. (2011). Transdifferentiation of glioblastoma cells into vascular endothelial cells. Proc Natl Acad Sci USA *108*, 4274–4280.

Sofroniew, M.V. (2009). Molecular dissection of reactive astrogliosis and glial scar formation. Trends in Neurosciences *32*, 638–647.

Sofroniew, M.V., and Vinters, H.V. (2010). Astrocytes: biology and pathology. Acta Neuropathol *119*, 7–35.

Song, H.H., Stevens, C.F.C., and Gage, F.H.F. (2002). Astroglia induce neurogenesis from adult neural stem cells. Nature *417*, 39–44.

Takano, T., Tian, G.-F., Peng, W., Lou, N., Libionka, W., Han, X., and Nedergaard, M. (2005). Astrocyte-mediated control of cerebral blood flow. Nat Neurosci *9*, 260–267.

Uziel, T., Zindy, F., Xie, S., Lee, Y., Forget, A., Magdaleno, S., Rehg, J.E., Calabrese, C., Solecki, D., Eberhart, C.G., et al. (2005). The tumor suppressors Ink4c and p53 collaborate independently with Patched to suppress medulloblastoma formation. Genes & Development *19*, 2656–2667.

Velasco, M.E., Dahl, D., Roessmann, U., and Gambetti, P. (1980). Immunohistochemical localization of glial fibrillary acidic protein in human glial neoplasms. Cancer *45*, 484–494.

Wallace, V.A. (1999). Purkinje-cell-derived Sonic hedgehog regulates granule neuron precursor cell proliferation in the developing mouse cerebellum. Current Biology *9*, 445–448.

Wang, R., Chadalavada, K., Wilshire, J., Kowalik, U., Hovinga, K.E., Geber, A., Fligelman, B., Leversha, M., Brennan, C., and Tabar, V. (2010). Glioblastoma stem-like cells give rise to tumour endothelium. Nature *468*, 829–833.

Wang, V.Y., Rose, M.F., and Zoghbi, H.Y. (2005). Math1Expression Redefines the Rhombic Lip Derivatives and Reveals Novel Lineages within the Brainstem and Cerebellum. Neuron *48*, 31–43.

Wang, X., Lou, N., Xu, Q., Tian, G.-F., Peng, W.G., Han, X., Kang, J., Takano, T., and Nedergaard, M. (2006). Astrocytic Ca2+ signaling evoked by sensory stimulation in vivo. Nat Neurosci *9*, 816–823.

Wechsler-Reya, R.J., and Scott, M.P. (1999). Control of neuronal precursor proliferation in the cerebellum by Sonic Hedgehog. Neuron *22*, 103–114.

Wetmore, C., Eberhart, D.E., and Curran, T. (2001). Loss of p53 but not ARF accelerates medulloblastoma in mice heterozygous for patched. Cancer Research *61*, 513–516.

Wright, J.H. (1910). Neurocytoma or neuroblastoma, a kind of tumor not generally recognized. J Exp Med *12*, 556–561.

Yang, Z.-J., Ellis, T., Markant, S.L., Read, T.-A., Kessler, J.D., Bourboulas, M., Schüller, U., Machold, R., Fishell, G., Rowitch, D.H., et al. (2008). Medulloblastoma Can Be Initiated by Deletion of Patched in Lineage-Restricted Progenitors or Stem Cells. Cancer Cell *14*, 11–11.

Zhao, X., Liu, Z., Yu, L., Zhang, Y., Baxter, P., Voicu, H., Gurusiddappa, S., Luan, J., Su, J.M., Leung, H.C.E., et al. (2012). Global gene expression profiling confirms the

molecular fidelity of primary tumor-based orthotopic xenograft mouse models of medulloblastoma. Neuro-Oncology *14*, 574–583.

Zhukova, N., Ramaswamy, V., Remke, M., Pfaff, E., Shih, D.J.H., Martin, D.C., Castelo-Branco, P., Baskin, B., Ray, P.N., Bouffet, E., et al. (2013). Subgroup-Specific Prognostic Implications of TP53 Mutation in Medulloblastoma. J Clin Oncol *31*, 2927–2935.

Zong, H., Espinosa, S., Su, H.H., Muzumdar, M.D., and Luo, L.Q. (2005). Mosaic analysis with double markers in mice. Cell *121*, 479–492.

Figure Legends

Figure 1. The Establishment of a MADM-based Medulloblastoma Model.

(A-C) Normal developmental process of cerebellum. Granule neuron progenitors are derived from a small number of embryonic neural stem cells (NSCs) (A, magenta dots in the ventricular zone-VZ) that migrate through the rhombic lip (A, yellow dot) and eventually settle on the surface of the cerebellar anlage (A, blue dots in the external germinal layer- EGL). While GNPs are unipotent and only give rise to granule neurons (B, right), NSCs generate all other neurons and astrocytes (B, left). GNPs proliferate in the postnatal EGL, then migrate along Bergmann glia processes (GFAP staining in C) in the molecular layer (ML) into the inner granule layer (IGL) and differentiate into mature granule neurons.

(D) MADM-based medulloblastoma model. From a colorless, $Ptch^{+/-}$ and $p53^{+/-}$, heterozygous mouse, GNP-specific *Math1-Cre* drives inter-chromosomal mitotic recombination to generate GFP-expressing $Ptch^{+/-}; p53^{-/-}$ GNPs and RFP-expressing $Ptch^{+/-}; p53^{+/+}$ GNPs. While red and most green GNPs differentiate into granule neurons, one or a few green GNPs eventually transform into medulloblastoma.

(E) In MADM-generated medulloblastoma, tumor cells will be GFP+ while niche cells will be unlabelled, allowing single-cell resolution analyses of niche establishment and tumor-niche interactions throughout tumor progression.

(F) In MADM mice without mutations, *Math1-Cre* labels sparse cells in IGL.

(G) *Math1-Cre* is restricted in GNPs since all MADM-labeled cells are granule neurons in IGL.

(H) MADM model allows observation of gradual tumor progression. Around P60, small tumors appear as focal GFP+ cell clusters, mainly on the surface of cerebellum as the remnant of EGL (left). Around P75, GFP+ cells in medium-sized tumors start infiltrating into normal cerebellar structure(middle). After P90, large tumors infiltrate multiple folia and distort normal cerebellar structure (right).

(I) Small, focal accumulations of GFP-positive cells are neoplastic (Ki67-positive, from boxed region in H).

[VZ= ventricular zone, NSC= neural stem cell, RL= rhombic lip, EGL= external germinal layer, GNP= granule neuron precursor, ML= molecular layer, IGL= internal granule layer]

Scale bars: A= 100μm; C,I= 50μm; F, H= 500μm; G= 10μm.

See also Figure S1.

Figure 2. Detailed Analyses of the Tumor Niche With MADM Reveals a Transdifferentiation Phenomenon.

(A) Blood vessels (CD34+) show enlarged lumen in GFP+ tumor regions compared to adjacent normal tissue, in both small and large tumors. Third and fourth column show GFP+ tumor cells are in close contact with vessels.

(B) Microglia/macrophages (IBA-1+) are enriched with activated morphology in GFP+ small tumor regions compared to adjacent normal tissue (second column) and persist in large tumors (fourth column). Many of them appear to have phagocytosed GFP+ tumor cell fragments in the cytoplasm (circled).

(C) Oligodendrocyte progenitor cells (PDGFRα+) are enriched in tumors (note few PDGFRα+ cells in normal cerebellum).

(D) Astrocytes (GFAP+) are present in small and large tumors. Distinct from all other niche cells, GFAP+ cells are also GFP+ (arrowheads, third column), suggesting transdifferentiation of GFP+ tumor GNPs into astrocytes (GFP+/GFAP+). All GFAP+ cells in large tumors are also GFP+.

(E-F) Another astrocyte marker, BLBP, is colocalized with GFP+ cells only in tumor regions (E, inset). BLBP+ astrocytes outside of the tumor region show no colocalization with GFP (F, from boxed region in E), suggesting the transdifferentiation is a tumor-specific phenomenon. [N= normal tissue]

(G) Transdifferentiation of tumor cells into astrocytes occurs in tiny lesions.

Scale bars: A-D (from left to right) panel 1,2,4= 50μm, panel 3= 10μm; E,F= 100μm, E inset= 10μm. G= 100μm

See also Figure S2.

Figure 3. TuAstros Bear Salient Astrocytic Features and Can Be Transdifferentiated From Postnatal GNPs.

(A-D) Tumor astrocytes displayed stereotypic astrocyte morphologies. In the normal cerebellum, Bergmann glia are GFAP+ and have distinct radial processes through the ML of all folia (A). Similar organization can be found in focal areas of tumors (B, middle outlined in dotted magenta lines), where the morphologies of TuAstros closely resemble Bergmann glia (C, D).

(E) TuAstros (GFP/GFAP+) closely interact with blood vessels (CD34+), often wrapping an entire vessel.

(F) To determine the ability of postnatal GNPs to transdifferentiate into tumor astrocytes an inducible *Math1-CreER; Ptc+/-; p53flox/p53flox; ROSA26-LSL-RFP* conditional knockout model was used. Mutation of GNPs was induced by tamoxifen administration between P7 and P10, and mice were assessed at P90 for tumor formation.

(G) Tumors induced from postnatal GNPs contained TuAstros (RFP/BLBP+).

[ML= Molecular Layer, TAM= tamoxifen, P= postnatal day]

Scale bars: A-E= 50μm; E bottom panel= 10μm; G= left panel 500μm, right panels 50μm

See also Figure S3.

Figure 4. Astrocytes in Human Medulloblastoma Are Lineage-Related to Tumor Cells.

(A) Schematic illustration of possible cytogenetic patterns of astrocytes in human medulloblastoma. Left: astrocytes are entrapped normal cells and are not lineage-related to tumor cells. Right: astrocytes are lineage-related to tumor cells.

(B) CD34+ endothelial cells in the tumor mass have normal karyotype at the *PTCH1* locus, while surrounding tumor cells show the missing of one *PTCH1* allele, suggesting the loss of chromosomal fragment occurred in somatic cells but not in germline.

(C) The identical loss of one allele from the *9q21.33* region to the *PTCH1* locus is seen in astrocytes and surrounding tumor cells, suggesting that they are lineage-related.

Cartoon: green FISH probe marks *9q21.33* and red FISH probe marks *PTCH1* locus. Asterisk marks a GFAP+ astrocyte that has a single allele of 9q chromosome fragment, similar to surrounding tumor cells [arrowheads] (DAPI+ nuclei are blue).

(D) Serially xenografted SHH-subtype human medulloblastoma cells (passage 12 shown here) give rise to sporadic cells with astrocytic morphology that stain positive for human GFAP throughout the tumor mass. While surrounding tumor cells are dividing, hGFAP+ astrocytes are not dividing.

[FISH= Fluorescent In Situ Hybridization, IF= immunofluorescence]

Scale bars: B,D= 50μm, B-C= left panel 25μm, right panel 10μm.

See also Figure S4.

Figure 5. TuAstros do not Function as Cancer Stem Cells to Give Rise to Tumor GNPs.

(A) Schematic illustration of the mouse model used for lineage tracing of TuAstros and expected outcomes.

(B) TuAstros do not give rise to tumor GNPs in primary tumors within two weeks.

(C) TuAstros do not give rise to tumor GNPs in secondary tumors within two months.

[Glast= Glutamate Transporter]

Scale bars: B-C = 50μm.

See also Figure S5.

Figure 6. Proliferation of Mutant GNPs in Pre-neoplastic Lesions Strongly Correlate With the Presence of TuAstros.

(A) Pre-neoplastic lesions, manifested as small clusters of GNPs on the surface of folia after cerebellar developmental period, occur at high frequency in *Ptch+/-* mice, but only 15-20% of them will eventually progress to form tumors (Oliver, 2005).

(B) Proliferation of mutant GNPs in the presence of TuAstros.

(C) Lack of proliferation of mutant GNPs in the absence of TuAstros.

(D) Examination of 33 different PNLs revealed a strong correlation between GNP proliferation and the presence of TuAstros.

Scale bars: B-C = 50μm.

See also Figure S6.

Figure 7. TuAstros Support Tumor GNP Survival and Proliferation in Culture.

(A) Schematic illustration of experimental paradigm and expected outcomes.

(B) Dissociated tumor cells cultured in serum-free medium tailored for astrocytes can enrich TuAstro-like cells after 3 DIV, which have fan-like astrocytic morphologies. Most of them express GFAP.

(C) Tumor GNPs (*Math1-GFP+*) were sparsely seeded onto RFP+ TuAstros, which divided irrespective to their distance to TuAstros initially.

(D) 72hr later, most proliferating tumor GNPs situate near or on TuAstros.

(E) Among all survived GNPs, most of them reside within the 30μm radium from TuAstros (left graph, **p=0.03,* n=3). The percentage of proliferative tumor GNPs is significantly higher when they are near or on TuAstros (right graph, **p=0.028,* n=3).

(F-I) Live imaging of co-cultures for 48hr revealed that GNPs far from TuAstros (panels in G are time series images of red box in F) initially proliferated (G, 24h), but eventually

died (G, 48h), and that GNPs in close proximity or on top of TuAstros (panels in H are time series images of green box in F) either migrate onto TuAstros (H, arrowhead 0-14h) or continue to survive and proliferate (H, 48h).

(J) Tumor GNPs within 30μm of TuAstros migrated and survived, whereas those beyond 30 μm did not survive.

(K) While tumor GNPs within 30μm to TuAstros double in number within 48hr, the number of tumor GNPs beyond 30μm shows more than 50% decrease in >20 TuAstros field of a single imaging experiment.

[DIV= days *in vitro]*

Scale bars: B-F,I,J= 50μm; G,H= 20μm.

See also Figure S7.

Tables

Table 1. Detailed Quantification of FISH Results.

Case	Tumor Cells -9q/ -PTCH/ -GFAP	Tumor Astrocytes -9q/ -PTCH/ +GFAP
1	53/58 (91%)	17/21 (81%)
2	36/43 (84%)	16/18 (89%)
3	50/57 (88%)	15/18 (83%)
4	71/81 (88%)	31/35 (89%)
5	51/56 (91%)	8/10 (80%)
6	59/66 (89%)	26/32 (81%)
TOTAL	320/361 (89%)	113/134 (84%)

Figure 1

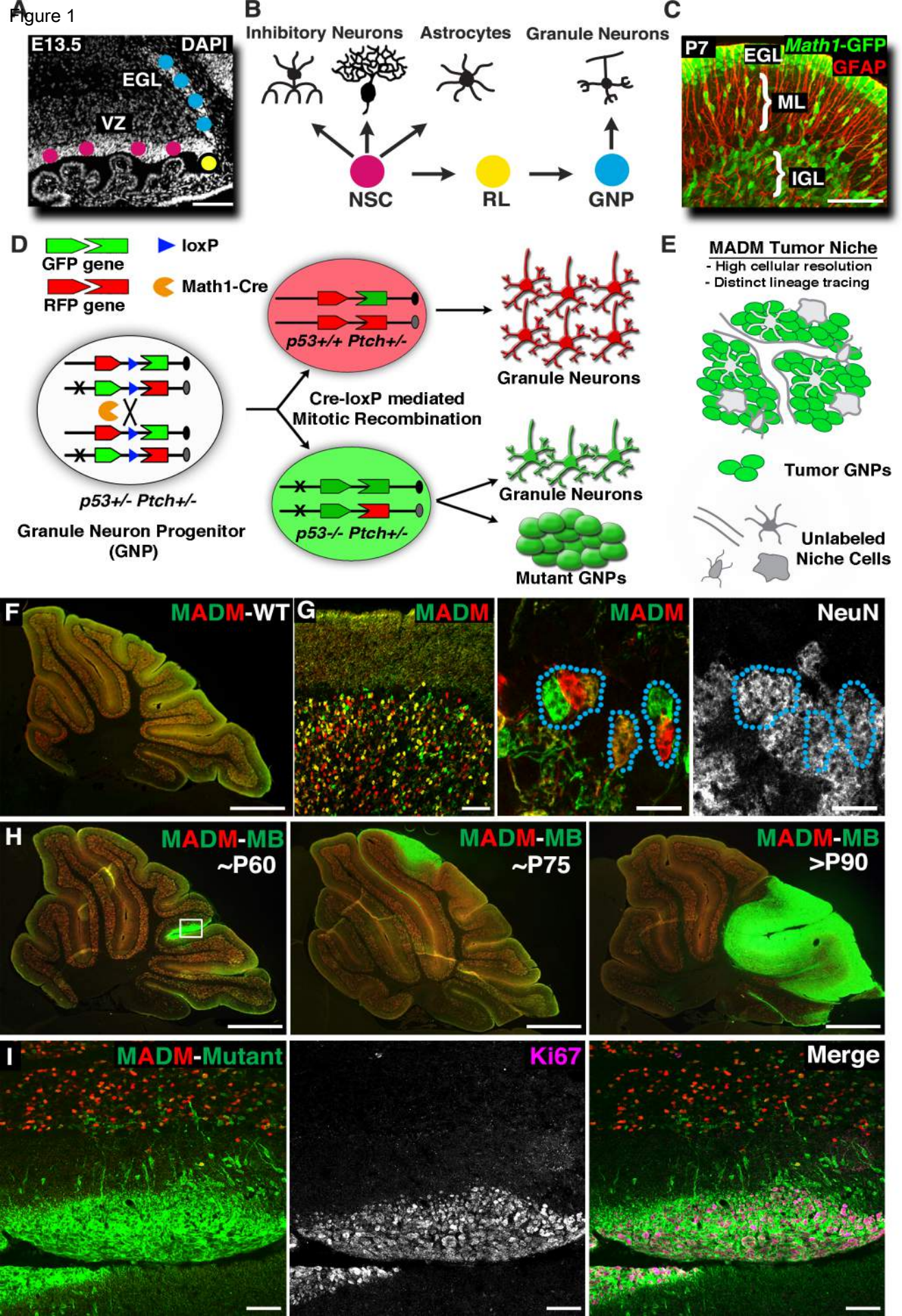
A
E13.5
DAPI
EGL
VZ
B
Inhibitory Neurons
Astrocytes
Granule Neurons
NSC
RL
GNP
C
P7
EGL
Math1-GFP
GFAP
ML
IGL
D
GFP gene
RFP gene
loxP
Math1-Cre
p53+/- Ptch+/-
Granule Neuron Progenitor (GNP)
p53+/+ Ptch+/-
Cre-loxP mediated Mitotic Recombination
p53-/- Ptch+/-
Granule Neurons
Granule Neurons
Mutant GNPs
E
MADM Tumor Niche
- High cellular resolution
- Distinct lineage tracing
Tumor GNPs
Unlabeled Niche Cells
F
MADM-WT
G
MADM
MADM
NeuN
H
MADM-MB ~P60
MADM-MB ~P75
MADM-MB >P90
I
MADM-Mutant
Ki67
Merge

Figure 2

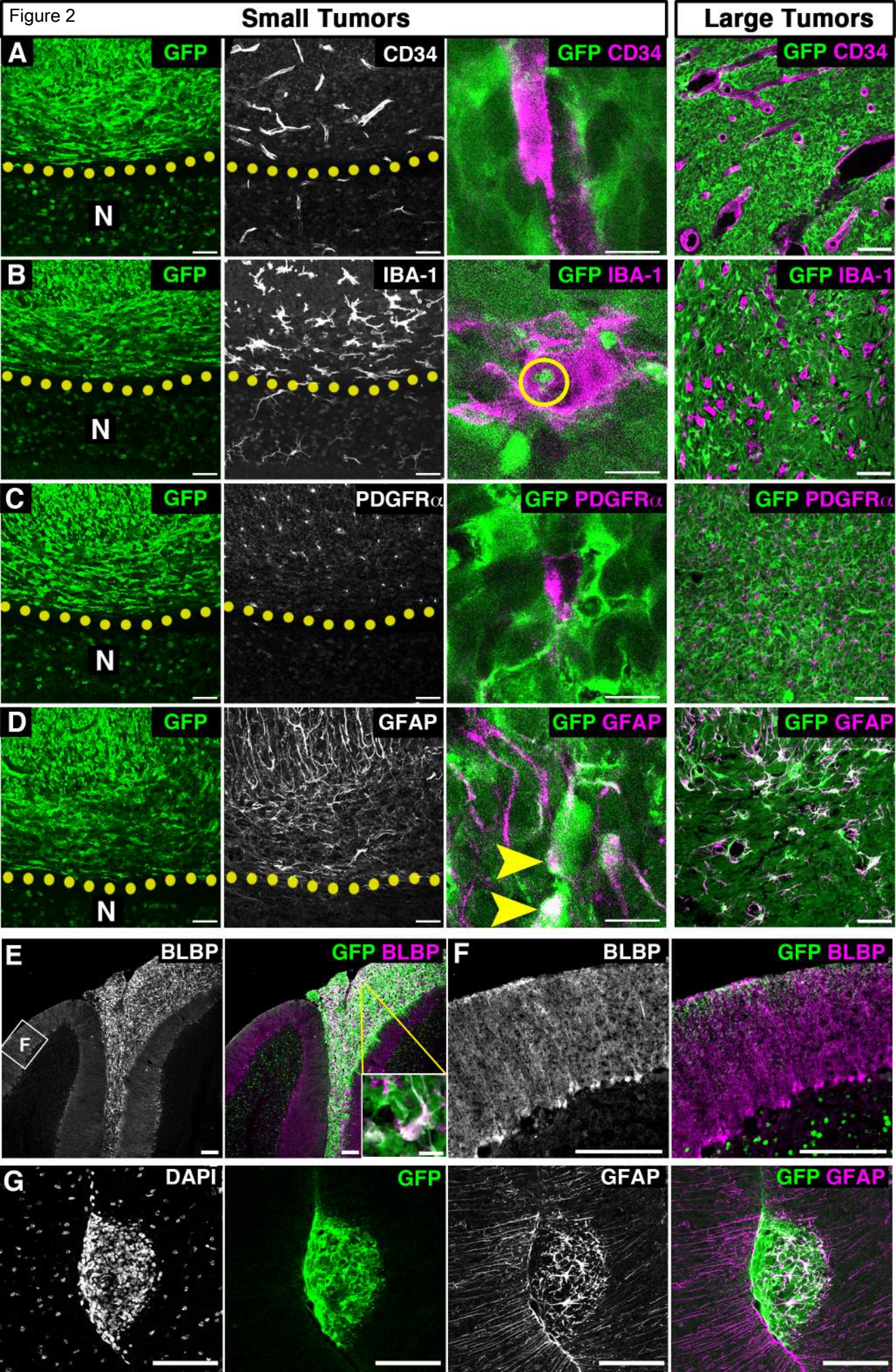
Small Tumors
Large Tumors
A
GFP
CD34
GFP CD34
GFP CD34
N
B
GFP
IBA-1
GFP IBA-1
GFP IBA-1
N
C
GFP
PDGFRα
GFP PDGFRα
GFP PDGFRα
N
D
GFP
GFAP
GFP GFAP
GFP GFAP
N
E
BLBP
GFP BLBP
F
F
BLBP
GFP BLBP
G
DAPI
GFP
GFAP
GFP GFAP

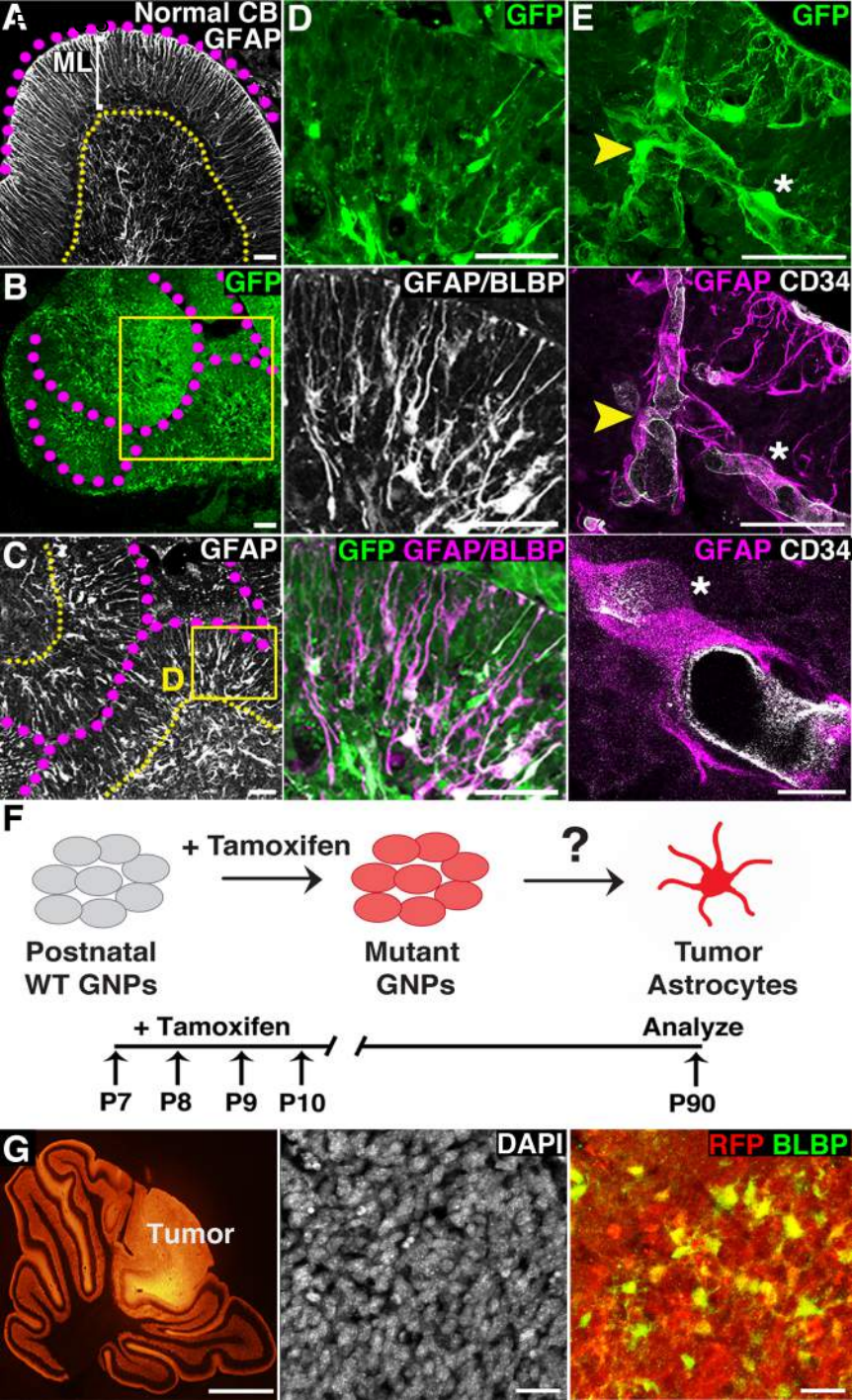
A
Normal CB
GFAP
ML
D
GFP
E
GFP
B
GFP
GFAP/BLBP
GFAP CD34
C
GFAP
D
GFP GFAP/BLBP
GFAP CD34
F
+ Tamoxifen
?
Postnatal
WT GNPs
Mutant
GNPs
Tumor
Astrocytes
+ Tamoxifen
Analyze
P7
P8
P9
P10
P90
G
Tumor
DAPI
RFP BLBP

A
Distinct Lineages
vs.
Related Lineage
Tumor Cell
self renew
Tumor Cell
Normal Cell
Infiltrates tumor
Normal Cell
Proliferation
Tumor Cell
Tumor Cell
Trans-differentiation
Tumor Astrocyte
B
Human Tumor Endothelial Cells
Normal Karyotype
CD34 PTCH1 DAPI
PTCH1
C
Human Tumor Astrocytes
Mutant Karyotype
GFAP/9q PTCH1 DAPI
9q21.33 PTCH1
D
Human Tumor Xenograft
DAPI
human GFAP
human GFAP KI67

Figure 4

Figure 5

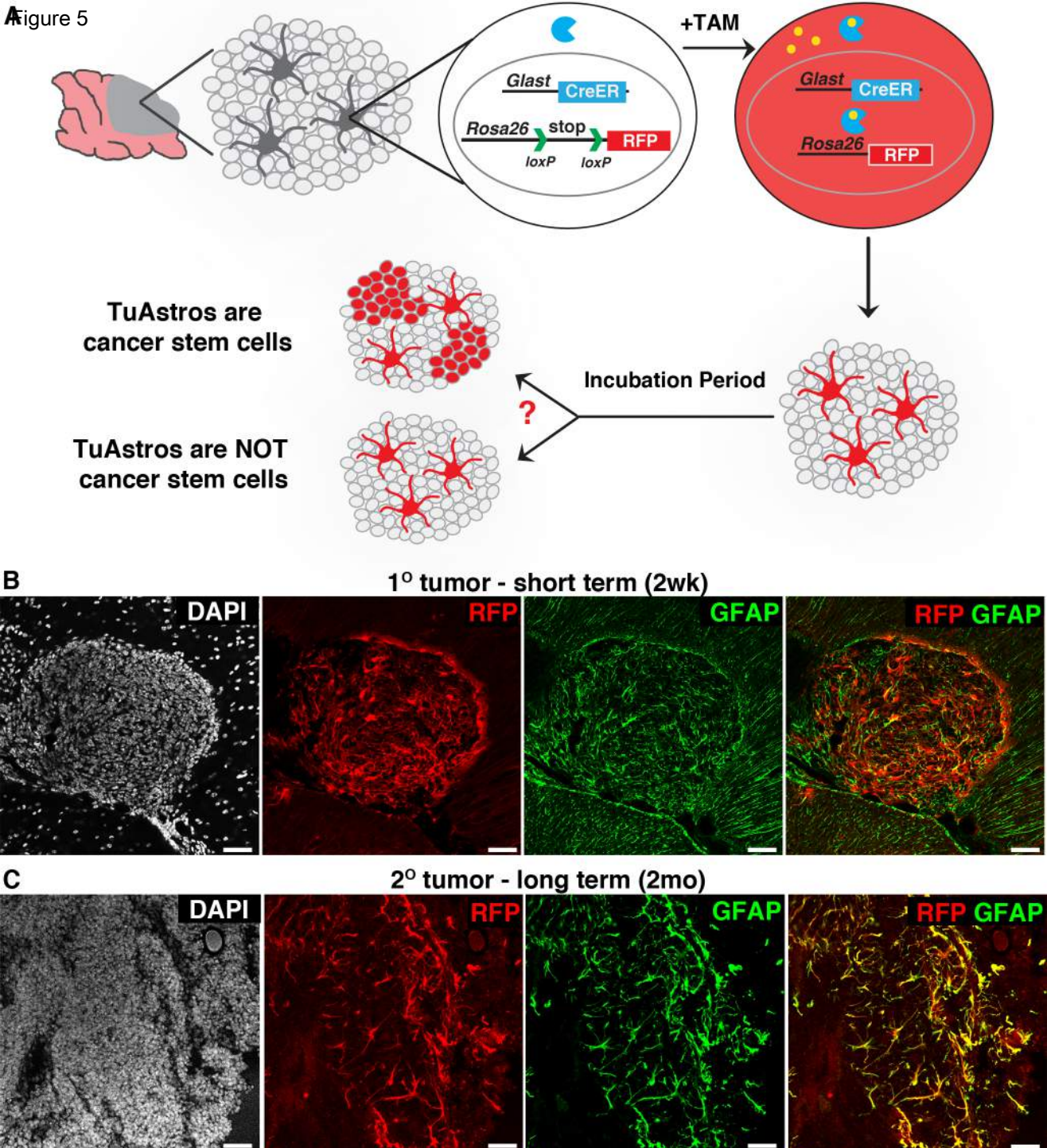
A
Glast
CreER
Rosa26
stop
RFP
loxP
loxP
+TAM
Glast
CreER
Rosa26
RFP
TuAstros are cancer stem cells
TuAstros are NOT cancer stem cells
?
Incubation Period
B
1° tumor - short term (2wk)
DAPI
RFP
GFAP
RFP GFAP
C
2° tumor - long term (2mo)
DAPI
RFP
GFAP
RFP GFAP

Figure 6

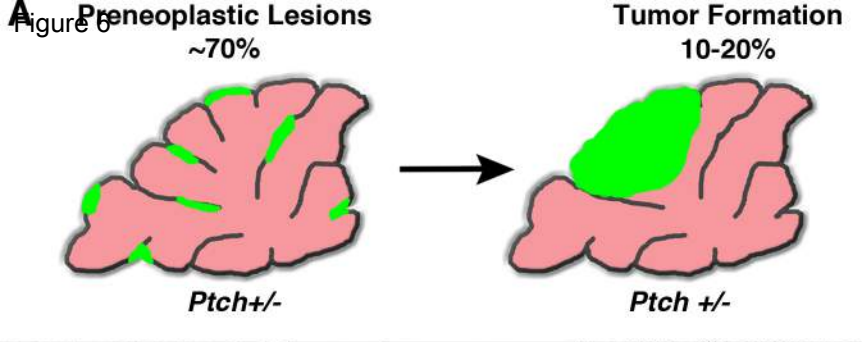

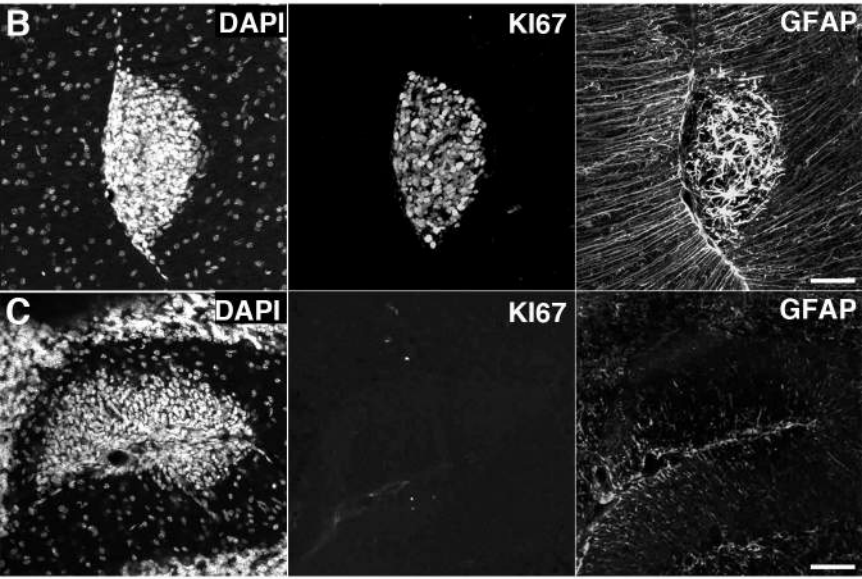

D

Astrocyte presence in proliferating PNLs

	KI67 +	KI67 -
GFAP +	14	1
GFAP -	2	16

Figure 7

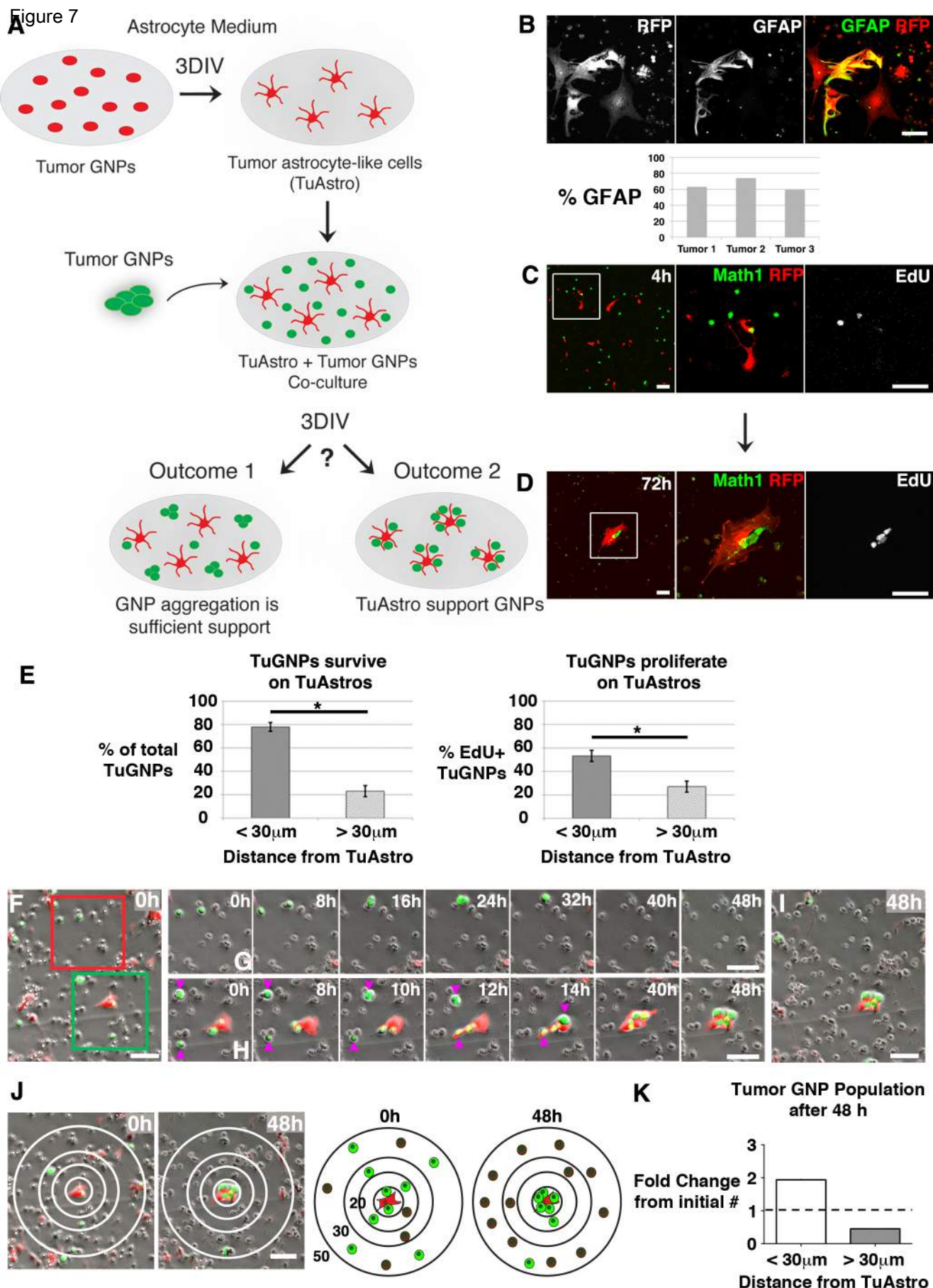
A
Astrocyte Medium
3DIV
Tumor GNPs
Tumor astrocyte-like cells (TuAstro)
Tumor GNPs
TuAstro + Tumor GNPs Co-culture
3DIV
?
Outcome 1
Outcome 2
GNP aggregation is sufficient support
TuAstro support GNPs
B
RFP
GFAP
GFAP RFP
% GFAP
100
80
60
40
20
0
Tumor 1
Tumor 2
Tumor 3
C
4h
Math1 RFP
EdU
D
72h
Math1 RFP
EdU
E
TuGNPs survive on TuAstros
% of total TuGNPs
100
80
60
40
20
0
*
< 30μm
> 30μm
Distance from TuAstro
TuGNPs proliferate on TuAstros
% EdU+ TuGNPs
100
80
60
40
20
0
*
< 30μm
> 30μm
Distance from TuAstro
F
0h
G
0h
8h
16h
24h
32h
40h
48h
H
0h
8h
10h
12h
14h
40h
48h
I
48h
J
0h
48h
0h
48h
20
30
50
K
Tumor GNP Population after 48 h
Fold Change from initial #
3
2
1
0
< 30μm
> 30μm
Distance from TuAstro

Supplemental Experimental Procedures

Mouse Lines

All animal procedures were based on animal care guidelines approved by the Institutional Animal Care and Use Committee (IACUC) at the University of Virginia. The following mouse lines were used to generate MADM experimental and control mice: *MADM-ML* pair *TG11ML*, *GT11ML* (Henner et al., 2013) JAX#022977, 022976, *Math1-Cre* (Matei et al., 2005) JAX#011104, *p53KO* (Jacks et al., 1994) JAX#002101, and *Ptc+/-* (Goodrich et al., 1997) JAX#003081. For the conditional knockout model these additional lines were used: *Math1-CreERT2* (Machold and Fishell, 2005) JAX#007684, *GLAST-CreER* JAX#012586, *p53flox* (Marino et al., 2000) JAX#008462, *Rosa-floxed stop- tdTomato* JAX#007908, *Math1-GFP* (Lumpkin et al., 2003), *Aldh1l1-GFP* MMRRC#011015-UCD.

Tamoxifen Administration

For perinatal mice, tamoxifen (Sigma T5648) was dissolved in 100% ethanol at 200 mg/mL in 37 ^{O}C water bath, then further diluted in corn oil to 20 mg/mL. Solution was injected subcutaneously at the nape. For adult mice, tamoxifen citrate tablets (10 mg/tablet; Mylan) were ground and dissolved at 200 mg/mL and delivered via oral gavage.

Tissue Preparation

Following anesthesia, mice were transcardially perfused with 4 ^{O}C pre-perfusion buffer (PBS, 1% Procaine, 0.01% Heparin) followed by 4 ^{O}C 4% paraformaldehyde (PFA) according to standard procedure. Brains were removed and postfixed in 4% PFA overnight, then cryoprotected in 30% sucrose overnight, all at 4^{O}C. Tissue was embedded in optimal cutting temperature (OCT) medium for cryosectioning and stored at -80^{O}C. Tissue blocks were sectioned at 20 □m on a cryostat, allowed to dry at room temperature for ~1bhr before storing at -80 - 80^{O}C or proceeding to immunostaining.

Tissue Immunostaining

Fluorescent labeling from MADM cassette recombination produces cells expressing GFP or tdTomato, which occupy the green (~488 nm) and red (~543 nm) spectra, therefore other antibodies used on MADM brains were primarily detected in the far-red (~635 nm) and ultraviolet (~405 nm) spectra. For conditional knockout models and secondary orthografts, tdTomato occupied the red (~543 nm) spectrum.

Detailed staining procedures:

Tissue section slides were re-hydrated and washed in phosphate buffered saline (PBS) for 5 minutes repeated 3 times. Slides were then incubated in permeabilizing/blocking buffer (0.3% Triton-X 100 in PBS [PBT] plus 5% normal donkey serum [NDS]) for 30 min at room temperature. Slides were then incubated with appropriate combination of primary antibodies (Table S1) in

PBT+0.5% bovine serum albumin overnight at 4 ^{O}C. Sections were washed three times in PBT (10 minutes each) followed by incubation with appropriate fluorophore-conjugated secondary antibody (Table S1) overnight at 4 ^{O}C or at room temperature (RT) for 4 hours. Sections were then washed three times in PBT (10 min each) and one time in PBS.

*To visualize nuclei slides were incubated in DAPI solution (1□g/mL in PBS) for 10 minutes then washed once with PBS before coverslip mounted with anti-fade mounting medium.

*If four primary antibodies were used and secondary antibodies to all four fluorescent channels were assigned (488,555,647,405), DAPI step is excluded. For extensive procedural details refer to (Liu et al., 2011).

Tissue Culture Staining

Coverslips of cells for immunofluorescence were fixed with 4% PFA for 20 minutes at RT and washed with PBS. Cells were permeabilized with 0.1% PBT for 10 minutes before addition of blocking solution (10% NDS in 0.1%PBT) for 20 minutes at RT. Appropriate primary antibodies (Table S1) were incubated on slides in antibody solution (PBS + 0.5% BSA) for 1 hr at RT then washed twice in PBS and once in 0.1% PBT (5 minutes each). Appropriate secondary antibodies were incubated on slides in 0.1% PBT for 30 minutes at RT. Slips were then washed twice in PBS and once in 0.1% PBT (5 minutes each). To visualize nuclei, slips were incubated in DAPI solution (1 □g/mL in PBS) for 3 minutes then

washed once with PBS before mounting on glass slides with anti-fade mounting medium.

EdU labeling and Click-iT Detection

To assess *in vitro* cell proliferation, 5-ethynyl-2'-deoxyuridine (EdU) (Invitrogen-A10044) was added to wells (10 □M final concentration) 2-3 hours prior to fixation.

Following fixation and permeabilzation as described above, Click-iT reaction was performed prior to incubation with block and primary antibody. Briefly, for a single reaction at 250 □L per coverslip the following are combined in this order: Distilled water (175 □L), 1M Tris-HCL pH 8.5 (25 □L), 1M CuSO4 (0.25 □L), Alexa Fluor 647 Azide (Invitrogen-A10277), mix, then just prior to application add 0.5M sodium L-ascorbate (50 □L) and mix. Apply 250 □L of reaction solution to permeabilzed cell coverslip and incubate for 30 minutes at RT protected from light. Wash twice with PBS (5 minutes each) and proceed with primary antibody incubation as described above while protecting from light.

Imaging

Fluorescent images were acquired on a Zeiss LSM 710 at the Advanced Microscopy Facility at the University of Virginia. For live imaging, an initial fluorescent image was taken at start of experiment followed by consecutive brightfield images taken every 2 hours for a 48 hour period and a final fluorescent image taken at the end. Sixty fields of view over six wells of a tissue culture plate

were imaged and analyzed. These experiments were performed on EVOS FL Auto Cell Imaging System (Life Technologies) equipped with environmental control platform. Both confocal and live images were processed with ImageJ and Adobe Photoshop.

Quantification & statistics

Quantification of niche cells throughout tumor development

Tissue sections from at least 3 mice at 3 distinct stages (early, mid, late) of tumor development were immunostained for MADM fluorescent proteins, CD34 for blood vessels, IBA-1 for microglia/macrophages, PDGFRα for oligodendrocyte precursor cells, BLBP to visualize astrocyte cell bodies, and DAPI for all nuclei. Three images were taken per tumor at 200X magnification throughout the tumor. Due to ambiguity in determining individual tumor GNPs, given the dense cellularity of these tumors, DAPI was used as a proxy for total tumor cell number. Some niche cells will also be included in this number, but their presence is so low, compared to GFP+ tumor cells, that inclusion of these cells in total tumor cell number will not significantly effect interpretation. Blood vessel density was determined by quantifying the % area occupied by CD34+ signal. Microglia/macrophage numbers were determined by counting the number of IBA-1+ cells per field of view. Oligodendrocyte precursor cell numbers were determined by counting the number of PDGFRα+ cells per field of view. Tumor astrocyte numbers were determined by counting the number of BLBP+ cells per field of view. The percentage of niche cell population numbers was calculated by

dividing the # of marker-positive cells by the # of total DAPI+ cells in the same field of view and multiplied by 100. ImageJ was used for image processing and counting. Excel and Graph Pad Prism were used to perform statistical analysis and t-test was applied to determine significance.

Quantification of in vitro proliferation, cell death, and differentiation in co-culture assay

After coverslips were immunostained for EdU (proliferation), DAPI (pyknotic nuclei for cell death), or Tuj1 (neuronal differentiation) 6 images (200X) were taken across two coverslips per group. Tumor cells were counted as tdT+ and verified with DAPI when cells were aggregated. Cell phenotype markers were counted and divided by the total number of tumor cells, then multiplied by 100 to represent % of population. Significance of quantification was determined using a paired Student's T-test with standard error of mean (SEM). Live images were quantified by identifying single astrocytes, by fluorescence and morphology, among images and then creating concentric circles about the origin of these cells to demarcate distances in ImageJ. GFP+ cells were tracked and counted over time within these delineations and averaged across fields of view. Fluorescence was confirmed at endpoint for each cell.

Purification of Tumor GNPs and FACS purification of Aldh1L1-GFP Astrocytes

Perinatal mice up to P5 were directly decapitated. >P5 tumor mice were anesthetized with ketamine/xylazine (80-100 mg/kg and 10-20 mg/kg, respectively) followed by cervical dislocation and decapitation.

Tissue Dissociation for tumor GNP purification and Aldh1L1-GFP cortical astrocytes

This procedure is adapted from (Foo, 2013; Foo et al., 2011).

Briefly, tumor tissue was microdissected away from normal tissue under a fluorescent macroscope to visualize GFP or tdTomato tumor regions. For Aldh1L1-GFP cells, P1-7 cortical caps dissected off and cut into ~2 mm pieces. Tissue pieces were digested in oxygen-equilibrated enzyme stock solution (final conc. 1XEBSS [Sigma E7510], 0.46% D-glucose, 26 mM $NaHCO_3$, 0.5 mM ethylenediaminetetraacetic acid (EDTA), deionized water) plus 150 U papain (Worthington LS003126) and DNaseI (250 mg/mL final conc; Sigma DN25) at 37 ^{O}C in 5% CO_2 for 45 minutes, swirling every 15 minutes. Digestion solution with tissue pieces was transferred to a 50 mL conical tube and liquid aspirated leaving tissue pieces. Enzyme neutralization was achieved by adding 3 ml of Low Ovo inhibitor solution (final conc. 1X Earl's balanced salt solution (EBSS), 0.46% D-glucose, 26 mM $NaHCO_3$, 0.15% BSA, 0.15% ovomucoid [Worthington LS003086], 250 mg/mL DNaseI), swirling then aspirating liquid, leaving tissue pieces. Begin trituration of tissue pieces by adding 5 mL of Low Ovo solution and using a 10 mL serological pipette slowly triturate tissue up and down approximately 5-10 times depending on amount of tissue. After remaining tissue

pieces settle, collect supernatant into a new 50 mL conical (these are all tumor cells). Repeat trituration with 5 mL Low Ovo and collect supernatant until only few tissue pieces are remaining (myelin-dense tissues). Underlay Low Ovo cell suspension with 10 mL High Ovo solution (final conc. 1X EBSS, 0.46% D-glucose, 26 mM NaHCO3, 0.3% BSA, 0.3% ovomucoid [Worthington LS003086], 250 mg/mL DNaseI). Spin down cells at 1000 rpm (180 rcf) for 7 minutes. Aspirate liquid and resuspend cell pellet in 8 mL panning buffer (final conc. 0.2% BSA, 1.2% D-glucose, DPBS-CMF [Invitrogen 14190-250]). To achieve single cell suspension, strain cell suspension from 70 □M cell strainer (Fisher 22-363-548).

Percoll gradient subfractionization for GNP purification

Adapted from (Baptista et al., 1994; Hatten, 1985):

Transfer cell suspension to a 15 mL polystyrene conical tube. Underlay cell suspension with 35% Percoll solution (For 10 mL: 4 mL sterile deionized water, 2.5 mL 4X calcium-, magnesium-free (CMF)-PBS-EDTA [NaCl 32 g/L, KCl 1.2 g/L, D-Glucose 8 g/L, NaH2PO4.H2O 2 g/L, KH2PO4 1 g/L, NaHCO3 8 ml/L of 2% stock, EDTA 10 ml/L of 1M EDTA, pH 8.0, deionized water, pH to 7.4 with NaOH, filter sterilize], 3.5 mL Percoll [Sigma P4937], Phenol red indicator to a light pink, 2N HCl 10-20 □L until solution is pink-orange) using a Pasteur glass pipette full of percoll solution. Underlay cell suspension/35% Percoll solution with 60% Percoll solution (For 10 mL: 1.5 mL sterile deionized water, 2.5 mL 4X CMF-PBS-EDTA, 6.0 mL Percoll, Phenol red indicator to a light pink, 2N HCl 15-30 □L

until solution is pink-orange, then add 30 μL 0.4% Trypan Blue) again with Pasteur glass pipette full of percoll solution. Spin gradient suspension at 2700 rpm (1300 rcf) for 20 minutes at RT. Two bands of cells are present, one at the cell suspension/35% percoll interface and a second at 35%/65% percoll interface. Cells at the 35/65 interface are GNPs and are collected in new 15 mL conical tube, and washed with panning buffer filled to top then pelleted and resuspended in desired medium and volume.

In vitro transdifferentiation of tumor GNPs into tumor astrocytes and co-culture

Purified tumor GNPs (RFP+ from CKO model) are seeded at high density (500,000 cells/1.9 cm^2. Single well in 24 well plate) onto PDL-coated glass coverslips in astrocyte media: 50% Neurobasal (Invitrogen #21103-049), 50% DMEM (Invitrogen #11995-065), 2% B27 supplement minus insulin (Invitrogen #0050129SA), 1% Penicillin/Strepomycin (Invitrogen #15140122), 1 mM Sodium pyruvate (Invitrogen #11360-070), 292 μg/ml Glutamax (Invitrogen #35050061), 1x SATO (Foo, 2013), 5 μg/mL N-Acetyl-cysteine (Sigma #A8199), 500 ng/ml insulin (Sigma #I6634), 5 ng/ml human recombinant heparin-binding epidermal growth factor (HB-EGF) (Sigma #E4643). After 3DIV coverslip plate is vigorously shaken and a few horizontal taps to dislodge dead cells and any GNP aggregates (most cells will die), then media is replaced. Tumor astrocytes are very few (>500 per coverslip) and recognized by larger flat fan-like morphologies compared to smaller round GNPs. For co-culture, tumor GNPs are purified from

CKO mice with *Math1-GFP* instead of *Rosa-fsf-tdTomato*. GFP+ tumor GNPs are seeded at low density (50,000 cells/1.9 cm^2. Single well in 24 well plate) onto coverslips with RFP+ tumor astrocytes, or without astrocytes, and cultured for 2DIV in tumor GNP media: Neurobasal medium, 2% B27 supplement minus insulin, 1% Penicillin/Streptomycin, 0.45% D-glucose (45% stock in Dulbecco's PBS [DPBS]; Fisher #D16-1), 500 ng/ml insulin and 5 ng/ml HB-EGF for astrocyte survival.

Fluorescent Activated Cell Sorting (FACS) of *Aldh1L1-GFP* astrocyte and culture conditions

Strained cells from dissociation were sorted based on their GFP expression at the University of Virginia Flow Cytometry Core Facility on a BD FACSVantage SE TurboSort DIVA and BD Influx cell sorter according to standard gating for single cells and selection of all GFP+ cells. Sorted cells were spun down, resuspended and seeded into poly-D-lysine coated T25 cm^2 flask in growth medium base (tumor GNP media) with 50 ng/mL HB-EGF. To reduce growth and promote maturation when cells are seeded on coverslips for co-culture with tumor GNPs, HB-EGF was reduced to 5 ng/mL.

Fluorescent *In Situ* Hybridization of chromosome loci with immunofluorescence

TMA Paraffin sections were mounted on silanized slides, baked for 5 minutes at 90 °C, and then de-paraffinized in Xylene. Slides are briefly dehydrated in 100%

ETOH followed by 35 minutes in hot 1 mM EDTA. Sections were rinsed in dH_2O and incubated with GFAP or CD34 primary antibodies (Abcam) diluted in CAS Block (Invitrogen Corporation). Slides were washed in 1X PBS and then incubated with FITC conjugated fluorescent secondary antibody (Abcam) diluted in CAS Block. There is an additional wash in 1XPBS followed by fixation in 4% paraformaldehyde (USB Corporation) for 20 minutes. Slides are dehydrated in an ethanol series and air dried. 20 µl of PTCH1/CEP9 (with GFAP) or PTCH1 only (with CD34) probe working solution (Empire genomics) is applied to the hybridization area, a 24x50 mm coverslip is placed over the top, and the edges of the coverslip are sealed with a continuous bead of rubber cement. The slide and probe are co-denatured at 95°C for 4 minutes and hybridized 24 hours or more at 37°C in a humidified chamber. Slides are then washed in 2X saline sodium citrate buffer (SSC)/0.1%NP40 at 70 degrees C for 1 minute and DAPI counterstain (Vector Laboratories) is applied as well as a glass coverslip. Visualization of the dual FISH/immunoflourescence signals is accomplished by use of a fluorescent microscope with standard filters.

Orthotopic allografting of tumor cells into the brain of NOD/SCID mice

All appropriate aseptic techniques including PPE and sterilization were followed in accordance with the UVa Rodent Survival Surgery Module with prior approval from IACUC. Purified tumor cells were obtained from primary tumor mice and 10,000 cells were injected into the striatum of NOD-SCID mice. Briefly, following anesthesia mice were mounted in stereotaxic apparatus, scalp incision made at

midline and a hole drilled through skull at -1.0mm Bregma, 2mm lateral, and 2.5mm deep. A Hamilton syringe with 5,000 cells/uL was inserted and 2uL were slowly dispensed. Syringe was removed and scalp was sutured. Mice recovered and were given analgesics.

Quantitative reverse transcription polymerase chain reaction (qRT-PCR)

Total RNA was extracted with TRI Reagent (Sigma Aldrich) followed by phenol/chloroform extraction and ethanol precipitation (Gay et al., 2013). RNA was treated with DNase I to removed residual genomic DNA (Up to 10ug RNA were resuspended in 1X DNase I Reaction Buffer (NEB #B0303S-10X) to final volume of 100uL. Add 2 units of DNase I (NEB #M0303L), mix and incubate at 37 ^{o}C for 10 minutes. Add 1 uL of 0.5M EDTA, mix and heat inactivate at 75 ^{o}C for 10 minutes.). cDNA was synthesized RNA with iScript Reverse Transcription Supermix for RT-qPCR (Bio-Rad #170-8841). qPCR was performed using an ABI 7900HT Real-Time PCR System for 40 cycles by denaturing at 95 ^{0}C for 15 seconds, annealing at 58^{0}C for 30 seconds, and extending at 72 ^{0}C for 30 seconds, ending with a default dissociation curve program. Sample amplification was performed with KAPA SYBR FAST qPCR kit (Kapa Biosystems #KK4617) with 10ng per reaction of cDNA. Relative levels of cDNA were calculated based on expression of housekeeping control gene Glyceraldehyde-3-Phosphate Dehydrogenase (*Gapdh*) to normalize expression levels between samples. Cycle threshold (CT) values were measured within the geometric amplification pahse and averaged for duplicate reactions. CT values over 35 were not considered.

Arbitrary values for gene expression in samples were normalized by subtracting the average of the internal control gene *Gapdh*.

Primers used include:

Aldh1L1 (F; 5’-GCCTTCCAACCTTCTGTTGC-3’, R; 5’-CGCCACCGAGGGAACTTAAA-3’),

Id3 (F; 5’- GCAGCGTGTCATAGACTACATC-3’, R; 5’-GTCCTTGGAGATCACAAGTTCC-3’),

Gapdh (F; 5’-CGTCCCGTAGACAAAATGGT-3’, R; 5’-GAA TTTGCCGTGAGTGGAGT-3’)

Table S1. Antibodies Used in this Study, Related to Experimental Procedures

Primary Antibody	**Vendor**	**Catalog #**	**Dilution/Application**
Rabbit anti-BLBP	Millipore	ABN14	1:250/Tissue IF
Rat anti-BrdU	Accurate Chemical	OBT0030	1:500/Tissue IF
Rat anti-CD34	Santa Cruz Biotechnology	Sc-18917	1:250/Tissue IF
Goat anti-cmyc	Novus Biologicals	NB600-338	1:200/Tissue IF
Goat anti-dsRed	Santa Cruz Biotechnology	Sc-33353	1:200/Cells IF
Rabbit anti-GFAP	Dako	Z033429-2	1:500/Tissue IF, 1:700/Cells IF
Mouse anti-GFAP	Millipore	MAB360	1:500/Tissue IF
Chicken anti-GFP	Aves Labs	GFP-1020	1:500/Tissue IF, 1:700/Cells IF
Rabbit anti-Iba1	Dako	019-19741	1:500/Tissue IF
Mouse anti-Tuj1	Sigma Aldrich	T5076	1:700/Cells IF
Secondary Antibodies	**Vendor**	**Catalog #**	**Dilution/Application**
Donkey anti-chicken Alexa Fluor 488	Jackson Immunoresearch	703-545-155	1:250/Tissue IF, 1:500/Cells IF
Donkey anti-mouse Alexa Fluor 488	Invitrogen	A21202	1:250/Tissue IF, 1:500/Cells IF
Donkey anti-rabbit Alexa Fluor 488	Jackson Immunoresearch	711-545-152	1:250/Tissue IF, 1:500/Cells IF
Donkey anti-goat Alexa Fluor 555	Invitrogen	A21432	1:250/Tissue IF, 1:500/Cells IF
Donkey anti-rabbit Alexa Fluor 555	Invitrogen	A31572	1:250/Tissue IF, 1:500/Cells IF
Donkey anti-mouse Alexa Fluor 647	Jackson Immunoresearch	715-605-150	1:250/Tissue IF, 1:500/Cells IF
Donkey anti-rabbit Alexa Fluor 647	Jackson Immunoresearch	711-605-152	1:250/Tissue IF, 1:500/Cells IF
Donkey anti-rat Alexa Fluor 647	Jackson Immunoresearch	712-605-153	1:250/Tissue IF, 1:500/Cells IF
Donkey anti-rabbit DyLight 405	Jackson Immunoresearch	711-475-152	1:250/Tissue IF

Supplemental References

Baptista, C.A., Hatten, M.E., Blazeski, R., and Mason, C.A. (1994). Cell-cell interactions influence survival and differentiation of purified Purkinje cells in vitro. Neuron *12*, 243–260.

Foo, L.C. (2013). Purification of Rat and Mouse Astrocytes by Immunopanning. Cold Spring Harbor Protocols *2013*, pdb.prot074211–pdb.prot074211.

Foo, L.C., Allen, N.J., Bushong, E.A., Ventura, P.B., Chung, W.-S., Zhou, L., Cahoy, J.D., Daneman, R., Zong, H., Ellisman, M.H., et al. (2011). Development of a Method for the Purification and Culture of Rodent Astrocytes. Neuron *71*, 799–811.

Gay, L., Miller, M.R., Ventura, P.B., Devasthali, V., Vue, Z., Thompson, H.L., Temple, S., Zong, H., Cleary, M.D., Stankunas, K., et al. (2013). Mouse TU tagging: a chemical/genetic intersectional method for purifying cell type-specific nascent RNA. Genes & Development *27*, 98–115.

Goodrich, L.V., Milenković, L., Higgins, K.M., and Scott, M.P. (1997). Altered Neural Cell Fates and Medulloblastoma in Mouse patched Mutants. Science *277*, 1109–1113.

Hatten, M.E. (1985). Neuronal regulation of astroglial morphology and proliferation in vitro. J Cell Biol *100*, 384–396.

Henner, A., Ventura, P.B., Jiang, Y., and Zong, H. (2013). MADM-ML, a Mouse Genetic Mosaic System with Increased Clonal Efficiency. PLoS ONE *8*.

Jacks, T., Remington, L., Williams, B.O., Schmitt, E.M., Halachmi, S., Bronson, R.T., and Weinberg, R.A. (1994). Tumor spectrum analysis inp53-mutant mice. Current Biology *4*, 1–7.

Liu, C., Sage, J.C., Miller, M.R., Verhaak, R.G.W., Hippenmeyer, S., Vogel, H., Foreman, O., Bronson, R.T., Nishiyama, A., Luo, L., et al. (2011). Mosaic Analysis with Double Markers Reveals Tumor Cell of Origin in Glioma. Cell *146*, 209–221.

Lumpkin, E.A., Collisson, T., Parab, P., Omer-Abdalla, A., Haeberle, H., Chen, P., Doetzlhofer, A., White, P., Groves, A., Segil, N., et al. (2003). Math1-driven GFP expression in the developing nervous system of transgenic mice. Gene Expression Patterns *3*, 389–395.

Machold, R., and Fishell, G. (2005). Math1 is expressed in temporally discrete pools of cerebellar rhombic-lip neural progenitors. Neuron *48*, 17–24.

Marino, S., Vooijs, M., van Der Gulden, H., Jonkers, J., and Berns, A. (2000).

Induction of medulloblastomas in p53-null mutant mice by somatic inactivation of Rb in the external granular layer cells of the cerebellum. Genes & Development *14*, 994–1004.

Matei, V., Pauley, S., Kaing, S., Rowitch, D., Beisel, K.W., Morris, K., Feng, F., Jones, K., Lee, J., and Fritzsch, B. (2005). Smaller inner ear sensory epithelia in Neurog1 null mice are related to earlier hair cell cycle exit. Dev. Dyn. *234*, 633–650.

Figure S1. Niche Cells in Human Shh Subtype Medulloblastoma, and the Validation of the Lack of Labeling of Niche Cell Types by *Math1-Cre* in the MADM Model. Related to Figure 1.

(A) Qualitative scoring of various niche cells in human medulloblastoma samples, including astrocytes (GFAP+), microglia/macrophages (CD68+), and blood vessels (CD34+).

(B) Summary of the presence of niche cells in human medulloblastoma

(C-E) *Math1-Cre;MADM* does not label prospective niche cell types in normal cerebellar tissue, as there was no co-localization of MADM labeling with markers for BLBP+ Bergmann glia and astrocytes (C), IBA-1+ microglia (D), and CD34+ blood vessels (E). Scale bars: A,C-E= 50μm.

Figure S2. Quantification of Niche Composition During Tumor Progression. Related to Figure 2.

(A) Blood vessels (CD34+) show significantly increased area of coverage in medium and large tumors but not in small tumors, in comparison to adjacent normal cerebellar tissue (small, $p=0.47$; medium, $p=0.01$; large, $p=0.006$; n=3 each).

(B) Microglia/macrophages (Iba-1+ cells) are significantly enriched in medulloblastoma even at early stages (small, $p=0.03$; medium, $p=0.008$; large, $p=0.001$; n=3 each). Oligodendrocyte progenitor cells (PDGFRα+) are also significantly enriched in tumors (small, $p=0.01$; medium, $p=0.01$; large, $p=0.00003$; n=3 each).

(C) Niche cell composition in tumors (n=3 each).

(D) Astrocyte processes (visualized as GFP from Aldh1L1-GFP transgene expression) closely intercalate with surrounding tumor cells.

(E) Extended astrocytic processes cover ~20% of the tumor area based on the average of sampling from four regions (425μm^2 each) throughout each tumors (n=4).

Scale bars: D=; D, right panel= 10μm. D, left and middle= 50μm, right= 10μm

Figure S3. Transdifferentiation is an Intrinsic Feature of Tumor GNPs. Related to Figure 3.

(A) Conditional knockout (CKO) model of medulloblastoma with the genotype *Math1-Cre; Ptc+/-; p53flox/p53flox; ROSA26-LSL-RFP*. Both tumor GNPs and tumor astrocytes are RFP+.

(B) Tumor GNPs were purified by Percoll gradient size selection (tumor GNPs in lower fraction, astrocytes in top fraction) (Hatten, 1985). Purified GNPs were cultured briefly *in vitro* to ensure no astrocyte contamination, then injected into brains of NOD/SCID mice to assess their transdifferentiation ability.

(C) Cultured tumor GNPs had minimal/no astrocyte contamination prior to orthotopic injection based on qRT-PCR of astrocytic genes, *Aldh1L1* and *Id3* (n=2).

(D) Grafted tumor GNPs did not show astrocytic transdifferentiation at 10dpi. It should be note that, while grafts have GFAP+ cells, they are RFP-negative so likely are reactive astrocytes in response to the injection-induced injury.

(E) At 30dpi when grafted tumors grew into large sizes, some tumor GNPs had transdifferentiated into TuAstros (RFP+/GFAP+/BLBP+).

[GNP= granule neuron progenitor, RFP= red fluorescent protein, qPCR= quantitative real time polymerase chain reaction, DIV= days *in vitro*, dpi= days post injection]

Scale bars: D-E= 100μm.

Figure S4. Astrocytes in Human Desmoplastic Medulloblastoma. Related to Figure 4.

(A) GFAP+ astrocytes in human tumors often organize into nodules (N) that wrap around tumor cells.

(B) GFAP+ astrocytes form close contact with blood vessels (arrows). Boxed region in the left panel is magnified in the right panel.

(C) Anti-human GFAP antibody specifically labels sparse human astrocytes (arrowhead) in mouse brains grafted with human tumor cells. Arrows point to mouse astrocytes.

[N= nodule, BV= blood vessel]

Scale bars: A-C = 50μm.

Figure S5. Specific Labeling of TuAstros in the Tumor Mass by *Glast-CreER; ROSA26-LSL-tdT*. Related to Figure 5.

(A) Experimental paradigm. Brains were dissected two days after Tamoxifen administration to validate the specific labeling of TuAstros.

(B) BLBP+ TuAstros are labeled while BLBP- tumor GNPs are not labeled in the tumor mass. The labeling of Bergmann glia but not other cell types in normal molecular layer (ML) further demonstrate the specificity of *Glast-CreER* transgene.

[Glast= Glutamate Transporter, ML= Molecular layer]

Scale bars: B macro view = 500μm, Higher magnification panels = 20μm.

Figure S6. Examples of Varied Presence of TuAstros in PNLs. Related to Figure 6.

(A-C) The presence of multiple PNLs in the same brain.

(D) Numbers of proliferating mutant GNPs are limited in a PNL with limited TuAstros.

(E) Occasionally, PNLs with proliferating GNPs show no obvious presence of TuAstros.

Scale bars: A= 500μm, B-E= 50μm.

Figure S7. The Support of Normal Astrocytes to Both Wildtype and Tumor GNPs. Related to Figure 7.

(A) Normal astrocytes support wildtype GNP proliferation *in vitro.* Normal astrocytes were isolated from the perinatal cortex of *Aldh1L1-GFP* mice by FACS and co-cultured with wildtype RFP+ GNPs. A 2hr EdU-pulse was used to label actively proliferating cells. GNPs cultured alone were used as a control.

(B) Quantification of %EdU+ GNPs is represented as x-fold change in co-cultures normalized to GNPs cultured alone, set as 1 (*n=3*, *p= 0.029*).

(C) RFP+ tumor GNPs were co-cultured with FACS-purified *Aldh1L1-GFP*+ astrocytes or alone for 1, 3, and 6 DIV (3DIV shown here).

(D) Proliferation of tumor GNPs determined by EdU labeling is increased in the presence of normal astrocytes. 1DIV *n.s. p=0.267*, 3DIV **p=0.025*, 6DIV **p=0.031*.

(E) Apoptosis of tumor GNPs determined by DAPI+ pyknotic nuclei is suppressed in the presence of normal astrocytes. 1DIV *n.s. p=0.202*, 3DIV **p=0.042*, 6DIV **p=0.003*.

(F) Neuronal differentiation of tumor GNPs determined by TUJ1-staining is suppressed in the presence of normal astrocytes. TUJ1 can only be detected beyond 1DIV, so this timepoint was not analyzed. 3DIV *n.s. p=0.193*. 6DIV **p=0.012*.

(G) Representative images of RFP+ tumor GNPs that are proliferating (EdU+), going through cell death (pyknotic nuclei from DAPI stain), and neuronal differentiation (TUJ1+).

[DIV= day *in vitro*]

Scale bars: A = 50μm; C = 100μm; G = 20μm.

Supplemental Figure 1

Click here to download Supplemental Text & Figures: Ventura_Figure S1.pdf

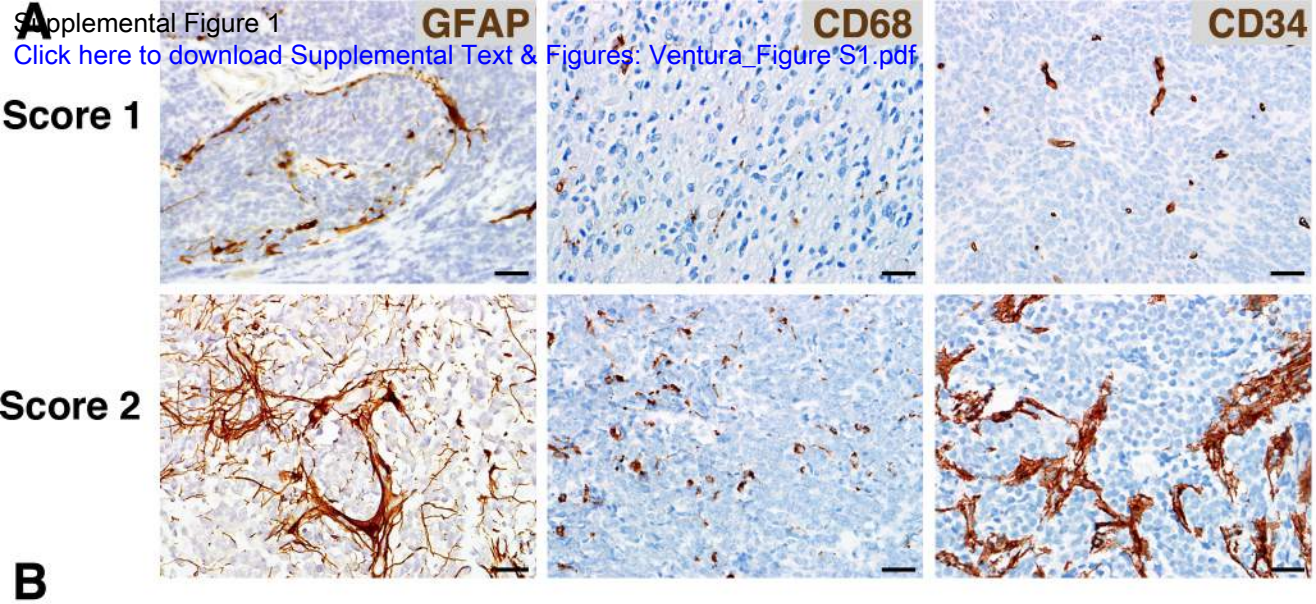

B

Score (0=none, 1=few, 2=many) (#score/#cases)	Astrocytes (GFAP)	Microglia/ Macrophages (CD68)	Blood vessels (CD34)
0	8/26	1/21	0/22
1	5/26	12/21	18/22
2	13/26	8/21	4/22
% tumors with cell type	**69.23**	**95.23**	**100**

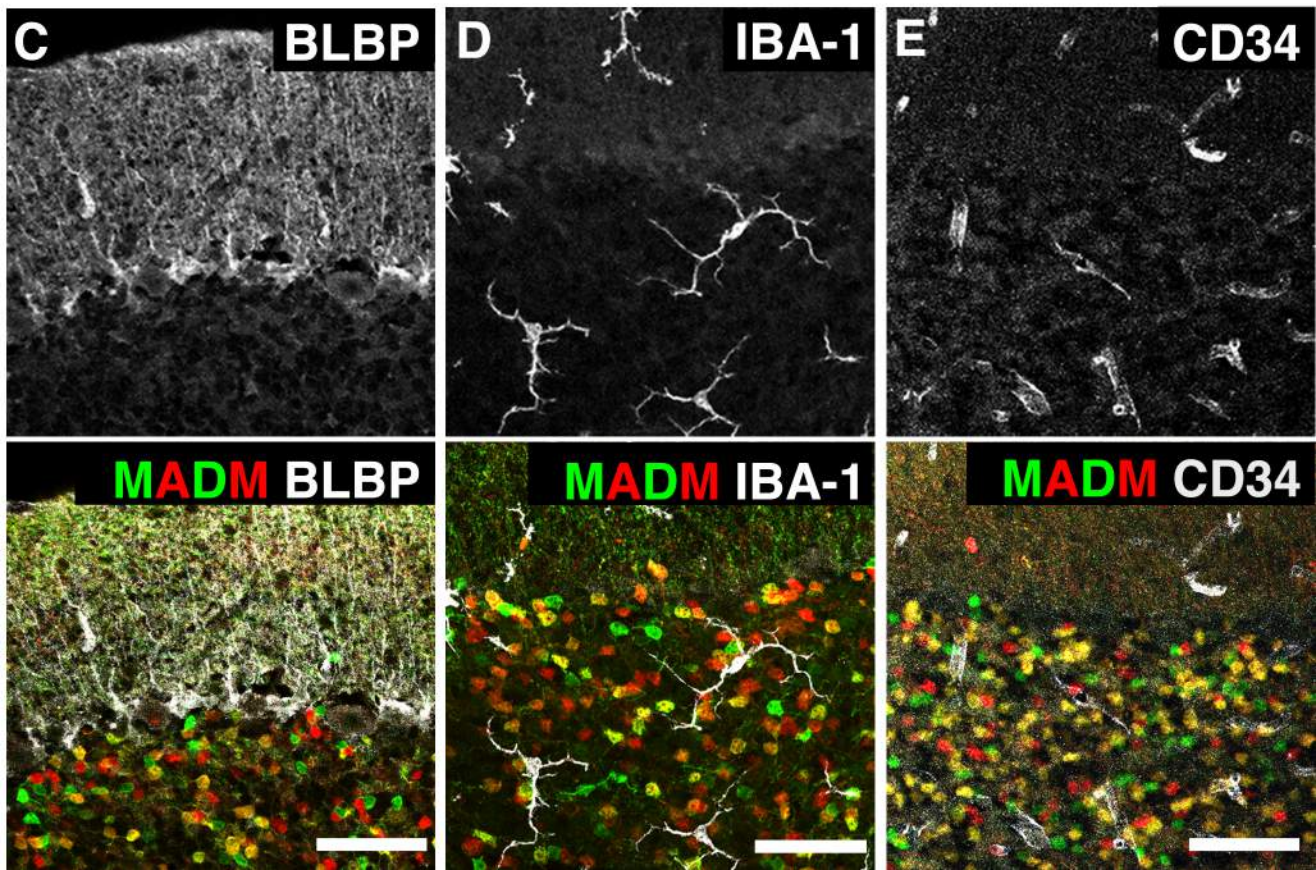

Supplemental Figure 2

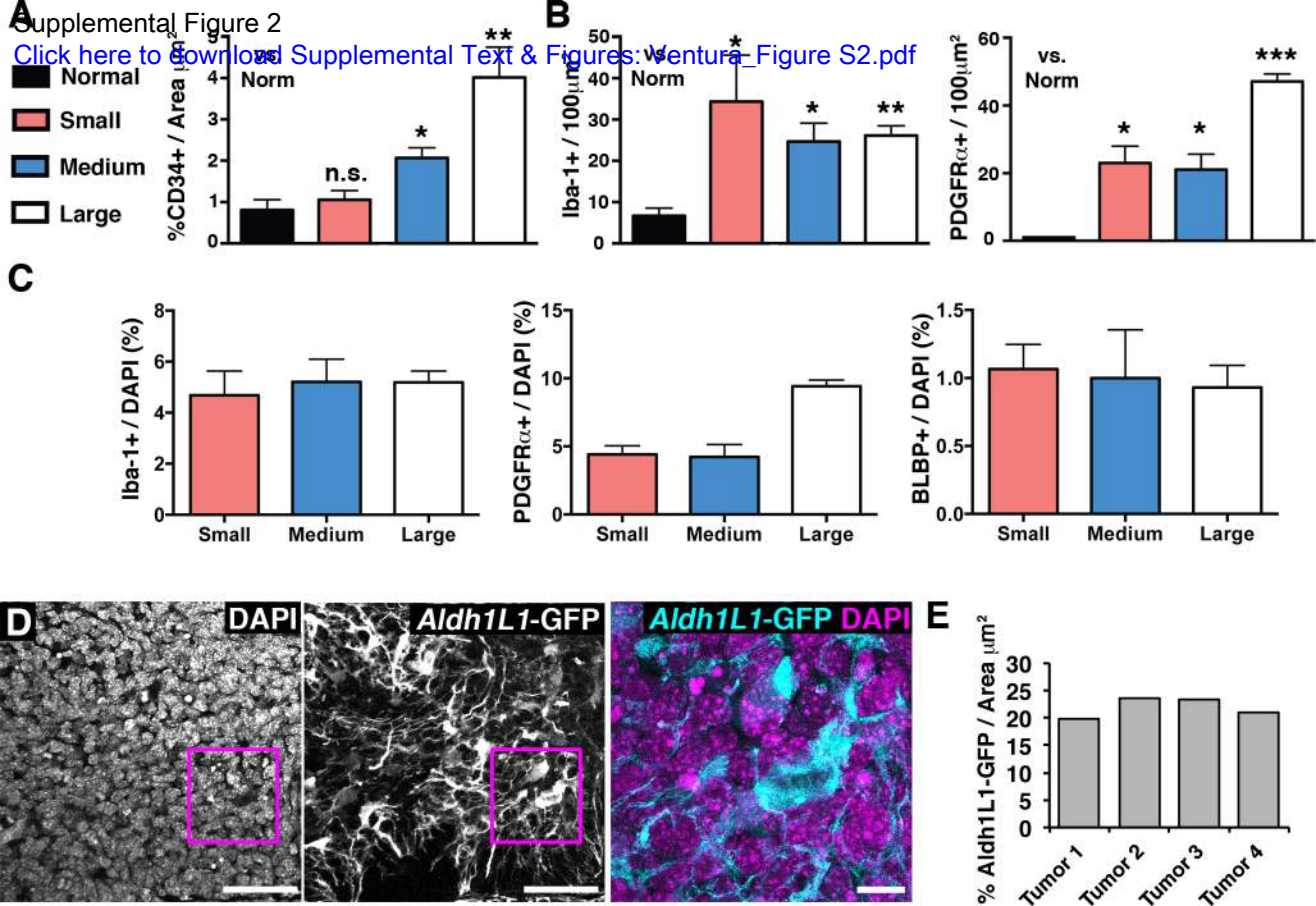

Supplemental Figure 3

Click here to download Supplemental Text & Figures: Ventura_Figure S3.pdf

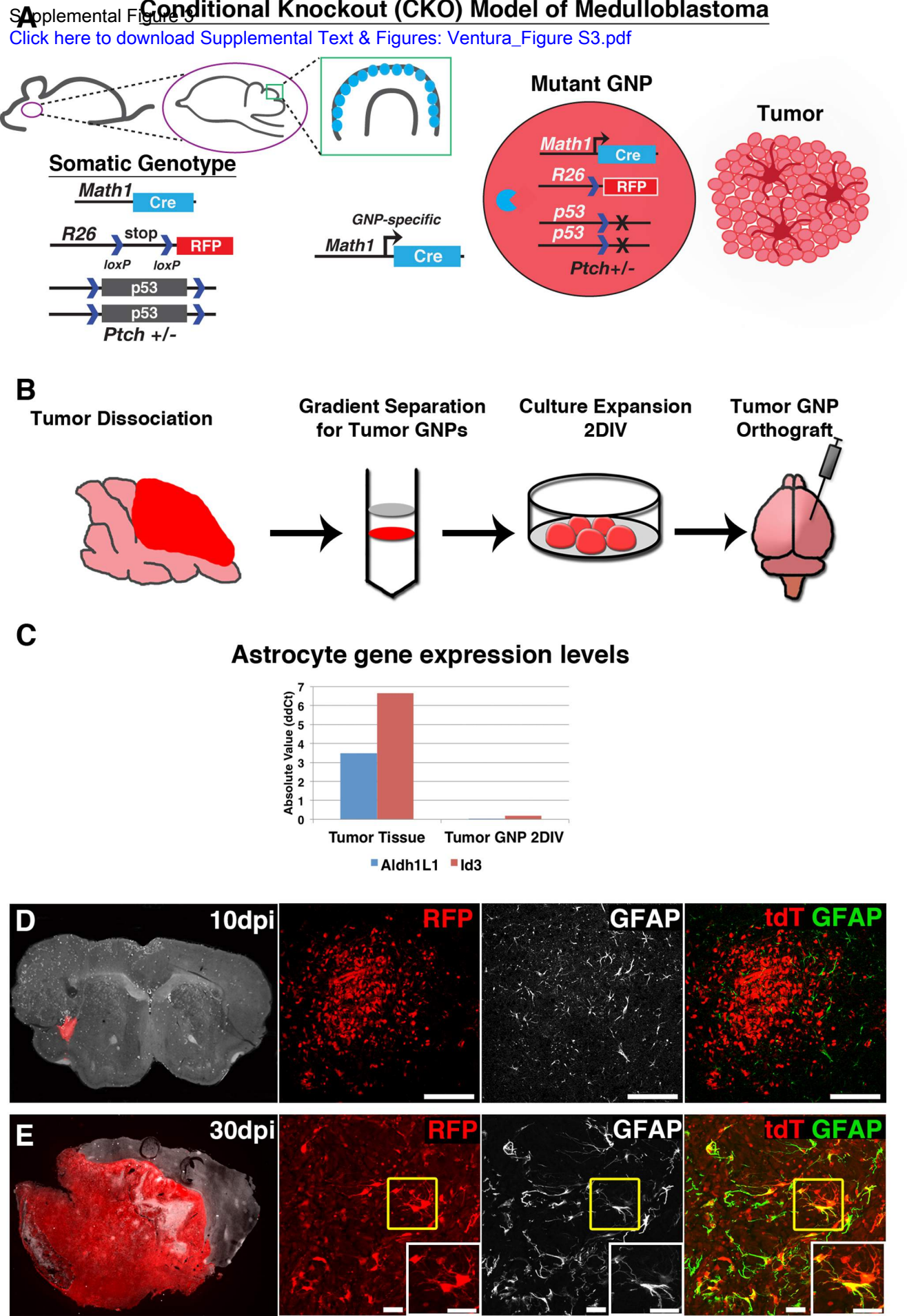

Supplemental Figure 4

Click here to download Supplemental Text & Figures: Ventura_Figure S4.pdf

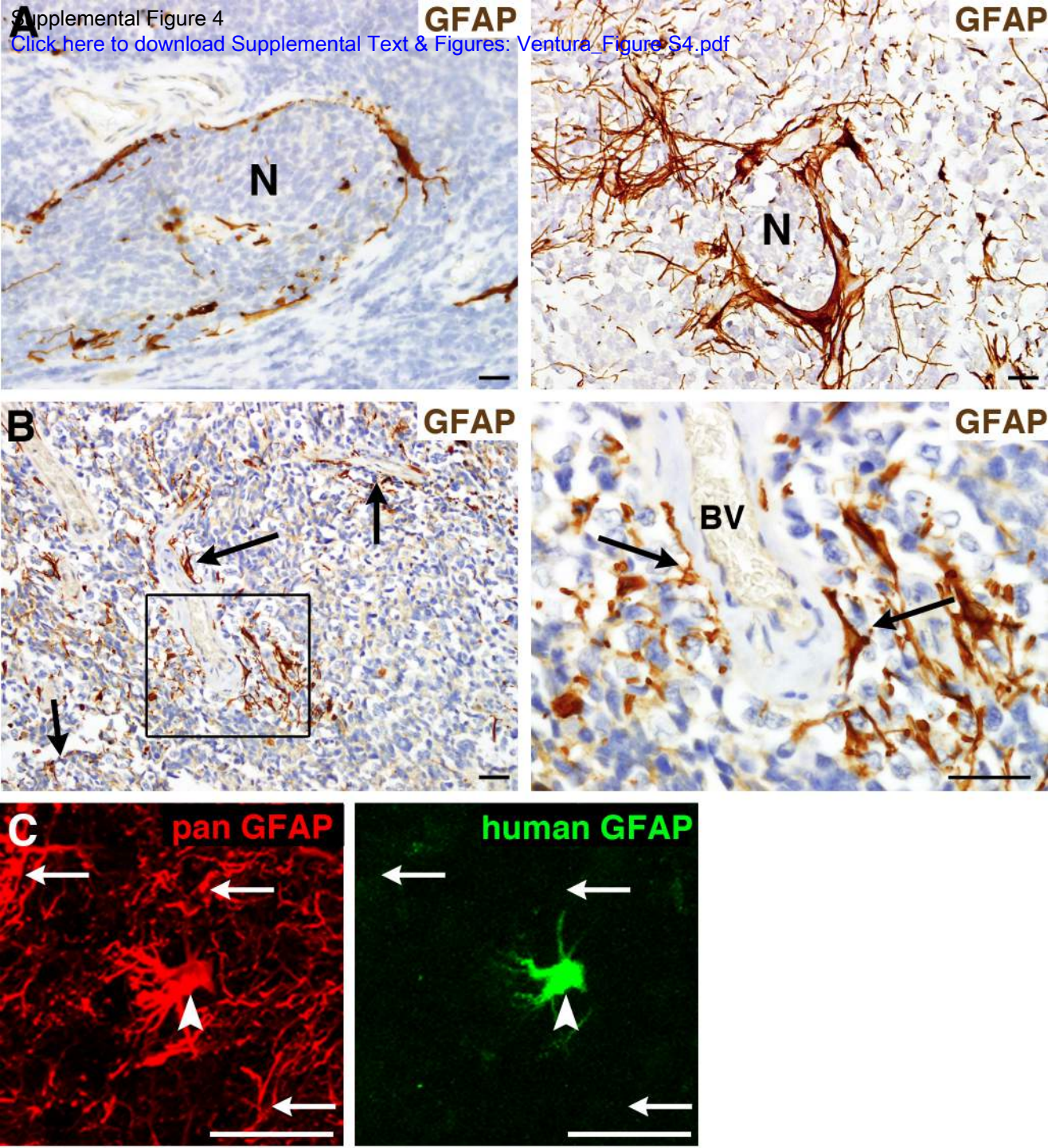

Supplemental Figure 5

A

Glast-CreER; ROSA26-LSL-tdTomato; Ptch+/-

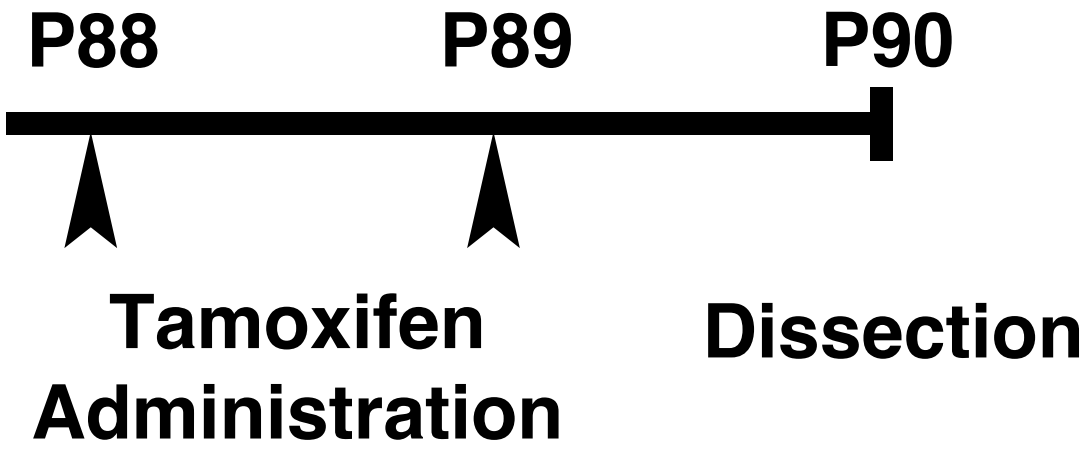

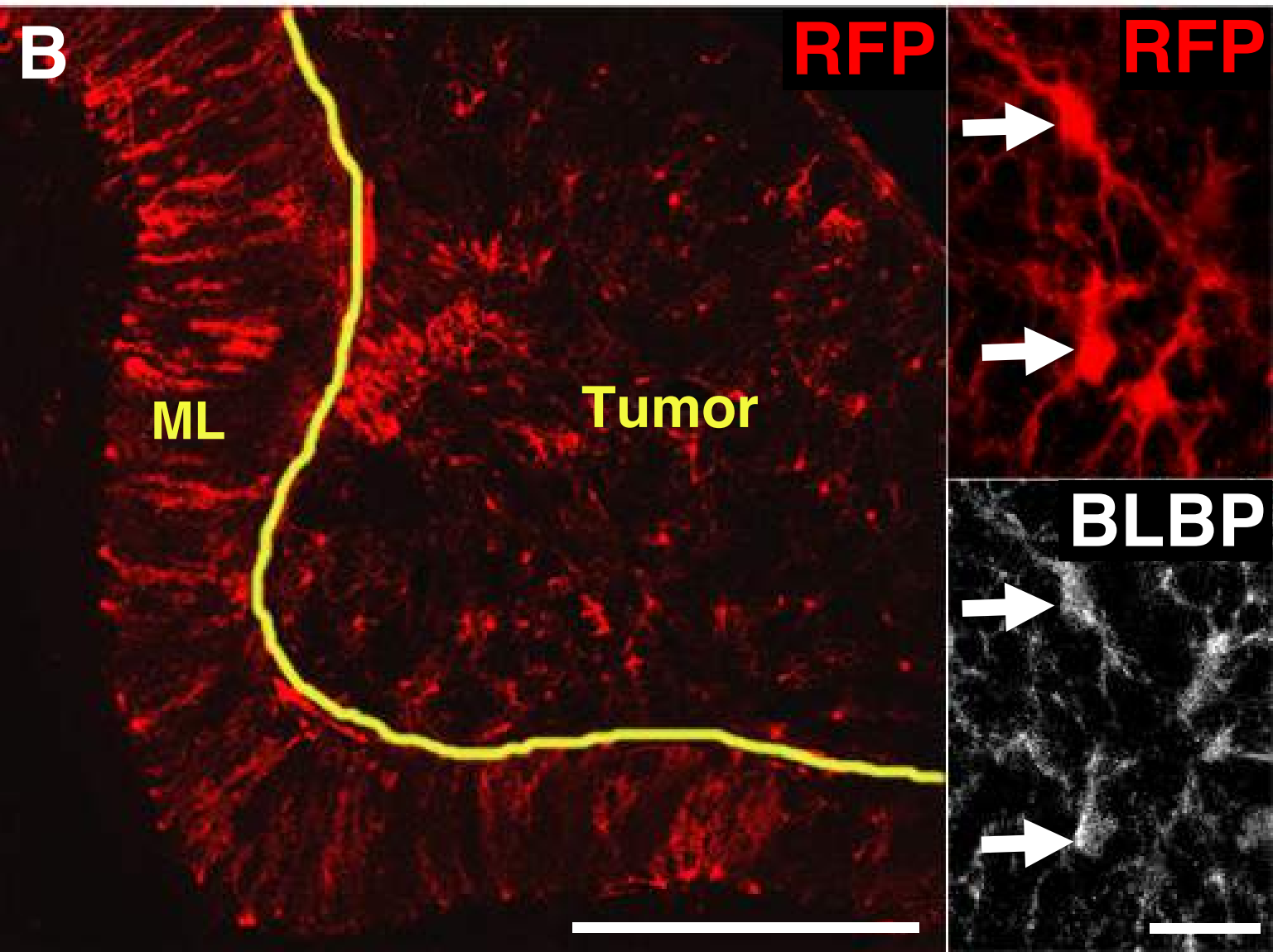

Supplemental Figure 6

Click here to download Supplemental Text & Figures: Ventura_Figure S6.pdf

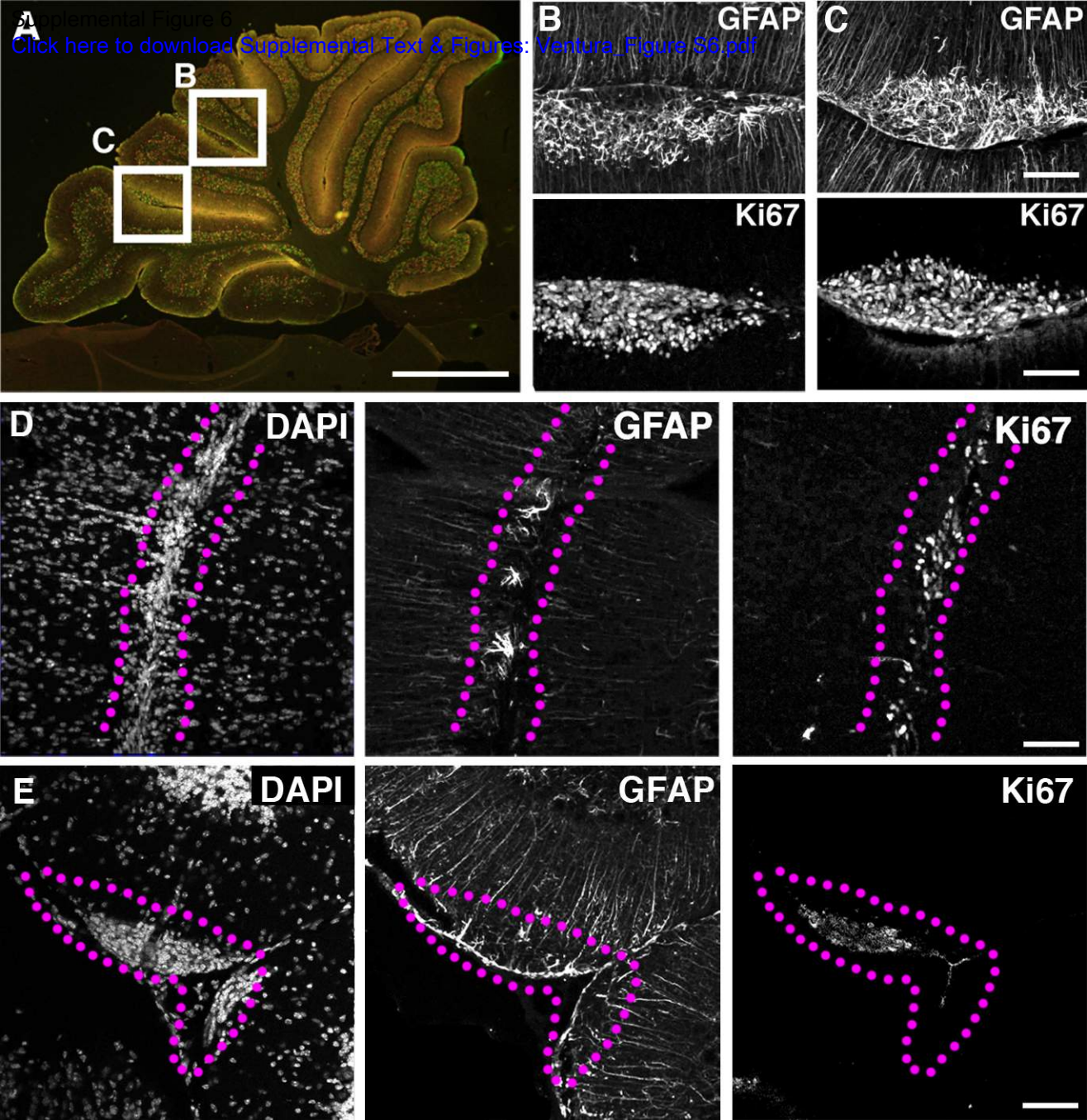

Supplemental Figure 7

Click here to download Supplemental Text & Figures: Ventura_Figure S7.pdf